Wrocław University of Technology
Centre of Advanced Materials and Nanotechnology

Materials Science

International Conference on Sol-Gel Materials
SGM 2003, Szklarska Poręba, Poland

Vol.21 • No. 4 • 2003

Oficyna Wydawnicza Politechniki Wrocławskiej

Materials Science is an interdisciplinary journal devoted to experimental and theoretical research into the synthesis, structure, properties and applications of materials.

Among the materials of interest are:

- glasses and ceramics
- sol-gel materials
- photoactive materials (including materials for nonlinear optics)
- laser materials
- photonic crystals
- semiconductor micro- and nanostructures
- piezo-, pyro- and ferroelectric materials
- high-T_c, superconductors
- magnetic materials
- molecular materials (including polymers) for use in electronics and photonics
- novel solid phases
- other novel and unconventional materials

The broad spectrum of the areas of interest reflects the interdisciplinary nature of materials research. Papers covering the modelling of materials, their synthesis and characterisation, physicochemical aspects of their fabrication, properties and applications are welcome. In addition to regular papers, the journal features issues containing conference papers, as well as special issues on key topics in materials science.

Materials Science is published under the auspices of the Centre of Advanced Materials and Nanotechnology of the Wrocław University of Technology, in collaboration with the Institute of Low Temperatures and Structural Research of the Polish Academy of Sciences and the Wroclaw University of Economics.

All accepted papers are placed on the Web page of the journal and are available at the address:
http://MaterialsScience.pwr.wroc.pl

The Journal is supported by the State Committee for Scientific Research

Editorial Office

Łukasz Maciejewski

Editorial layout

Hanna Basarowa

Printed in Poland

Drukarnia Oficyny Wydawniczej Politechniki Wrocławskiej
Zam. nr 7/2004.

Contents

Materials Science, *Vol. 21*, *No. 4*, *2003*

Electrochemical evaluation of protective properties of one-component SiO_2 and TiO_2 coatings obtained by the sol-gel method

EWA SZAŁKOWSKA[1*], JAN MASALSKI[2], JÓZEF GŁUSZEK[2]

[1]Department of Chemistry, Częstochowa University of Technology,
al. Armii Krajowej 19, 42-200 Częstochowa, Poland

[2]Institute of Inorganic Technology and Mineral Fertilizers, Wrocław University of Technology,
Wybrzeże Wyspiańskiego 27, 50-370 Wrocław, Poland

The paper presents the corrosion resistance of uncoated steel and steel coated with one-component films in 0.5 M H_2SO_4 at 22.0±0.2 °C. One-component coatings were obtained by the sol-gel method. The coatings were obtained by the dip coating method. Quantitative composition of the coatings and their thickness were estimated by means of X-ray Photoelectron Spectroscopy (XPS). The corrosion behaviour of steel coated with one-component films was evaluated with the use of electrochemical direct and alternating current methods.

Key words: *sol-gel method; XPS method; potentiodynamic curves; impedance*

1. Introduction

The main focus of research on corrosion-resistant materials nowadays is the modification of the surface layer. The most popular methods involve coating the metal or admixing some elements into it. The interest in ceramic coatings deposited on various materials has been increasing in recent years, due to such properties of the ceramics as high mechanical strength, high melting point, abrasion and corrosion resistance even in aggressive environments. The sol-gel technique applied to depositing ceramic films on materials has been gaining increasing recognition, as it offers wide possibilities of producing both one-component and multicomponent coatings [1–4]. Among other advantages of the sol-gel technique, one has to mention the control of microstructure of the coating films, their high purity and relatively low temperatures as compared to the conditions of obtaining solid ceramics.

[*]Corresponding autor, e-mail: ewas@mim.pcz.czest.pl.

The sol-gel coatings are used for protection against electrochemical and high-temperature corrosion [5–8]. The significance of the sol-gel technique in general is best evidenced by the variety of its applications for obtaining new materials in the form of fibres, films, powders, devitrificates, monolithic glass, ceramics, and, last but not least, coatings [9–14].

The aim of the present project is to obtain one-component coatings on chromium steel by means of the sol-gel technique, and to assess the protective properties of the coatings in the environment of 0.5 M H_2SO_4.

2. Experimental

The substrate was chromium steel which is a modification of the AISI 403 type. In the sol-gel method, one of the steps is a high-temperature treatment of oxide coatings. The steel substrate might show a phase transition during this operation if the iron steel is used. To avoid this, the chromium steel (modification of AISI 403) was chosen. The additional elements – molibdenium and vanadium (absent in AISI 403) stabilize the precipitated carbides making the steel more temper-resistant. For the chemical composition, see Table. The samples were in the form of discs 12.0 mm in diameter and 1.0 m thick. Before coating, the surfaces were ground with an emery paper #1000, rinsed with distilled water and degreased with tetrachloromethane in an ultrasound washer.

Table. Chemical composition of the stainless steel (% w/w)

C	Mn	Si	P	S	Cr	Ni	Mo	V	W	Cu
0.12	0.51	0.35	0.026	0.029	12.4	0.43	0.11	0.04	0.13	0.12

To obtain an SiO_2 sol, the solution containing 25.0 g of tetraethoxysilane $Si(C_2H_5O_4)$ and 11.0 g of anhydrous ethanol (C_2H_5OH) was used, to which another solution of 11.1 g of anhydrous ethanol and 8.6 g of distilled water was added. Subsequently, the solution obtained was stirred by means of a magnetic stirrer with a constant speed (300 r.p.m.) for one hour. Then, the solution was left in an open vessel at the temperature of 20 ± 5 °C, until the sol of required viscosity (about 3 cP) had been obtained. The time needed for obtaining the appropriate sol depends also on the factors affecting the ratio of solvent evaporation, i.e. the temperature, air humidity and circulation. In the sol obtained, the content of the coating material was 13% (m/m) with respect to SiO_2. The reaction of hydrolysis of the tetraethoxysilane (TEOS) proceeds in the following way:

$$Si(C_2H_5O)_4 + (2+n)\,H_2O \rightarrow SiO_2{\cdot}nH_2O + 4C_2H_5OH \qquad (1)$$

The viscosity of the solutions used for SiO_2 coatings was 3.3–3.4 cP, as measured with a Hoopler viscosimeter at 20 °C.

To obtain a TiO_2 sol, a solution containing 6.0 cm^3 of tetraisopropyl orthotitanate $Ti(C_3H_7O)_4$ and 45.0 cm^3 of anhydrous ethanol was used, to which a solution containing 6.0 cm^3 30% (m/m) of hydrous acetic acid and 45.0 cm^3 of anhydrous ethanol was added while stirring. The solution obtained was left in a closed vessel to age. After 3–5 hours the solution became turbid, yielding 2.0% (m/m) of TiO_2 sol. The reaction of the hydrolysis of tetraisopropyl orthotitanate proceeds as follows:

$$Ti(C_3H_7O)_4 + (2+n)\ H_2O \rightarrow TiO_2 \cdot nH_2O + 4C_3H_7OH \qquad (2)$$

The viscosity of the solution at 20 °C was 3.4 cP as measured with a Hoppler viscosimeter.

The films were deposited on the substrates by dip coating. First, the sol was homogenized for 45 minutes in an ultrasound washer, then the samples were dipped in the sol for 2 minutes in order to establish equilibrium at the boundary of the substrate/solution phases. The dipping and withdrawing of samples was performed at a constant rate of 1.0 mm/s. The samples were then dried in the cool air for 24 hours, and heated in an electrical furnace, which was heated to the maximum temperature at the rate of 2.0 °C/min. The samples examined were coated with five layers of the film in such a way that the first four layers were heated at 500 °C for 10 minutes, and the fifth, external layer was heated at 750 °C for 30 minutes.

The one-component coatings obtained by means of the sol-gel method on the chromium steel were examined with a scanning microscope Cambridge Stereoscan SC-180.

The X-ray Photoelectron Spectroscopy was performed by means of an electron analyzer AMICUS (KRATOS Analytical). The coated samples were cut to the size of 5.0 mm^2, covered with a conducting tape on both sides, and placed in a vacuum chamber. The tape carried away the electrostatic charge from the samples, thereby minimizing shifts in the peaks of the bonds energy. The spectra were recorded using the pass energy of 75 eV and an X-ray energy of 240 W. The analysis of the surfaces was enhanced with a depth profile obtained by etching with a fast Kauffman ion Argon gun. The stable parameters of the gun operation ($p = 1\times10^{-2}$ Pa, emission current 100 mA, and acceleration voltage 200 V) enabled the scaling of the profile. Both etching of the samples surfaces and their analysis were performed at various locations on the films, which minimized the risk of damaging the surface. The quantitative analysis of the coatings was carried out with the original software of the AMICUS spectrometer.

Electrochemical examinations were performed with direct and alternating currents. Polarization curves were measured in a conventional three-electrode thermostated system which enabled maintaining constant temperature of 22.0±0.2 °C during the measurements. In the potentiodynamic tests a platinum electrode was used as the auxiliary one and a saturated calomel electrode (SCE) as the reference one. The analysis of the dependence of current density on the potential applied in a 0.5 M H_2SO_4 solution was performed by means of an automated measuring system consisting of a EP-20 potentiostate, an EC 20B generator, a 5D logarithmic amplifier (ELPAN, Poland)

and a system for signal recording (AMBEX, Poland) connected to a PC. The potential was changed from the cathodic to the anodic values with respect to the SCE, the rate of change being small (1.0 mV/s), since the passivation process is typically slow. Impedance spectroscopy was carried out with a HF FRA 1255 device (Schlumberger) connected to an impedance interface ATLAS 9181. The measuring system was controlled by an IBM PC program Imp-opt v. 4.0, through the GPIB interface. The impedance measurements were performed within a Faraday cage in order to reduce external interferences. The two-electrode arrangement enabled the measurements of impedance up to 1.0 GΩ. The platinum electrode was used as an auxiliary electrode. The upper limit of frequency was 3.0 kHz, whereas the lower limit was 0.001 Hz. The amplitude of the sinusoidal interference signal was 25.0 mV. The measurements were carried out at the corrosion potential occurring after various periods of exposure of the samples to the solution. Repeatability was checked by making two measurements for one sample, first starting at low frequencies and the second starting at high frequencies. The spectra were virtually identical, it can be thus concluded that the examined systems did not change during the measurements. The impedance spectra are presented in the Bode diagram system recorded at 22.0±0.2 °C. The resulting impedance spectra were numerically processed by an Equivalent Circuit (version 4.51) Boukamp program in order to obtain the best-fit values of the circuit elements.

3. Results and discussion

The surface topographies of one-component films are presented in Figs. 1, 2. In Figure 1, showing the surface of the TiO_2 coating, one can see uneven spherical grains of various sizes. The TiO_2 coating is non-homogeneous and cracked. The cracks probably result form contractions occurring during the process of drying and heating, even though the heating ratio was low (2 °C/min). The increase in the density of the coating at higher temperatures (above 700 °C) makes the crystalline layer of Cr_2O_3 thicker at the substrate/coating boundary, which may cause cracks at lower temperatures [15]. On the other hand, applying higher temperatures was necessary to remove excess of water adsorbed physically and chemically from the dried gel [16]. As evidenced in Fig. 2, the SiO_2 coating is also cracked.

The results of the XPS analyses are presented in Figs. 3, 4, where the contents of elements considered are functions of the etch time and the thickness of the substrate. The estimated thickness of the TiO_2 coating was approx. 600–800 nm (Fig. 3). In the whole profile of the TiO_2 coating, there are actually no peaks from the substrate, i.e. iron or chromium. Initially high concentration of carbon atoms in the film decreases rapidly, almost disappearing below 50 nm, thereby providing evidence for surface adsorption of the carbon compounds. Down to the depth of 600 nm the composition of the coating is stable, the oxygen concentration is approx. 50%, and titanium concentration is only slightly lower than that of oxygen – 42%. The gradual decrease in the titanium concentration can be ascribed to uneven thickness of the coating. One can

also observe an increase in the chromium concentration associated with its diffusion towards the surface, occurring during the high-temperature treatment. Chromium is present in the oxidized form (Cr_2O_3), hence a small increase in the oxygen concentration is observed. Manganese present on the surface comes from the steel substrate. Its concentration seems to be out of proportion as compared to that of other elements

coming from the substrate. This is caused by the process of surface segregation occurring during steelmaking.

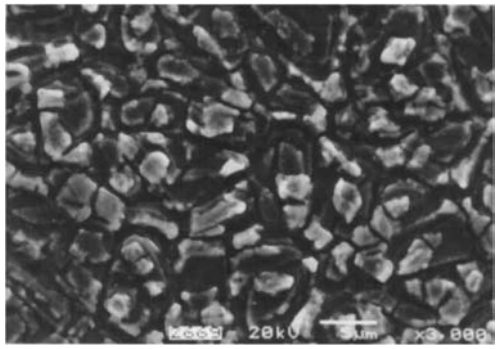

Fig. 1. Microstructure of the TiO_2 film on the chromium steel surface

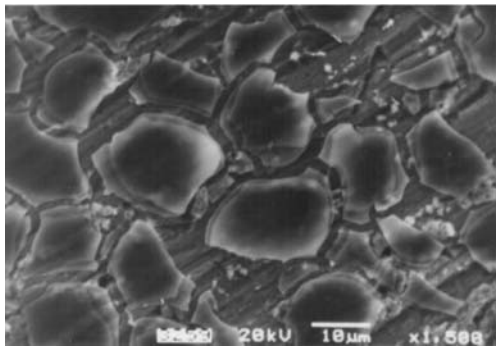

Fig. 2. Microstructure of the SiO_2 film on the chromium steel surface

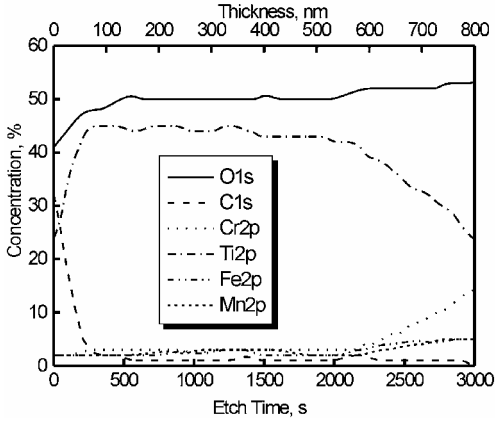

Fig. 3. Depth profile of the TiO_2 film on the chromium steel surface

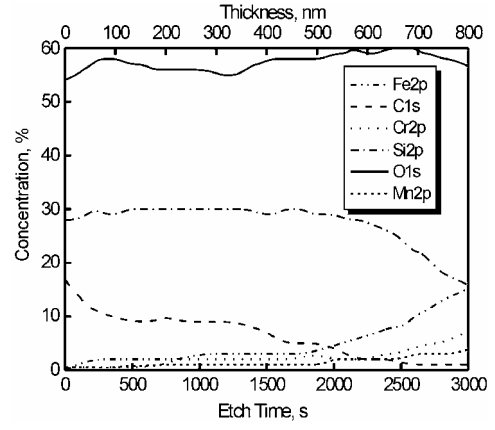

Fig. 4. Depth profile of the SiO_2 film on the chromium steel surface

The thickness of silica layer covering the steel substrate was estimated as about 800 nm (Fig. 4); it is therefore relatively thick. Down to 600 nm the silicon concentration is constant, at the level of 30% (Fig. 4, line Si2p). The coating is characterized by a high carbon content in all its volume. The surface layer is of organic origin and builds into the structure of the silica coating in the process of the high-temperature treatment. The ultimate drop of the carbon concentration is caused by the decrease in silicon concentration, the two being probably bound. The coating is homogeneously

oxidized throughout all its thickness, the concentration of oxygen is maintained at the level of 55–60% (Fig. 2, line O1s). Interestingly, no diffusion of chromium towards the surface has been observed, therefore the iron concentration exceeds the chromium concentration throughout the depth of the coating.

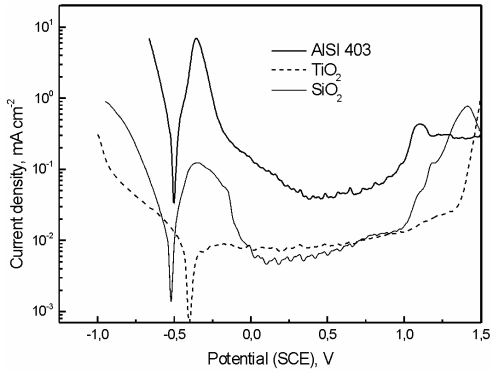

Fig. 5. Potentiodynamic curves for steel samples, uncoated and coated with the SiO_2 and TiO_2 films, in 0.5 M H_2SO_4

Effectiveness of the oxide layers was assessed by the polarization measurements carried out in 0.5 M H_2SO_4. As can be clearly seen in the polarization curves shown in Fig. 5, both the cathodic and anodic current densities are significantly lowered by the coatings. The rate of the anodic process at the corrosion potential for the TiO_2 and SiO_2 coatings is reduced by approx. two orders of magnitude as compared to the steel surface. The comparison of various one-component coatings (Fig. 5) indicates that the best barrier against corrosion is provided by the 5-layer TiO_2 coating.

The results of the impedance measurements recorded on the uncoated and coated steel samples are presented in Fig. 6 as the Bode diagrams for various periods of exposure to the H_2SO_4 solution. The impedance spectra obtained for the uncoated steel differ significantly from those obtained for the coated samples. The value of the impedance module is higher for the coated steel, indicating its higher chemical resistance to the corrosive solution.

The 'Equivalent-Circuit' program (Boukamp) was used for developing electrical equivalence models for the bare steel (Figs. 7a, 7b) and for the one-component coatings (Fig. 7c). The program gave a good match between the calculated spectra and the spectra obtained experimentally. The impedance spectra recorded for the steel exposed to the 0.5 M solution of H_2SO_4 obtained after exposure periods ranging from 10 minutes to 4 hours correspond to the equivalent model R1(R2Q3) (Fig. 7a). In this model, R1 represents the resistance of the electrolyte and of the products of the film corrosion, R2 is the resistance of the charge transfer, and Q3 models the electrical double layer by means of the so-called constant-phase element.

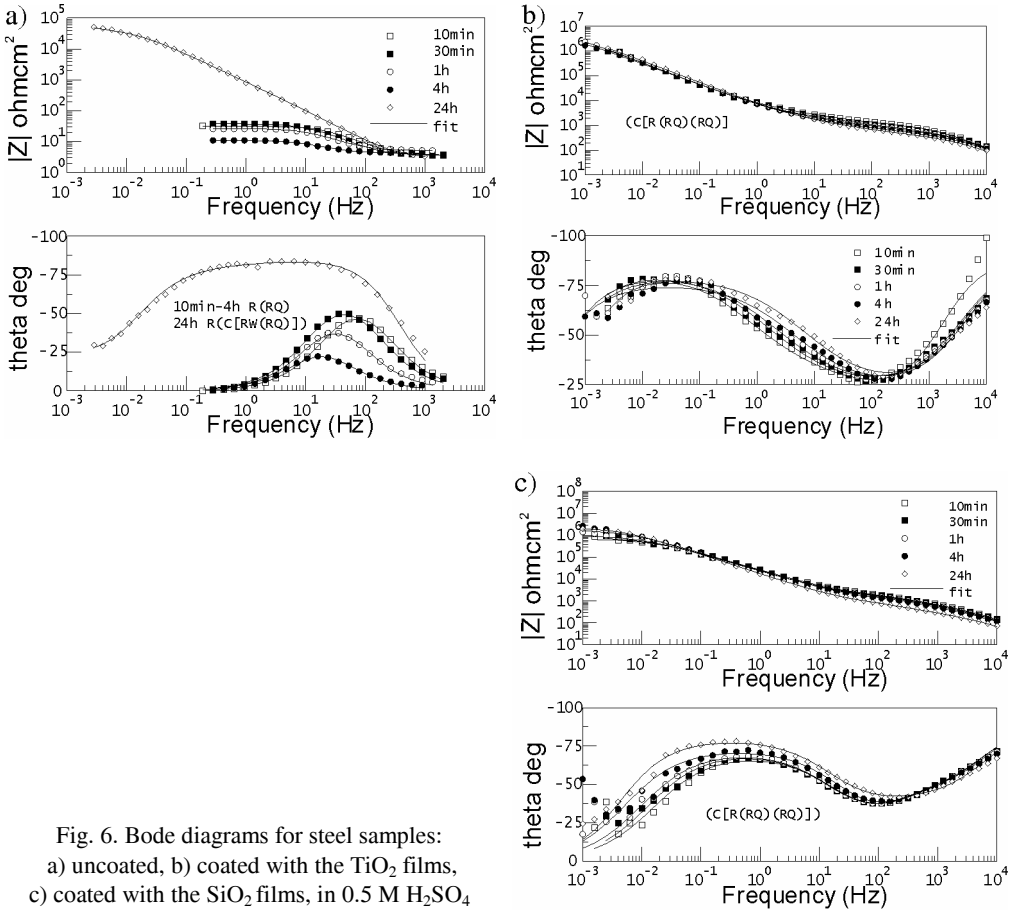

Fig. 6. Bode diagrams for steel samples:
a) uncoated, b) coated with the TiO_2 films,
c) coated with the SiO_2 films, in 0.5 M H_2SO_4

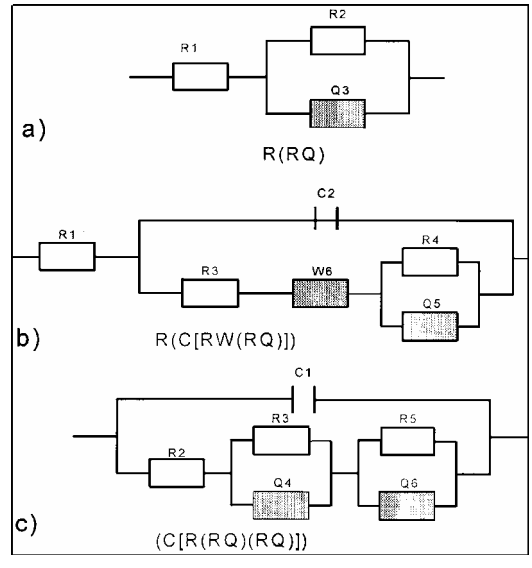

Fig. 7. Electrical equivalent circuits for uncoated steel (a, b) and the steel coated (c) in 0.5 M H_2SO_4

Extending the exposure time to 24 hours renders the R1(R2Q3) equivalent circuit, obtained by means of the Boukamp circuit description mode, inadequate. The spectrum obtained after 24-hour exposure of the steel samples to the acidic solution exhibits high low-frequency impedance module and high constant value of the phase angle within the broad range of frequencies, the latter probably resulting from joining two maxima of the phase angle (Fig. 6a).

The occurrence of the two inseparable maxima of the phase angles is a consequence of an additional element appearing in the electrical equivalent circuit. Figure 7b presents a circuit generating an impedance spectrum correlating with the experimental spectrum. The elements R1, R4, and Q5 in Figure 7b correspond to R1, R2, Q3 in Fig. 7a. Element C2 is the capacitance of the corroded layer adhering tightly to the steel surface, elements R3 and W6, are the resistance of the electrolyte in the pores of the corroded layer and Warburg pseudo-impedance associated with diffusion processes, respectively.

The best fit between the simulated spectra of the coated steel and the experimental ones is obtained with the use of the (C[R(RQ)(RQ)]) model of the electrical equivalent circuit, presented in Fig. 7c. This model is very similar to the one used in the description of stainless steel 304 coated with CeO_2 film exposed to a 1.0 M solution of NaCl [17]. The model presented in Fig. 7c contains additionally the element C1 (electrode capacitance) [18]. The physical sense of the elements R2, R5, and Q6 presented in Fig. 7c is identical to that of the elements R3, R4, and Q5 in Fig. 7b. The elements R3 and Q4 in Fig. 7c are connected to certain properties of the coatings and denote, a resistive element and a constant-phase element, both characterizing electrical properties of the passive layer.

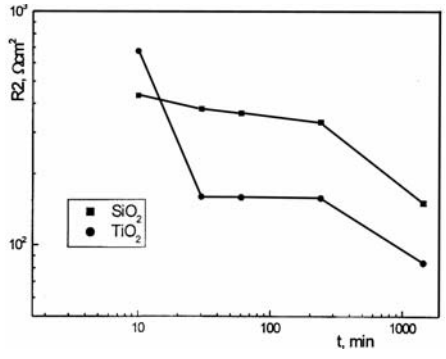

Fig. 8. Resistance of the electrolyte in through -coatings pores (R2) versus exposure time of SiO_2- and TiO_2-coated steel

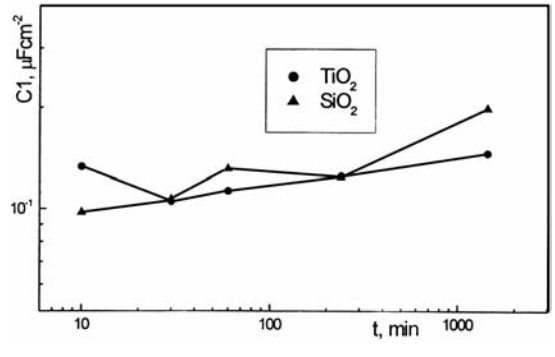

Fig. 9. Capacitance of coatings (C1) versus exposure time of SiO_2- and TiO_2-coated steel

On one hand, the use of two constant-phase elements in the electrical equivalent circuit facilitates the match between the calculated and experimental curves. On the other hand, it introduces four additional parameters, whose physical sense cannot be

easily determined. In spite of this complication, the model developed adequately reflects the physical properties of the investigated system: metal–coating–electrolyte.

In Figure 8, changes in the R2 value of the TiO_2 and SiO_2 coatings are presented as a function of the exposure time to the corrosive solution. As the exposure time increases, the conductivity of the solution also increases (i.e. the resistance decreases), indicating appearance of micro-cracks and new conduction paths (or broadening of the existing ones). The changes in the capacitance (C1) of the coating film typically result from the penetration of water. Water affects the dielectric constant of the coating and, consequently, increases its capacitance. The changes in capacitance of the samples immersed in the corrosive solution are presented in Fig. 9. The capacities of the TiO_2 and SiO_2 coatings increase during the exposure to the 0.5 M H_2SO_4 solution, possibly indicating that the penetration by water is preceded by a several-hour period of induction. The capacitance of the SiO_2 coating is higher than that of the TiO_2 coating. The value of Q6 reflects the degree of delamination of the coating. The fact that this parameter does not show any significant variation over time (Fig. 10) means that no delamination occurs. The decrease in the value of Q6 with the time of exposure in the case of the TiO_2 coating can result from diminishing the metal surface being in contact with the electrolyte through pores and cracks. From the point of corrosion protection, the most crucial parameter is the charge transfer resistance (R5) (Fig. 11) which is inversely proportional to the corrosion rate and to the area corroded. The increase in the value of R5 can be attributed to the process of reconstruction of the internal layer or to the process of 'self-repair' occurring in the layer. In the case of the TiO_2 and SiO_2 coatings, the value of R5 increases, depicting continuous inhibition of corrosion.

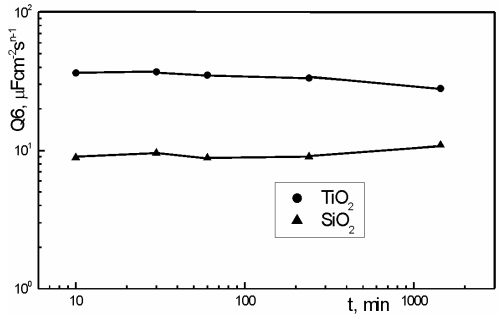

Fig. 10. Constant phase element (Q6) versus exposure time of SiO_2- and TiO_2-coated steel

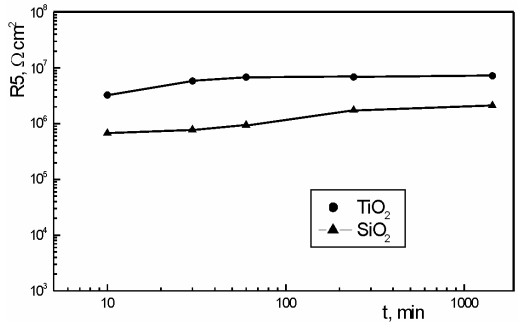

Fig. 11. Charge transfer resistance (R5) versus exposure time of SiO_2- and TiO_2-coated steel

The analysis presented above indicates that the corrosion processes occurring in the systems of coatings obtained by the sol-gel method on chromium steel are of a highly complex nature. It has to be also noted that the TiO_2 and SiO_2 coatings are not electrical barriers and that their defects cause considerable scatter of the results.

4. Conclusion

It is possible to obtain one-component coatings on chromium steel by means of the sol-gel method. The TiO_2 and SiO_2 coatings, enhancing the corrosion resistance in the environment of 0.5 M H_2SO_4, are about 800 nm thick. The one-component coatings are non-homogeneous, with many cracks (Figs. 1, 2). The cracks probably result from contractions occurring during the process of drying and heating. The impedance measurements indicate that the coatings are poor barriers due to the presence of numerous cracks through which charge transfer can occur.

References

[1] BRINKER C.J., SCHERER G.W., *Sol-gel: the physics and chemistry of sol-gel processing*, Academic Press, San Diego, 1990.
[2] KLOTZ M., AYRAL A., GUIZARD C., COT L., Bull. Korean Chem. Soc., 20 (1999), 879.
[3] KUNDU D., BISWAS P.K., GANGULI D., J. Non-Cryst. Solids, 110 (1989), 13.
[4] ANDRIANOV K.A., *Organic Silicon Compounds* (in Russian), Gos. Nauchno-Tekhn. Izd. Khim. Lit., Moscow, 1955.
[5] ATIK M., DE LIMA NETO P., AEGERTER M. A., AVACA L. A., J. Appl. Electrochem., 25 (1995), 142.
[6] ATIK M., ZARZYCKI J., J. Mat. Sci. Letters, 13 (1994), 1301.
[7] VASCONCELOS D.C.L., CARVALHO J.A.N., MANTEL M., VASCONCELOS W.L, J. Non-Cryst. Solids, 273 (2000), 135.
[8] GŁUSZEK J., MASALSKI J., ZABRZESKI J., NITSCH K., GŁUSZEK P., Thin Solid Films, 349 (1999), 186.
[9] MAKISHIMA A., OOHASHI H., WAKAKUWA M., J. Non-Cryst. Solids, 42 (1980), 545.
[10] KAMIYA K.,. SAKKA S., TATERNICKI T, J. Mater. Sci., 15 (1980), 1765.
[11] MAKISHIMA A., ASAMI M., WADA K., J. Non-Cryst. Solids, 121 (1990), 310.
[12] ANDERSON M.L., STROUD R.M., MORRIS C.A., MERZBACHER C.I., ROLISON D.R., Adv. Eng. Materials, 8 (2000), 481.
[13] GARBASSI F., BALDUCCI L., UNGARELLI R., J. Non-Cryst. Solids, 223 (1998), 190.
[14] HOLMES-FARLEY S. R., YANYO L. C., Adhesion Sci. Technol., 5 (1991), 131.
[15] ATIK M., MESSADDEG S.H., LUMA F.P., AEGERTER M.A., J. Mat. Sci. Letters, 15 (1996), 2051.
[16] HENCH L.L., WANG S.H., Phase Trans., 24 (1990), 785.
[17] BISWAS R.G., SANDERS R.D., J. Mat. Eng. Perf., 7 (1998), 727.
[18] JUTTNER K., Electrochim. Acta, 35 (1990), 1501.

Received 15 June 2003
Revised 9 August 2003

Materials Science, *Vol. 21*, *No. 4*, *2003*

CeMn/AlSiO ceramic layers on metallic supports for high-temperature catalytic processes

WŁODZIMIERZ TYLUS*

Institute of Inorganic Technology and Mineral Fertilizers, Wrocław University of Technology, Wybrzeże Wyspiańskiego 27, 50-370 Wrocław

The CeO_2–Mn/$SiO_2Al_2O_3$ coating (also as γ-Al_2O_3 or $AlOOH \cdot H_2O$) on metallic supports was found to be best suited for high-temperature catalytic oxidation of diesel soot. With a thickness of 15–20 μm, the ceramic layer coated by the sol-gel method showed no cracks either before or after a thermal shock. Scanning micrographs revealed a tight contact between coating and substrate. The crystallites of active cerium oxides were uniformly distributed in the top part of the layer. No segregation of Cr or Fe from substrate bulk to surface was evidenced, but – advantageously – it was Al that segregated (surface concentration rose from 14 to 24 wt. %), forming a protective layer on the metal surface and a bond with SiO_2/Al_2O_3 coated by the sol-gel method. Making use of DTA and DTG techniques, the catalytic activity of the coating in the diesel soot oxidation reaction was determined. Two temperature peaks (at 350 °C and 470 °C) corresponding to the maxima of the soot oxidation rate were distinguished.

Key words: *sol-gel; ceramic layer; high-temperature corrosion*

1. Introduction

Three-way catalysts have long been used in spark ignition engines. A major element of such a catalyst is a ceramic washcoat deposited onto a metallic monolith support by the sol-gel method. With compression-ignition engines, however, where emission of particulates (especially from heavy duty engines) creates serious hazards, the problem is far more sophisticated [1–3]. The key point is the need of combining two functions in one device which has to act as a particulate filter and a catalyst reducing the ignition temperature from 550 °C to at least 400 °C [4]. During regeneration, when the soot depositing in the filter undergoes catalytic combustion, the process conditions are extremely harsh (thermal shocks, exhaust gas temperature above 1000 °C).

*E-mail: tylus@itn.pwr.wroc.pl.

The response of the ceramic catalytic coatings to the harsh conditions of regeneration was investigated. The application of the heat-resisting metal foam made of FeCrAl alloy increased noticeably the strength of the filter as compared to the conventional ceramic monolith [5]. Owing to a better thermal conductivity, metal monoliths become easier heated and are easier to handle. This metallic support was covered with ceramic and catalytic layers by the sol-gel method.

A certain part of the study, which was carried out to obtain a catalytic layer resistant to a harsh external environment, involved the following procedures: preparation of the metallic surface of the support [6], preparation of coating mixtures, deposition of the ceramic layer and active substances, as well as laboratory tests and physicochemical characterization of the layers obtained in this way. In the present study, a $CeMn/Al_2O_3SiO_2$ coating is described, which meets relevant requirements and has been prepared by mixing silica sols with Ce- and Mn-impregnated aluminium powders. The layers obtained were tested for resistance to high-temperature corrosion and for catalytic performance (DTA, DTG). The surface was analyzed with AES, XRD and electron scanning techniques.

High-temperature corrosion resistance of both uncoated and ceramic-coated FeCrAl foils was determined by thermal shocks, a well-known method dealt with in metallurgy. The samples were treated by approximately 3000 cycles of alternating heating (10 s at 1200 °C) and cooled to room temperature. The measured weight increment of a sample resulting from the oxidation of the material was regarded as a measure of the resistance to high-temperature corrosion. The oxidation of the metallic substrate is the lesser, the tighter is the contact between the coating and the substrate.

2. Experimental

2.1. Preparation of silica sols

Silica sols were obtained from TEOS (tetraethoxysilane >98%) made by FLUKA. They differed in SiO_2 content, which was achieved by adding appropriate portions of water and ethanol. The best starting compound was found to be the partly hydrolyzed $Si(OC_2H_5)_4$. Following the water addition, some part of the ethoxy groups hydrolyzed to form Si–OH groups. Of these, a certain portion condensed to produce Si–O–Si compounds. Another portion preserved its reactive groups.

$$(\mathrm{Si-OC_2H_5}) + \mathrm{H_2O} \xrightarrow{\mathrm{H^+}} (\mathrm{Si-OH}) + \mathrm{C_2H_5OH} \tag{1}$$

$$(\mathrm{S-OH}) + (\mathrm{HO-Si}) \xrightarrow{-\mathrm{H_2O}} \mathrm{Si-O-Si} \tag{2}$$

On changing the proportion of water, it is possible to obtain products of various storage lives or gelation rates. For example, a sol with a low water content and a 20%

SiO_2 ingredient did not gelify within a 12-month period. The hydrolysis was carried out with a solvent of choice. Water-miscible solvents, e.g. ethanol, ethyl glycol or isopropanol, can be used in a wide range of proportion. The rate of coating, the duration of drying and viscosity depend on the type of the solvent applied. Methanol and ethyl glycol accelerated crosslinking, while isopropanol or butanol retarded it.

2.2. Preparation of catalytic powders

Alumina sols were obtained from aluminium isopropanolate which was synthesized under laboratory conditions via the following reaction:

$$2Al + 6(CH_3)_2CHOH = 2((CH_3)_2CHO)_3Al + 3H_2 \quad (3)$$

The hydrolysis reaction occurred according to the equation

$$2((CH_3)_2CHO)_3Al + (3 + n)H_2O = Al_2O_3{\cdot}nH_2O + 6(CH_3)_2CHOH \quad (4)$$

With alumina sols, it was also the proportion of water that contributed to their storage lives and gelation rates. However, the gelation rate was less important in that particular case because the AlO(OH) sol was directly used to produce the desired forms of powdered aluminium oxides, γ-Al_2O_3 and boehmite. As a matter of fact, boehmite was found to act much better as a filling material for the washcoats. During annealing, together with SiO_2, boehmite formed coatings firmly attached to the metallic substrate.

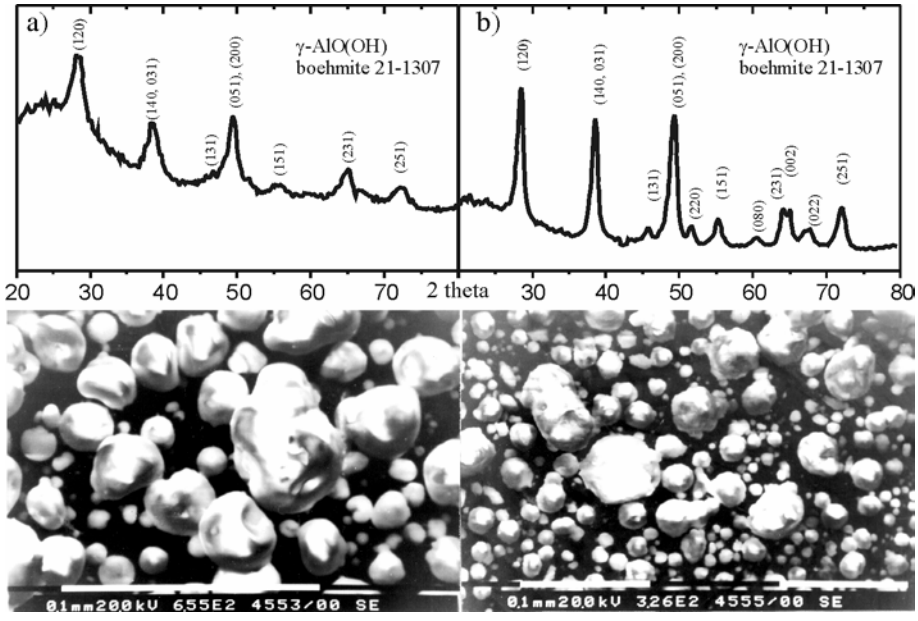

Fig. 1. XRD spectra and micrographs of boehmite powders: a) < 100 μm, b) < 25 μm

The boehmite form of aluminium oxide, $AlOOH \cdot H_2O$, was obtained by alternating drying at 120–200 °C and ball-grinding of the gelified aluminum sol. Figure 1 shows the diffraction patterns identifying the type of the boehmite: Boehm25 (fraction < 25 μm) and Boehm100 (<100 μm). The Boehm25 peaks are more distinct, which indicates that the particles of Boehm25 are more homogeneous than those of Boehm100. The bottom part of the figure shows the microscopic images of both fractions. Boehm25 was used as a filling agent to improve the tightness of the contact between the SiO_2-based coatings and the metallic substrate.

2.3. Catalytic performance of the powders

Aluminium powders were impregnated with catalytic compounds in the course of diesel soot oxidation. The activities of the metal oxides tested in this work can be arranged in the following sequence:

$$CeO_2 \text{ (from nitrate)} > PbO > La_2O_3 > CeO_2 > V_2O_5 > CuO > Co_3O_4$$

$$> Bi_2O_3 > Mo_2O_3 > NiO > Fe_2O_3 > MnO_2 > Cr_2O_3 > ZnO > MgO > ZrO_2 > WO_3$$

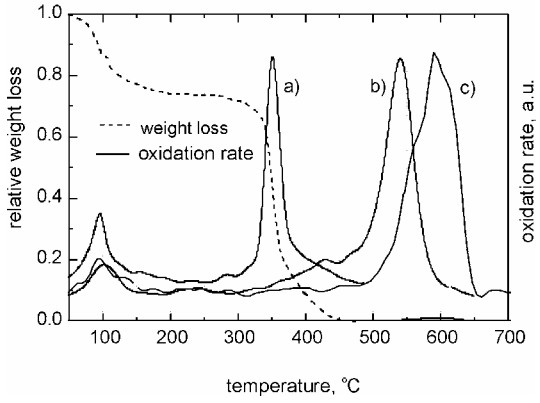

Fig. 2. Curves of oxidation and oxidation rate for diesel soot mixed with CeO_2/Al_2O_3 powder (a), mixed with Al_2O_3 only (b), and for synthetic soot mixed with Al_2O_3 (c)

Figure 2 shows the DTA/DTG plots of diesel soot oxidation over CeO_2/Al_2O_3, where the relative soot mass decrement and the soot combustion rate are related to the temperature-programmed reactor (2 °/min increment). These results were compared with those for diesel soot combustion over pure Al_2O_3 and for synthetic soot, the temperature of the maximum soot combustion rate (mass decrement) being adopted as the temperature of soot ignition. With CeO_2 from cerium nitrate, the ignition temperature amounted to 350 °C. Such a decrease in the soot ignition temperature substantiates the need of incorporating CeO_2 into ceramic catalytic coatings. There are noticeable dif-

ferences between the diesel soot and synthetic soot. The combustion temperature with synthetic soot approaches 600 °C, whereas that with diesel soot is approximately equal to 540 °C. Apart from water desorption, the curve depicting the combustion of the flame soot is a plane one up to about 520 °C. At the same time, the diesel soot sample has already 'lost' half of its mass, which should be attributed to the presence of soluble organic fractions (SOF) burning at lower temperatures and initiating the ignition of the solid soot fraction. In the majority of instances, an active catalyst influences SOF (which resorb from the surface of the soot particulates at elevated temperatures) and decreases their ignition temperature [7].

Selected powders with an active phase – after thorough mixing with the silica sol of appropriate physicochemical parameters in a homogenizer – were deposited onto a suitably prepared support surface. The support was a heat-resisting steel foil, containing FeCr (23%) Al (5%) with admixed lanthanides.

2.4. Preparation of metallic surfaces

The preparation of the metallic surfaces prior to the deposition of the oxide layers plays an important role. In our study it included the following procedures: degreasing, development of the external surface (in order to increase the adhesion of the layer) and rinsing. The development of the surface was carried out with two methods, by selective etching or roughening. In the first method, the samples underwent thermal etching with mineral acid solutions until a mass decrement of 3 to 7% was achieved. With a 10%H_2SO_4+10g/l HCl mixture at 70 °C, this took about 3 minutes. The homogeneous etching requires an appropriate degreasing as a prior step. Using the etching method together with the developed geometrical surface yielded a selective enrichment with aluminium in oxide form. This supported the adhesion of the deposited oxide layer to the substrate. The samples were then rinsed many times. However, he surface analysis by the Auger electron method revealed the presence of sulfur, which must have penetrated there as a result of the etching operation. Sulfur is a highly undesirable element, as it becomes a high-temperature corrosion centre. For this reason, the pneumatic roughening method seemed to be far more advantageous. Thus, the 100 μm corundum ejected at a pressure of 1.8 atm from a distance of approximately 20 cm was adopted as the optimum procedure. The homogeneous surfaces obtained in this way were cleaned pneumatically to remove the abrasive material, and then rinsed in an ultrasonic washer.

2.5. Catalytic coatings and their resistance to high-temperature corrosion

Metallic surfaces were coated in single or multiple operations by immersion or via a pneumatic shower. All samples were dried at 20 to 90 °C for 48h and then calcined in a temperature-programmed oven up to 750 °C. High-temperature corrosion resistance was tested according to a procedure described elsewhere [6].

3. Results and discussion

In Figure 3, the dependence of the relative mass increment of the optimum catalysts, (57%) Ce–(3%) Mn/(18%) SiO_2 + (22%) Al_2O_3 on the number of thermal shock cycles for various thicknesses of the ceramic coatings is shown. The silica sols prepared were found to be good binders which provided an appropriately tight contact not only with the metallic substrate but also with the catalytic oxides added. These oxides accounted for up to 90% of the total ceramic layer mass. We obtained durable 'thick' layers constituting up to 30% of the catalyst mass. These large amounts of active substances are of a great importance in that particular case, because the external geometrical surface alone can be in contact with the soot particulates. In all of the investigated samples, the corrosion was lower than in the reference. According to expectations, thick coatings are best suited for the protection of metallic surfaces. With a 31 wt.% layer, the increment in the catalyst mass (due to the oxidation of the metallic surface) amounted only to 0.2% and was the lowest one determined in the samples under study.

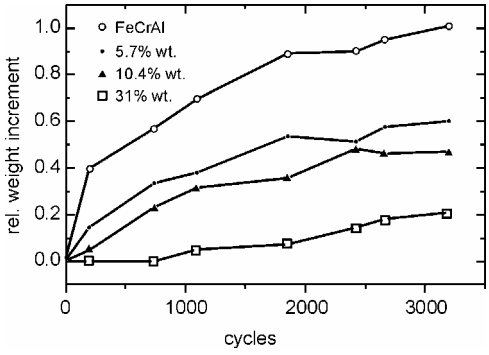

Fig. 3. High-temperature corrosion (oxidation) in thermal shock cycles for various thicknesses of the CeMn/AlSiO optimal ceramic coatings and FeCrAl foil as a reference sample*

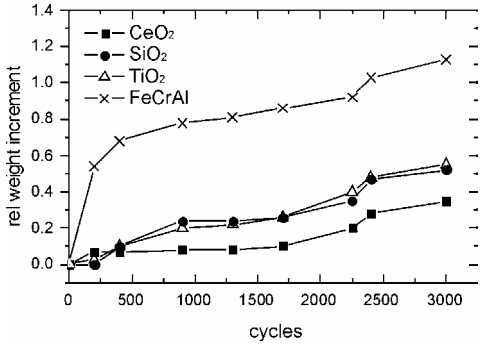

Fig. 4. High-temperature corrosion (oxidation) in thermal shock cycles for various ceramic coatings

Figure 4 characterizes the Al_2O_3 coatings with TiO_2, SiO_2 or CeO_2 admixtures. They were obtained by the shower method, using an AlO(OH) sol solution with the addition of the SiO_2 sol or the TiO_2 sol (or TiO_2 anatase), with the aim to impregnate them with active substances. Each of the three coatings seems to protect the metallic surface sufficiently well against high-temperature corrosion. After 3000 cycles, there was no visible indication of destruction. This finding holds for coatings whose mass did not exceed 3 wt. % of the total catalyst mass. Thicker coatings were comparatively prone to abrasion and cracks already after the initial cycles of thermal shocks.

*Percentage concentration of ceramic coating in the total weight of a catalyst was regarded as a measure of thickness.

The samples displayed a slight mass increment, which fell below 0.6 wt. %. The coating with the CeO_2 additive (20 wt. %) was only moderately better, showing a mass increment of 0.4% compared to the 1.2% increment in the sample with no ceramic layer.

3.1. Electron scanning of the surface

The ceramic layer 15–20 μm thick showed no cracks either before or after a thermal shock (Fig. 5). The micrographs of Fig. 6 display the cross-sections of the CeO_2-$Mn/SiO_2Al_2O_3$ coating. The micrograph 4446 reveals a tight contact between the coating and the substrate (uniform area on the right-hand side).

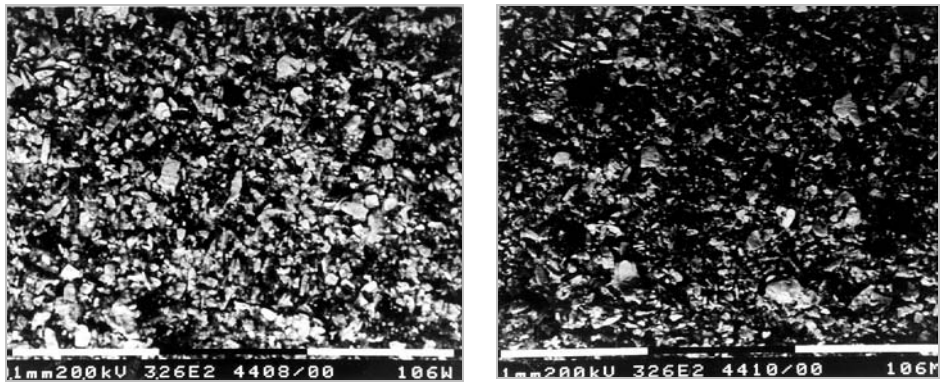

Fig. 5. SEM micrographs of the ceramic layers before (left) and after (right) thermal shocks

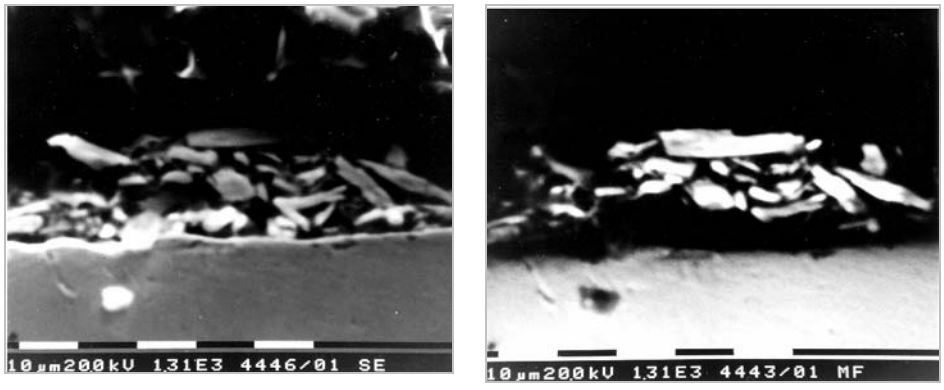

Fig. 6. SEM micrographs of the cross-sections of the CeO_2-$Mn/SiO_2Al_2O_3$ coating

The bright crystallites visible in the micrograph 4443 taken with the material contrast are active cerium oxides uniformly distributed in the top part of the layer. No segregation of Cr or Fe from substrate bulk to surface was evidenced, but – advantageously – it was Al that segregated (surface concentration rose from 14 to 24 wt. %), forming a protective layer on the metal surface and a bond with SiO_2/Al_2O_3 (coated by

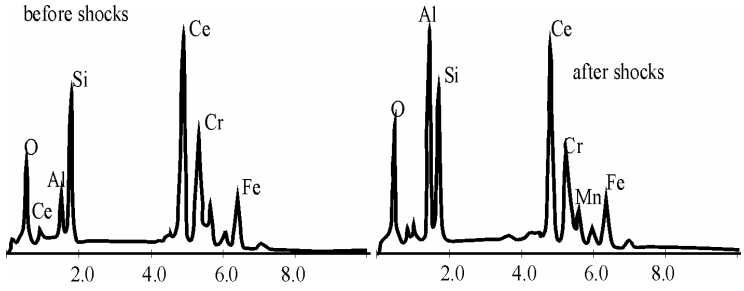

Composition	O	Al	Si	Ce	Cr	Mn	Fe
Before shocks	17.9	13.8	10.7	48.5	2.2	1.1	5.8
After shocks	23.3	24.1	9.3	36.1	1.7	0.9	4.6

Fig. 7. XRD spectrum of the CeMn/$SiO_2Al_2O_3$/FeCrAl catalyst surface. Composition (wt. %) of the catalyst surface before and after exposure to high temperature

the sol-gel method). These findings are all evidenced by the spectra (Fig. 7) from XRD analysis.

3.2. Verification of the catalytic protective layer

Making use of the DTA and DTG techniques, the catalytic activity of the coating in the diesel soot oxidation reaction was determined. Soot was spread onto the trap-catalyst directly from the exhaust pipe of an SW 400 ANDORIA diesel engine and was combusted in a temperature-programmed reactor. Two peaks (at 350 °C and 470 °C) corresponding to the maxima of the soot oxidation rate were distinguished (Fig. 8).

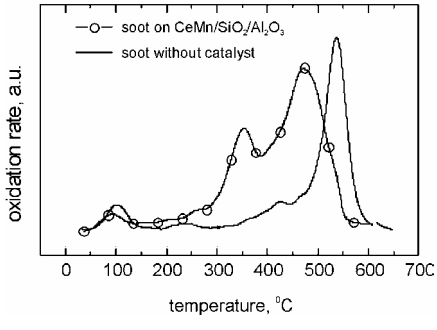

Fig. 8. Curves of oxidation rate for diesel soot spread on the CeMn/$SiO_2Al_2O_3$/FeCrAl catalyst and for diesel soot without any catalyst

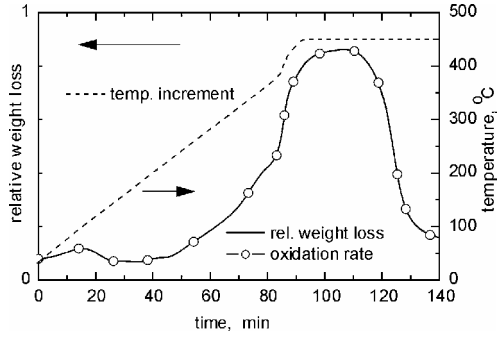

Fig. 9. Curves of oxidation and oxidation rate for diesel soot spread on the CeMn/$SiO_2Al_2O_3$/FeCrAl catalyst at a surface density of 6.5 g/m^2 in a temperature programmed reactor (increment 4 °/min up to 450 °C; flashed line)

This indicates that the soot combustion proceeded first in the tight contact mode and then in the loose contact mode [8]. It should be noted that real exhaust gas temperature to which the trap-catalyst will be exposed hardly ever surpasses 400 °C. To

provide a complete oxidation of the soot collected in the filter, it is necessary for the catalyst to act as an igniter so as to initiate the reaction at 350 °C. The heat released in the course of the reaction raises the temperature of the catalyst, thus enabling combustion of the remaining soot portion. With a programmed temperature increment of 4 degrees per minute up to 450 °C and a soot surface density of 6.5 g/m^2_{filter}, soot conversion amounted to 96% (Fig. 9).

4. Conclusions

Considering the promising results of the laboratory tests, prototypes of trap-catalysts (made of FeCrAl foams varying in pore size) were constructed and coated

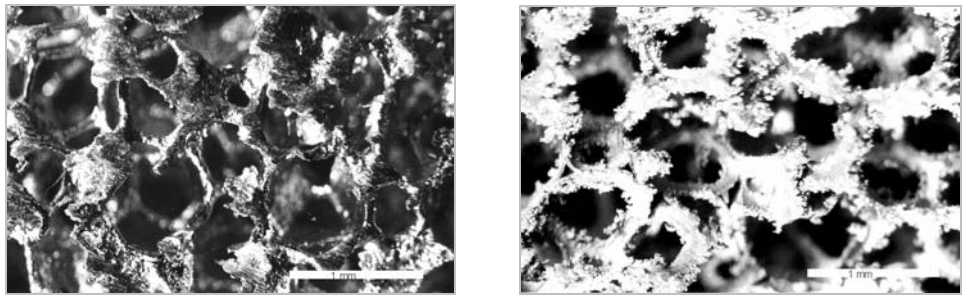

Fig. 10. FeCrAl foam support uncoated (left) and coated with $CeMn/SiO_2Al_2O_3$ layer (right)

with a catalytic protective layer, $Ce\text{-}Mn/SiO_2\text{-}Al_2O_3$ (Fig. 10). They are now tested on the buses of municipal transport.

Acknowledgement

The author is grateful to the State Commitee for Scientific Research for financial support through the grant no. 4T09B 049 22

References

[1] TYLUS W., Wiad. Chem, 53 (1999), 11.
[2] ZELENKA P., CARTELLIERI W., HERZOG P., Appl. Catal. B: Environ., 10 (1996), 3.
[3] FERRAUTO R., VOSS K., Appl. Catal. B: Environ., 10 (1996), 29.
[4] SUTO H., MIKAMI T., HIRAI H., HORI M., SAE Paper 910334 (1991).
[5] HOFFMAN U., RIECKMAN T., Chem. Eng. Technol., 17 (1994), 149.
[6] TYLUS W., KUCHARCZYK B. GODOWSKI P., Inż. Mat., 102 (1998), 28.
[7] KANESAKI N., SEKIJA Y., SHINZAWA M., AOJAMA S., JSAE Rev., 14 (1993), 49.
[8] NEEFT J.P.A., *Catalytic oxidation of soot*, Proefschrift Technische Universiteit Delft, 4, 1995.

Received 10 July 2003
Revised 30 September 2003

Materials Science, *Vol. 21*, *No. 4*, *2003*

The effect of sequence of sol-gel multilayer coatings deposition on corrosion behaviour of stainless steel 316L

JACEK GRZEGORZ CHĘCMANOWSKI, JÓZEF GŁUSZEK, JAN MASALSKI*

Institute of Inorganic Technology and Mineral Fertilizers, Wrocław University of Technology, Wybrzeże Wyspiańskiego 27, 50-370 Wrocław

The possibility of producing protective coatings by the sol-gel process is discussed. Metaloorganic complexes open new possibilities for the syntheses of ceramic materials. The most important applications of Si alkoxides for the synthesis of inorganic-inorganic composites are presented. The SiO_2 protective coatings on surgical stainless steel 316L have been synthesized by the sol-gel techniques. The multi-layer coatings were deposited by the dip method using sols containing appropriate molar ratios of the precursor (tetraethoxysilan), anhydrous ethanol, nitric acid and acetic acid. Nanosilica with the surfactant didodecyldimethyl-ammonium bromide were added to the sols applied. Coatings were annealed from 200 °C to 300 °C. The electrochemical characterization by dc measurements of the protective coatings in Ringer's solutions is reported. The coatings performance has been compared using polarization characteristics. Two arbitrarily chosen values were taken: the current density at –750 mV and the potential corresponding to the current density of 2 $\mu A/cm^2$. The coatings were chosen and ranked with regard to additional parameters: the polarization resistance and the through-coating porosity. It has been established that the way of applying of the coatings had an influence on the protective properties. The best protective properties have the coatings obtained from sols consisting of three SiO_2 layers with nanosilica and three SiO_2 layers without nanosilica. The positive effect of nanosilica on the protective properties of the coatings was determinated. Small changes in the preparation process can often have disproportionate large effects on the quality of the coatings.

Key words: *sol-gel; nanosilica; potentiodynamic curves; surfactant; wet corrosion*

1. Introduction

Surface engineering techniques enable us to improve properties of metallic materials, raise their corrosion resistance, as well as reduce their 'wear and tear'. One of these techniques is the sol-gel process, which enables the synthesis of new ceramic materials. Coatings from sols can be obtained by dipping, spinning or spraying [1].

*Corresponding author, e-mail: masalski@novell.itn.pwr.wroc.pl.

Surface layers may be single- or multicomponent systems [2–5]. A major advantage of this method is that at no stage of the synthesis of ceramic material high temperatures are needed [6, 7]. The drawbacks inherent to the sol-gel method are shrinkage and porosity. The porosity of the coating can be reduced either by appropriate thermal treatment [6] or by increase of their thickness. However, inorganic coatings of the thicknesses smaller than 0.3–1.0 μm [8] are prone to cracks during drying or thermal treatment [9]. Higher thicknesses are obtained by decreasing the hydrolytic ratio R_h [10] or by reducing the temperature of the thermal treatment [11].

Inorganic-inorganic composite coatings (where one of the components is an inorganic polymer obtained from the sol (the matrix), and the other inorganic component is a powder added to the sol) display lower porosity and shrinkage during drying and thermal treatment processes. In this way, so-called nanocomposites are obtained, i.e. composites of grain sizes (particle sizes) below 100 nm [12]. Experiments with stainless steel 316L [13, 14] using nanosilica and surfactants have revealed that the protective properties of the coatings obtained from modified sols are better than those prepared with sols containing no ceramic powders.

2. Experimental

The substrate investigated was stainless steel of the type 316L (surgical steel) of the chemical composition shown in Table 1. The steel samples were in the form of disks 14.8 mm in diameter and 1 mm thick. Prior to the deposition of the coatings, the surface of the steel was ground successively with abrasive papers of the grain-size distribution of 400, 600 and 800. The samples were then washed with distilled water, dried and degreased in a two-stage procedure using an ultrasonic bath (for 45 min in tetrachloroethylene (C_2Cl_4) and 15 min in anhydrous ethyl alcohol (C_2H_5OH)). The coatings were deposited on the steel samples.

Table 1. Chemical composition of stainless steel 316L (wt. %)

C	Cr	Ni	Mo	Mn	Si	Cu	V	S	P
0.03	17.28	14.80	2.8	1.96	0.19	0.07	0.035	0.03	0.024

For the preparation of the SiO_2 coatings, tetraethoxysilane ($Si(OC_2H_5)_4$; TEOS) was used. TEOS was diluted with anhydrous ethyl alcohol and homogenized in an ultrasonic bath for 75 min. Then, the remaining components were added to the solution and homogenization was carried out for 85 min. The starting sols (referred to as A and B, Table 2) obtained in this way were applied to the preparation of the sols used for the deposition of the coatings. A certain amount of nanosilica in the presence of an appropriate surfactant was added to the sol B, and the mixture was then stirred in an ultrasonic bath for 60 min at a constant temperature (T = 20 °C). The surfactant, DoDAB (didodecyldimethylammonium bromide, $(C_{12}H_{25})_2N(CH_3)_2Br$)) was used to reduce agglomeration of nanosilica with the particle size from 5 to 32 nm. Table 3 shows the composition of the sol K, which was used for preparation of the coatings.

Table 2. Chemical composition of the sols A and B

Sol	Composition			
	TEOS [g]	C_2H_5OH [g]	HNO_3 [g]	CH_3COOH [g]
A	18.660 (20 ml)	15.800 (20 ml)	–	4.202 (4 ml)
B	26.050	43.043	0.0062	0.0068

Table 3. Chemical composition of the sol K

Sol	Composition			
	Sol B [ml]	Sol A [ml]	Nanosilica [g]	DoDAB [g]
K	15.0	–	0.0065	0.0105

The coatings were deposited on the substrate by dip-coating. The samples were dipped in the sol for 2 min in order to establish equilibrium at the substrate–solution phase boundary. The dipping and withdrawing of samples was performed at a constant rate of 1.0 mm/s. The samples were subsequently dried in the cool air for 24 h, and fired in an electrical furnace which was heated to the ultimate temperature at a rate of 2.0 °C/min. The samples were sintered for 60 min. In this way, six-layer coatings were obtained. The coatings have been assigned the following symbols: capital letter K followed by a number (from 0 to 7). The compositions of particular layers of the coatings and the sintering temperatures are shown in Table 4.

Table 4. Preparation of the coatings

Layer	Sample								Sintering [°C]
	K0	K1	K2	K3	K4	K5	K6	K7	
1	A	B	K	K	B	A	A	K	300
2	A	B	B	A	K	K	K	A	280
3	A	B	K	K	A	B	A	K	260
4	A	B	A	B	K	K	K	A	240
5	A	B	K	K	B	A	A	K	220
6	A	B	B	A	K	K	K	A	200

The dc measurements designed for the assessment of corrosion resistance involved recordings of polarization curves in a conventional three-electrode system. The measuring set (fully automatic) consisted of a measuring vessel, an SI 1286 potentiostate and a computer. Prior to the measurements, the samples were soaked in the Ringer solution (NaCl, 8.60 g/dm^3; KCl, 0.30 g/dm^3; $CaCl_2$, 0.48 g/dm^3) for 10 min and then polarized in the same solution in the anodic direction at the rate of 1 mV/s, starting with the potential of –1000 mV (the electrochemical potential is related to the saturated calomel electrode (SCE) in all cases presented).

3. Results and discussion

Figure 1 shows the values of the corrosion potential (E') measured after 10-min exposures of the samples of stainless steel 316L (both coated and uncoated) to the Ringer solution. The appropriate thermal treatment, as well as addition of nanosilica as a filling material, accounts for the 'refining' of the surface. The comparison of the measured E' values suggests that the sequence of film deposition and thermal treatment could decrease the number of cracks in the coatings. It is well known that reducing the ratio of cathode area to anode area results in a decrease of the corrosion potential [15]. From the results reported in our previous papers [16,17] it can be inferred that when the number of layers in coating increases so does the E' potential.

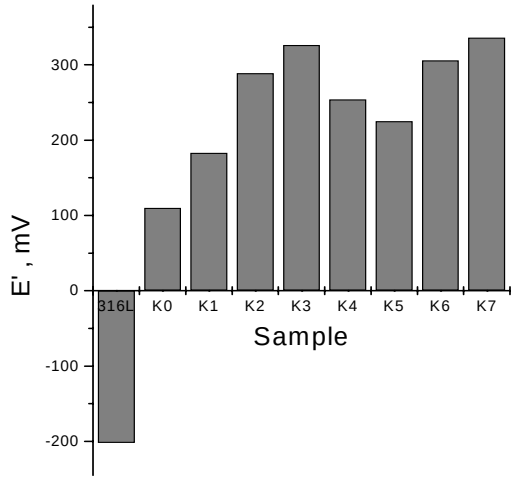

Fig. 1. Corrosion potential values E' for coated and uncoated stainless steel 316L measured after 10 min exposure to the Ringer's solution

Figure 2 presents the polarization curves of stainless steel 316L with the coatings deposited from the sols. The values of the cathode and anode current densities are much lower for the coated samples as compared to the uncoated stainless steel 316L samples. Low anode current values up to the potential slightly exceeding 1000 mV were determined for the sample K5.

The polarization curves for the bare and coated steel samples are plotted in Figs. 3–5. As shown in the figures, the coatings with their first layers obtained from the sols with no nanosilica additives display lower cathode current densities than those prepared from the sols with nanosilica additions (Figs. 3 and 4). The value of the pitting potential ($E_{2\mu A/cm^2}$), however, is influenced by the last (6th) deposited layer. Thus, when this layer is deposited from the sol with the silica additive, the pitting potential reaches higher values than when it is deposited from the sol with no additive (Figs. 3 and 4).

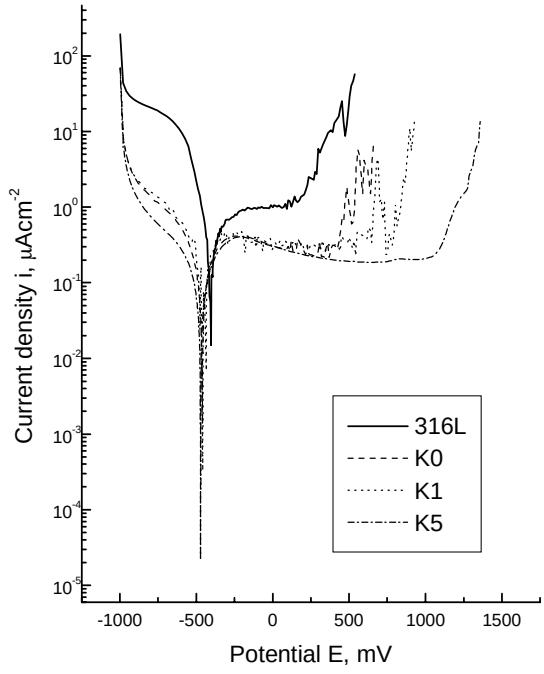

Fig. 2. Polarization curves for sol-gel coated stainless steel 316L

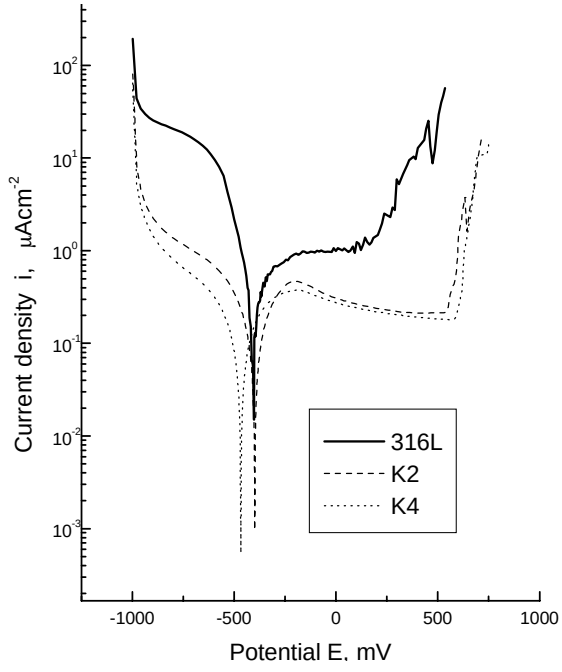

Fig. 3. Polarization curves for sol-gel coated stainless steel 316L

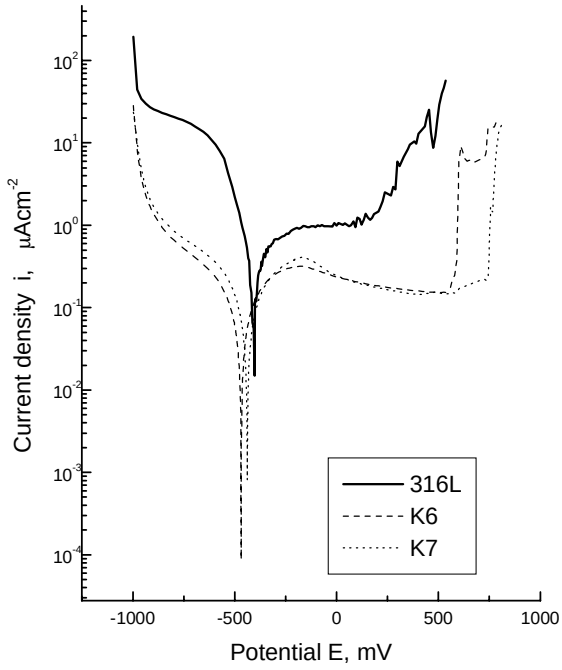

Fig. 4. Polarization curves for sol-gel coated stainless steel 316L

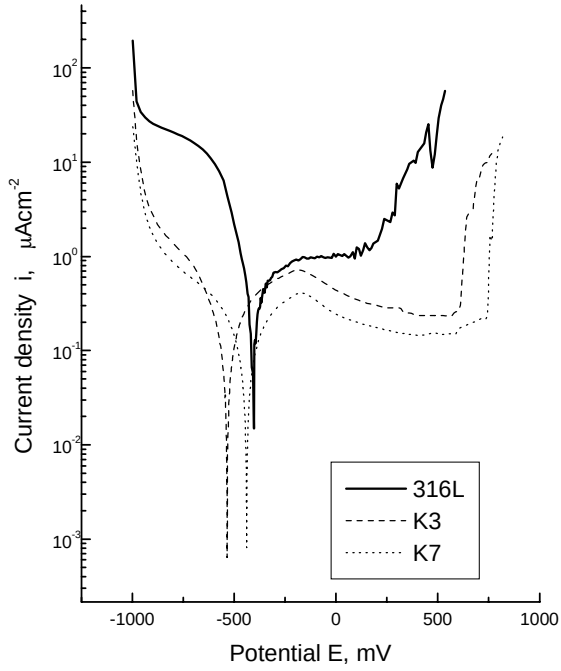

Fig. 5. Polarization curves for sol-gel coated stainless steel 316L

The fourth layer of the coating, which is not the external one and has no direct contact with the solution, exerts an influence on the cathodic-to-anodic transition potential (E_{C-A}). There is also a distinct change in the values of the anode currents and corrosion pit nucleation potentials (Fig. 5). A similar pattern can be observed for the coated samples K2 and K3 where the sequence of the layers deposition from the sol A and the sol B has been changed. Figure 2 reveals a distinct change in the values of the E_{C-A} transition and the anode currents.

To assess the behaviour of the coatings, two quantities have been chosen from the polarization curves, i.e. the current density obtained from the cathodic curves recorded at – 750 mV (the porosity measure) and the potential obtained from the anodic region corresponding to the current density of 2 μA/cm^2. The explanation supporting this choice of parameters can be found in our previous paper [18]. The potential chosen can be considered as the pitting potential. Figure 6 presents (in the current-potential co-ordinates) the parameters i_{-750mV} and $E_{2\mu A/cm^2}$ which correspond to each of the polarization curves. Thus, the best and the worst protective properties are supposed to be those of the coating in the top left-hand corner and bottom right-hand corner of the figure, respectively. Figure 6 introduces the electrochemical parameters which are needed for assessment of the anticorrosive properties of the coatings. Analysis of these data demonstrated that, although each of the samples displays protective properties, those of K5 are the most advantageous.

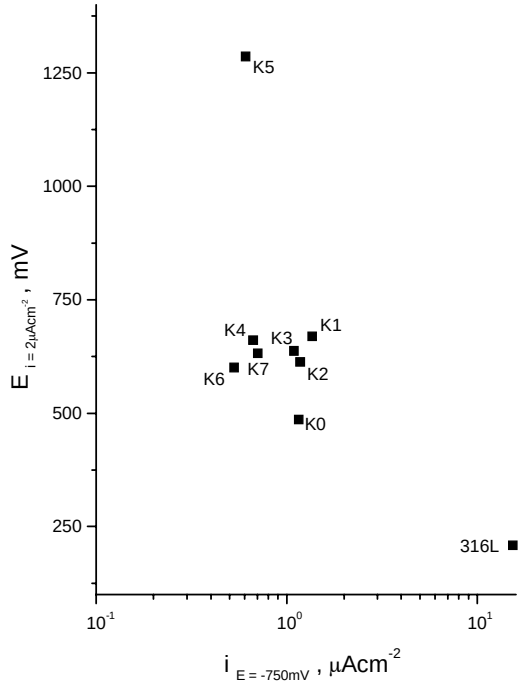

Fig. 6. Electrochemical parameters used for estimation of the protective properties of the coatings

Another parameter useful for the quality assessment of coatings is the polarization resistance R_p. To determine its value, we have used the data chosen from the proximity of the cathodic-to-anodic transition potential. In the linear system (E–i) one obtains a straight line with a slope yielding directly the polarization resistance. The R_p values were determined using the linear regression method and are plotted in Fig. 7.

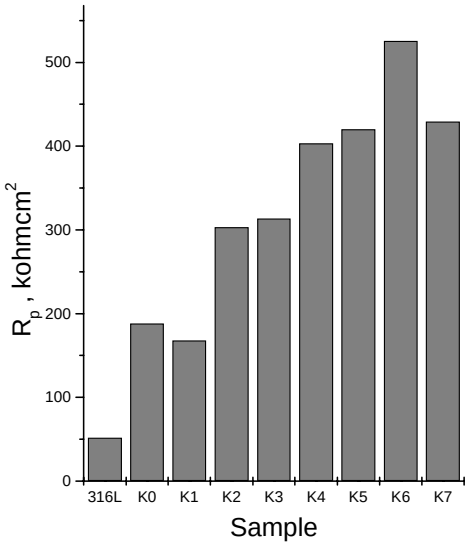

Fig. 7. Comparison of polarization resistances R_p for coated and uncoated stainless steel 316L

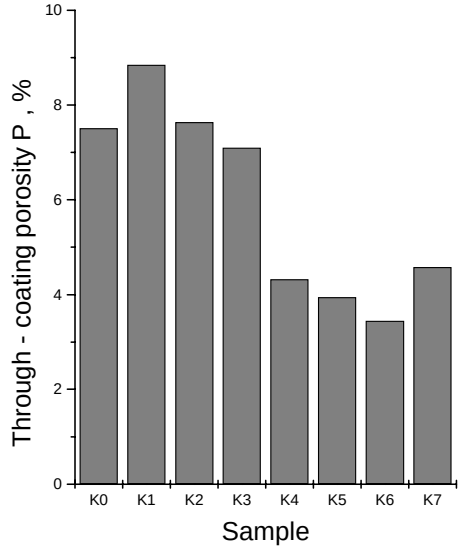

Fig. 8. Comparison of the through-coating porosity for coated stainless steel 316L

From these plots it can be seen that a change in the method of deposition is connected with a change in the values of polarization resistance of the samples of coated stainless steel 316L. This is particularly evident when comparing K2 with K3, K2 with K4, K3 with K7 and K6 with K7. It can be concluded that each sample of stainless steel 316L with the coating displays protective properties. However, the best ones are those of the K6 sample.

Figure 8 depicts the through-coating porosity P, defined as the ratio of the cathode current density of the coated samples i to the current density of the uncoated substrate i' at the potential of –750 mV.

$$P = \frac{i}{i'} \cdot 100\%$$

There is a correlation between the polarization resistance R_p and the through-coating porosity P. Thus, the sample K6 (which has the highest R_p value), shows the lowest P value, while the sample K2 exhibits the highest P value at the lowest polarization resistance. The complex nature of the system causes, however, that no general criteria seem to apply to the assessment of the protective properties when the coatings are prepared by the sol-gel method. It should be also stressed that the corrosion resistance is strongly influenced not only by through-coating porosity but also by the character of the coating–substrate interface [19].

4. Conclusions

Addition of nanosilica and the cation surfactant DoDAB has a favourable effect on the protective properties of the sol-gel coatings on stainless steel substrates of the type 316L. It is also the sequence of deposition at the layers that contributes to the protective properties of the coatings obtained.

References

[1] BRINKER C.J., SCHERER G.W., *Sol-Gel Science. The Physics and Chemistry of Sol-Gel Processing*, Academic Press, San Diego, 1990.
[2] GŁUSZEK J., *Tlenkowe powłoki ochronne otrzymywane metodą sol-gel* (*The protective oxide coatings prepared by the sol-gel metod*, in Polish), Ofic. Wyd. Politechniki Wrocławskiej, 1998.
[3] GŁUSZEK J., ZABRZESKI J., Inżynieria Powierzchni, 3 (1996), 16.
[4] GUGLIELMI M., J. Sol–Gel Sci. Techn., 8 (1997), 443.
[5] ATIK M., DE LIMA P., AVACA L.A., AEGERTER M.A., ZARZYCKI J., J. Mater. Sci. Letters, 13 (1994), 1081.
[6] ULRICH D.R., J. Non-Cryst. Solids, 100 (1988), 174.
[7] HENCH L.L., ULRICH D.R., *Ultrastructure Processing of Ceramics, Glasses and Composites*, Wiley, New York, 1984.
[8] STRAWBRIDGE I., JAMES P.F., J. Non-Cryst. Solids, 82 (1986), 366.

[9] ZARZYCKI J., [in:] L.L. Hench and D.R. Urlich (Eds.), *Ultrastructure Processing of Ceramics, Glasses and Composites*, Wiley, New York, 1987, p. 27.
[10] GARINO T.J., Mater. Res. Soc. Symp. Proc., 180 (1990), 497.
[11] GALLARDO J., GALLIANO P., DURAN A., J. Sol-Gel Sci. Techn., 19 (2000), 393.
[12] JURCZYK M., *Nanomatriały* (*Nanomaterials*, in Polish), Wyd. Politechniki Poznańskiej, 2001.
[13] CHĘCMANOWSKI J.G., GŁUSZEK J., MASALSKI J., KRYSZTAFKIEWICZ A., Inż. Mat., 5 (2002), 359.
[14] CHĘCMANOWSKI J.G., GŁUSZEK J., MASALSKI J., JESIONOWSKI T., Ochrona przed Korozją, 11A (2002), 214.
[15] WEST J.M., *Basic Corrosion and Oxidation*, Wiley, New York, 1986.
[16] MASALSKI J., CHĘCMANOWSKI J.G., SOBAŃSKA D., Raport SPR 13/2001 ITNiNM Politech. Wrocł. 2001.
[17] CHĘCMANOWSKI J.G., GŁUSZEK J., MASALSKI J., Proc. 7th Polish Symp. Sci.-Tech. 83, Poraj 2001.
[18] GŁUSZEK J., MASALSKI J., KUCHARCZYK B., GOLUBSKI Z., Inż. Mat., 5 (2002), 355.
[19] PENTTINEN I.M., KORHONEN A.S., HARJU E., TURKIA M.A., FORSEN O., RISTOLAINEN E.O., Surf. Coat. Tech., 2 (1992), 161.

Received 18 July 2003
Revised 30 September 2003

Materials Science, *Vol. 21*, *No. 4*, *2003*

Behaviour of glucose oxidase during formation and ageing of silica gel studied by fluorescence spectroscopy

MAŁGORZATA PRZYBYT*

Institute of General Food Chemistry, Department of Biochemistry and Food Science,
Technical University of Łódź, 90-924 Łódź, ul. Wólczańska 171/173, Poland

Glucose oxidase was entrapped in silica gels obtained by the sol-gel process with the retention of a part of its activity. The stability of the enzyme molecule during the sol-gel transition and ageing of the wet gel was followed by the measurement of fluorescence of tryptophan and flavin adeninedinucleotide (FAD). The results indicate unfolding and denaturation of the enzyme protein caused by the changes of microenvironment inside gel, presence of ethanol, decomposition of FAD and photosensitised oxidation of tryptophan by FAD. Among the products of FAD decomposition, alloxazine derivatives were identified through their specific fluorescence characteristics. The results of the observation of the fluorescence variation and activity assay of the gel are in good agreement. The experiments with the dried gel indicate that illumination is not necessary to sensitise the reaction of oxidation of tryptophane by FAD although in the presence of light the effectiveness of this process is higher. Presumably the decomposition of FAD and tryptophan is not only induced by light but also by the paramagnetic (with free radical character) defects in the gel matrix. This reaction is enhanced by the presence of glucose and depends also on pH of the buffer used in the gel preparation. The products of the enzyme degradation are easily washed out from the gel. Leaching of active enzyme from the gel was also observed.

Key words: *sol-gel; glucose oxidase; fluorescence; flavin adeninedinucleotide; enzyme stability*

1. Introduction

Biosensors for assay of glucose with immobilised glucose oxidase are the most commonly developed and studied ones because of their biomedical, industrial and clinical applications. Since Clark and Lyons [1] have introduced the first concept of glucose sensing electrode, a tremendous variety of different types of biosensors were described [2]. Practically, all types of electrochemical, optical, thermal and other

* E-mail: mprzybyt@snack.p.lodz.pl.

sensors were used to construct glucose biosensors. All methods of enzyme immobilisation were also tested with glucose oxidase. The first glucose analyser was successfully introduced to the market in 1979 [2]. The replacement of a natural redox mediator – oxygen – by synthetic ones [3] allowed introducing in 1987 the first individual glucometer [2] for every-day control of blood glucose by diabetic patients. In last two decades, a substantial progress was made in construction of implantable biosensors for continuous glucose measuring [4]. In the case of *in vivo* application of the glucose biosensors, the immobilisation matrix must be non-toxic, biocompatible and stable. It must also give no immunological response, allow a free diffusion of oxygen and glucose and stabilise the activity of the immobilised enzyme. From that point of view, the silica gel obtained by the sol-gel technique has interesting properties as the immobilisation matrix because of the simplicity of preparation, tunable porosity, chemical inertness, optical transparency and mechanical stability. It shows also no toxicity and is biocompatible.

In 1990, Braun at al. [5] reported for the first time a successful immobilisation of enzymes in silica gel obtained from organic silica precursors via the sol-gel method. Since then the sol-gel technique has been widely used in construction of different types of biosensors and reviewed few times [6–9]. Glucose oxidase can be immobilised in pure silica gel or in composite materials with organic groups introduced into silica network (ORMOSIL) or mixtures of gel and other materials like graphite, colloidal gold, organic polymers and others [6–9]. Materials obtained by the sol-gel technique were mostly applied in electrochemical biosensors – amperometric with oxygen detection [10] or hydrogen peroxide detection [11–19] and with synthetic redox mediators [20–24]. Other types of biosensors with glucose oxidase immobilised in silica gel are optical biosensors with pH-dependent fluorophores [25], fluorophores quenched by oxygen [26, 27], based on optical properties of glucose oxidase prosthetic group (flavin adeninedinucleotide – FAD) [28, 29]; thermal [30]; chemiluminescent [31] and electrochemiluminescent [32].

The glucose oxidase is a very stable enzyme while it is a glycoprotein [2, 33] and many biosensors with this enzyme show a great operational and storage stability deciding about their practical use. Unfortunately, many biosensors with glucose oxidase immobilised in silica gel show rather poor stability [12, 14–16, 24, 32]. Partially the instability of the sensor is ascribed to leaching of the enzyme from the gel [14, 15, 25, 30] or to changes of electrochemical mediator (ferrocene) properties [24]. To avoid the leaching of the enzyme it is sometimes cross-linked inside the gel [15] or covalently bound to the gel lattice [16, 23] but such an approach does not improve very significantly the properties of the biosensor. It is also very characteristic that the retention of the glucose oxidase activity after entrapment in silica gel is very low [26]. Such results indicate that the entrapment of glucose oxidase in silica gel changes the properties of the enzyme, especially its stability.

Generally, the properties of the enzyme molecule inside the gel are changed due to the change in its conformation leading sometimes to a denaturation of protein, restriction of molecule motion and lower accessibility of the entrapped enzyme by the

substrate [6]. As the result, the enzyme immobilised in silica gel has properties different from the native one. Typically the activity of the entrapped enzyme is lower. In general, enzymes immobilised in silica gel follow the Michaelis–Menten kinetics but the Michaelis K_M constants are greater and the catalytic constants k_{cat} lower as compared with the native ones. The stability of the enzyme in the silica gel can either be decreased or increased depending on the nature of protein and composition of the gel [6]. The changes of protein conformation and dynamic motion inside the gel are caused by interactions of the molecule with silica surface inside the pores and different microenvironment. The porosity of the gel and the interactions of the enzyme substrate with the gel surface change the diffusion conditions causing the lower accessibility of the active centre and thus leading to different kinetic properties [6]. Although glucose oxidase is often sequestered in silica gel in biosensor construction, there are only few papers on the properties of this enzyme inside the gel [29, 34, 35]. Practically none of them reports on the changes of the enzyme state during a dynamic sol-gel transition and ageing of the gel.

The research area of our group is the immobilisation of enzymes in silica gel in construction of biosensors. The results for the glucose oxidase immobilised in silica hydrogel on the tip of oxygen electrode indicate a very low stability of the enzyme in the gel partially caused by leaching [36]. The goal of our work is to construct the optode for glucose with glucose oxidase and fluorophore quenched by oxygen entrapped in silica gel. Thus there is a need to study the behaviour of glucose oxidase during the sol-gel process, ageing of hydrogel and drying of gel. A very useful method to examine the state of glucose oxidase molecule inside the gel is the measurement of the fluorescence. In glucose oxidase molecule, there are two fluorophores with different spectral properties: tryptophan in apoenzyme (protein) [35, 37, 38] and prosthetic group – FAD [29, 38] which can be observed independently.

The paper presents the results of fluorimetric investigations of glucose oxidase physically entrapped in silica gel obtained by the sol-gel method from tetraethoxysilane during the sol-gel transition, ageing of hydrogel and in a dried gel.

2. Experimental

2.1. Reagents

As a gel precursor, tetraethoxysilane (TEOS) (99%, Aldrich Chemie GmBh, Germany) was used. Glucose oxidase (GOD) from *Aspergillus niger* of activity 30 U/mg was purchased from Serva. GOD was dissolved in water (500 mg in 10 ml). Anhydrous glucose (analytical grade) was obtained from POCh (Gliwice, Poland). All other reagents were of analytical grade. Twice distilled water was used throughout.

At pH 5 an acetate buffer was used, at 7 and 9 – the phosphate ones. The buffers were adjusted to desired pH with a concentrated solution of NaOH.

2.2. Apparatus

Fluorescence measurements were done using Fluoromax-2 spectrofluorometer (Jobin Yvon-Spex Instruments S.A., Edison, New Jersey, USA). The fluorescence spectra were measured with 10 mm pathlength closed quartz cells during ageing experiments or with polymethacrylane ones during drying. The excitation and emission slits were set at 2 nm each. The increment was set at 1 nm and integration time at 2 s. The measurements were done at ambient room temperature.

Between measurements the hydrogels were kept at 20 ºC in a homemade air-circulated thermostat.

Oxygen concentration measurements were done using a galvanic silver–zinc oxygen electrode CTN-920.S (MES-EKO, Wrocław, Poland) connected with a microcomputer pH/oxygen meter CPO-551 (Elmetron, Zabrze, Poland). The results of measurements were expressed as the percentage of oxygen concentration in a solution saturated from air at 25 ºC. The constant stirring rate of the solutions was maintained by magnetic stirrer BMM 21 (DHN Wigo, Piastów, Poland). The temperature was maintained with a thermostat U1 (MLW, Medingen, Germany).

pH of the buffers was measured with combined glass electrode connected with a microcomputer pH/oxygen meter CPO-551.

2.3. Preparation of gels

The stock solution of the sol was prepared as follows: 4.5 ml of TEOS, 1.4 ml of water and 0.1 ml of 0.1 M HCl giving the molar ratio TEOS : H_2O: HCl equal to 1 : 4 : 10^{-5} were stirred vigorously at room temperature until transparent homogeneous solution was obtained (3 h). The sol was then cooled in a refrigerator (4 ºC) for about 30 mins.

Table 1. Composition of gels studied and the gelling times

Buffer	pH (estimation)	Gelling time [min][a]
Water	3	~15
Acetate	5	~9
Phosphate	7	~3.3
Phosphate	9	~1.2

[a]Gelling time is the time span from mixing all components until the bulk gel is formed.

The samples were prepared as follows: 1.5 ml of the stock sol was mixed with 0.5 ml of GOD solution and 1 ml of water or 0.03 M buffers (Table 1). In the case of water, pH of the mixture was 3.3, and with the acetate buffer pH = 5.4 was obtained. For phosphate buffers, pH of the mixtures could not be measured due to a short gel-

ling time. Thus, in all the cases when pH of the gel is mentioned, the reported value is the one of the buffer. Two samples of the gel were prepared, and to the second one 54 mg of glucose was added to obtain the final concentration 0.1 M. At such a concentration of glucose, the whole FAD in the GOD molecule occurs in a reduced form, while in samples without glucose added, the oxidised form of FAD is present.

2.4. Measurement procedure

Three different sets of experiments were done:

A. Because at given compositions of initial mixture of sol and enzyme solution the gelling times were short (Table 1), it was impossible to record the fluorescence spectra of tryptophan and FAD during the sol-gel transition; only kinetic measurements were done. The tryptophan fluorescence was excited at 295 nm and measured at 340 nm. The fluorescence of FAD was excited at 370, 396, 438, 450, 467 and 490 nm and measured at 520 nm. In this case, the integration time was 0.5 s. The mixtures were prepared in polymethacrylate cuvettes closed with parafilm. Immediately after preparation, the sample was placed in the spectrofluorimeter and the spectra were recorded for 2 h. After the measurement, the samples were taken out, some pinholes were made in the parafilm and the sample was left to dry at ambient room temperature for 22 days. Then the cuvettes were opened and left to dry for another day. During drying, the samples were placed on a shelf in the laboratory, not being protected from the light. The dimensions of the gel monoliths obtained were measured with the accuracy of 0.1 mm. Then the fluorescence spectra of FAD and tryptophan were recorded and the monoliths were subjected to 3 ml of 0.02 M acetate buffer, pH 5, and left for 2 days in a refrigerator. After that time the buffer was checked fluorimetrically for the presence of tryptophan and FAD.

B. The samples were prepared in closed quartz cuvettes and fluorescence spectra were measured about 0.5 h after a rigid gel was obtained. The measurements were repeated every day in the first week, then more rarely. The whole course of measurements lasted 4 weeks. Only for samples of pH 5, the time regime of measurement was a little different.

C. The samples were prepared as in (A). 1 hour after gelation, the fluorescence spectra were taken. Then the gels were left to dry in the same manner as in (A) but in darkness. The monoliths obtained were measured as in (A). Then they were weighted and powdered in a mortar. 0.3 g of the powder was immersed in 3 ml of 0.02 M phosphate buffer, pH 7, and left overnight in a refrigerator. Next day the samples were filtered and the supernatants were checked fluorimetrically for the presence of FAD and tryptophan and then for the activity of GOD.

2.5. Assay of GOD activity

100 ml of 0.1 M glucose solution in 0.02 M phosphate buffer, pH 6, saturated with oxygen from air was poured into the thermostated vessel. The oxygen electrode was

dipped in the solution and the vessel was closed. The measurements of oxygen were done at 25 ºC at a constant stirring rate of 500 rpm. When the signal of electrode became constant, the sample checked for GOD activity was added, and the oxygen concentration was recorded for 5 min. In the case of native GOD, 10 or 5 μl of the enzyme solution was added, in the case of supernatants (C) – 0.5 ml. For the assay of the GOD activity, 50 mg of the powdered gel was added. Each assay was triplicated.

From the recorded dependencies of oxygen concentration on time, the slope of the initial straight line equal to the initial rate of oxygen consumption was calculated and taken as the GOD activity. The results were corrected for actual atmospheric pressure.

3. Results and discussion

3.1. Fluorescence properties of glucose oxidase in solutions

The glucose oxidase molecule is a homodimer with two FAD molecules as prosthetic group. Each FAD residue is buried in a deep pocket formed in the protein subunit [33]. This pocket is a β-D-glucose binding domain. FAD is not covalently bound with the apoenzyme. Glucose oxidase is the catalyst of the reaction of oxidation of glucose with the use of oxygen dissolved in water. The mechanism of glucose oxidation is well established [2]: it consists of two half-reactions in which FAD is reduced and oxidised. Previously FAD in glucose oxidase was reported as non-fluorescent in both forms [39] but now it is well established that it shows fluorescence [29, 38, 40]. The fluorescence of reduced $FADH_2$ (in the presence of glucose) is reported to be higher than that of the oxidised form both in solution and when it is immobilised in an organic gel [29, 40] but lower when GOD is entrapped in silica gel [29]. The changes of FAD fluorescence caused by glucose were used as a basis for optical biosensors [29, 40].

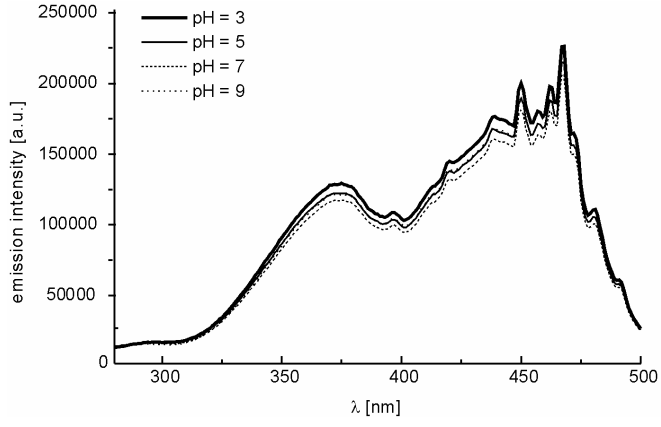

Fig. 1. Excitation spectra of FAD in oxidised glucose oxidase at different pH. The emission was collected at 520 nm

Figure 1 shows the excitation spectra of oxidised FAD in glucose oxidase at different pH values in solution. The intensity of emission is practically independent of pH; only at pH 3 it is a little higher. For free FAD, the emission intensity is decreasing with the pH increase. The excitation spectrum of FAD consists of two bands: one with the maximum at about 450 nm and vibronic structure corresponding to the HOMO-LUMO singlet $\pi \rightarrow \pi^*$ transition and the second with the maximum at about 370 nm corresponding also to singlet $\pi \rightarrow \pi^*$ transition but some results suggest mixing with an $n \rightarrow \pi^*$ transition [41]. In the presence of 0.1 M glucose, the fluorescence intensity of FAD increases slightly at pH 3 but at higher values of pH it decreases, especially in alkaline solutions (pH 9).

Because of the existence of two excitation bands, the emission spectra were excited at 370 nm and at 450 nm, and recorded between 460 nm and 600 nm. The wavelength of the maximum is practically independent of pH, red-ox state of GOD and excitation wavelength (Table 2). Only at pH 9, the maximum of the reduced form is shifted by 5 nm to higher values when excited at 450 nm (Fig. 2).

Table 2. Characteristics of FAD fluorescence in glucose oxidase

pH	Form	Ratio of emission intensity at 450 and 370 nm I_{450}/I_{370}	Maximum of the lower excitation band [nm]	Maximum of emission [nm]	
				λ_{exc} = 370 nm	λ_{exc} = 450 nm
3	ox	1.778	375	524	524
	red	1.841	373	524	525
5[a]		1.666	375	524	523
5	ox	1.789	372	525	526
	red	1.789	376	525	524
5[b]	ox	1.670	370	522	519
	red	1.583	371	518	520
7	ox	1.786	372	527	526
	red	1.594	375	524	522
9	ox	1.796	372	525	524
	red	1.501	372	522	530

[a]Free FAD (oxidised).
[b]In the presence of ethanol (6.74 M).

During the hydrolysis of TEOS and formation of gel, ethanol is produced. Assuming a complete hydrolysis 4 moles of ethanol would be produced from 1 mole of TEOS yielding the concentration in the final gel equal to 6.74 M. The presence of ethanol could influence the conformation of glucose oxidase molecule and change the fluorescence properties of FAD and tryptophan. Because of that, the spectra were recorded at pH 5 and at ethanol concentration equal to 6.74 M when the precipitation of glucose oxidase did not occur. Because of that, the silica gel with entrapped GOD

cannot be produced in the process in which ethanol is present in the initial mixture at a high concentration allowing the slow gelation, with gelling time measured in days [42]. The presence of ethanol caused the change of FAD fluorescence properties – increase of the emission intensity and blue shift of the maximum (Table 2).

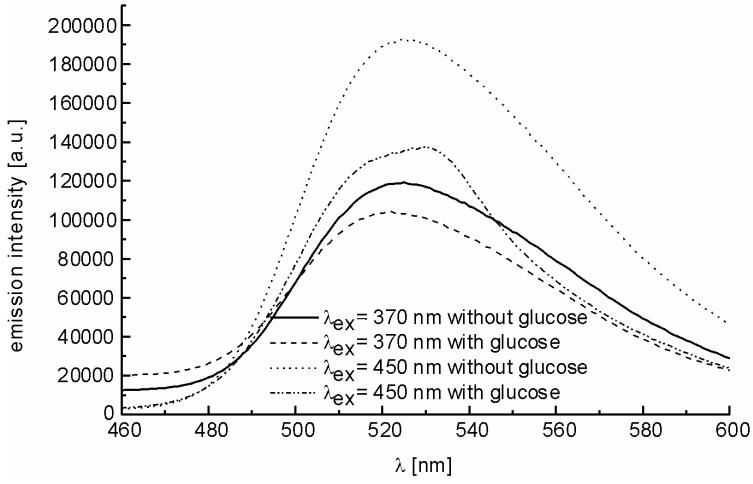

Fig. 2. Emission spectra of FAD in glucose oxidase at pH 9

The spectral parameters of tryptophan fluorescence are dependent on the dynamic and electronic properties of its environment. Thus the measurement of steady-state fluorescence of tryptophan can be used to obtain informations about the conformation of protein molecule, its dynamics and folding. There are 10 tryptophan residues in each monomer of GOD and 4 of them are located in the FAD binding domain [33]. The fluorescence of tryptophan in GOD molecule depends on the red-ox state of FAD prosthetic group and these changes can be interpreted as due to the Förster energy transfer from tryptophan residues to the FAD moiety [37]. In a reduced GOD molecule, the fluorescence of tryptophan is increased and the efficiency of the energy transfer from the apoenzyme to FAD is decreased indicating the greater freedom of FAD inside the pocket formed by the apoenzyme. The tryptophan fluorescence in GOD is also pH-dependent [38]. The properties of tryptophan residues in GOD at the pH under investigation and in the presence of ethanol at pH 5 are summarized in Table 3.

The results obtained are similar to those reported earlier [37, 38]. For the reduced form of GOD, the increase of tryptophan fluorescence as compared with the fluorescence of the oxidised form is observed at all pH values studied. This increase is the greater the higher pH is. The presence of ethanol caused an increase of fluorescence of both forms of the enzyme accompanied with practically no change of the λ_{max} suggesting a weaker contact of the tryptophan residues with FAD.

Table 3. Steady state tryptophan fluorescence characteristics in glucose oxidase (λ_{exc} = 295 nm)

pH	Form	λ_{max} [nm]	$\Delta\lambda$[a] [nm]	$I_{R\,max}$[b] [%]	I_{red}/I_{ox}[c]
3	ox	338	60.4	102.5	1.210
	red	342	62.2	124.0	
5	ox	339	60.7	100	1.245
	red	342	61.9	124.5	
5[d]	ox	338	62.5	141.6	1.367
	red	340	63.6	193.7	
7	ox	340	61,1	106.2	1.272
	red	342	62.8	135.1	
9	ox	341	62.1	101.2	1.365
	red	344	63.0	138.2	

[a] $\Delta\lambda$ bandwidth at a half intensity of the maximum intensity.
[b] $I_{R\,max}$ relative maximum intensity (intensity of oxidised GOD at pH 5 taken as 100%).
[c] I_{red}/I_{ox} ratio of intensities of reduced and oxidised forms of GOD.
[d] In the presence of ethanol (c = 6.74 M).

3.2. Kinetic fluorescence measurements during sol-gel transition

Because the longest gelling time was 15 min at pH 3 for the initial gel compositions studied, only kinetic measurements were done. Changes of fluorescence were studied continuously during first 2 h after all components had been mixed.

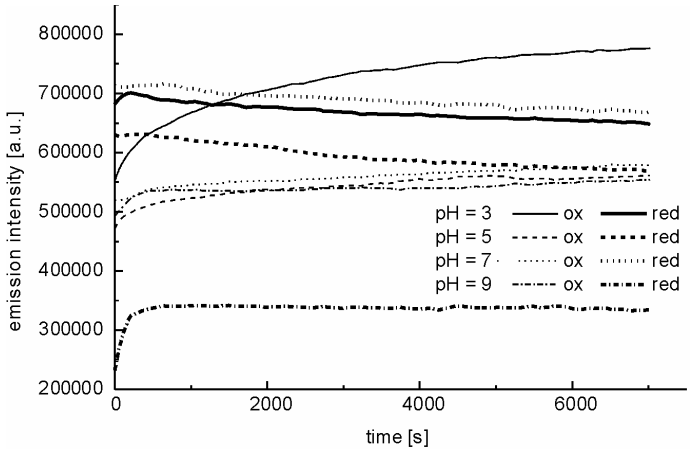

Fig. 3. Intensity of tryptophan fluorescence vs. time during gel formation (λ_{exc} = 295 nm; λ_{em} = 340 nm)

The tryptophan emission was excited at 295 nm and measured at 340 nm. The results are shown in Fig. 3. For the oxidised form of GOD, the tryptophan fluorescence intensity increases, the increase being most significant at pH 3. For the reduced form at pH 3, 5 and 7, a very slow decrease of fluorescence is observed. Only at pH 9 the

tryptophan fluorescence increased to about 145% of its initial value during first 7 min and then it was slowly decreasing.

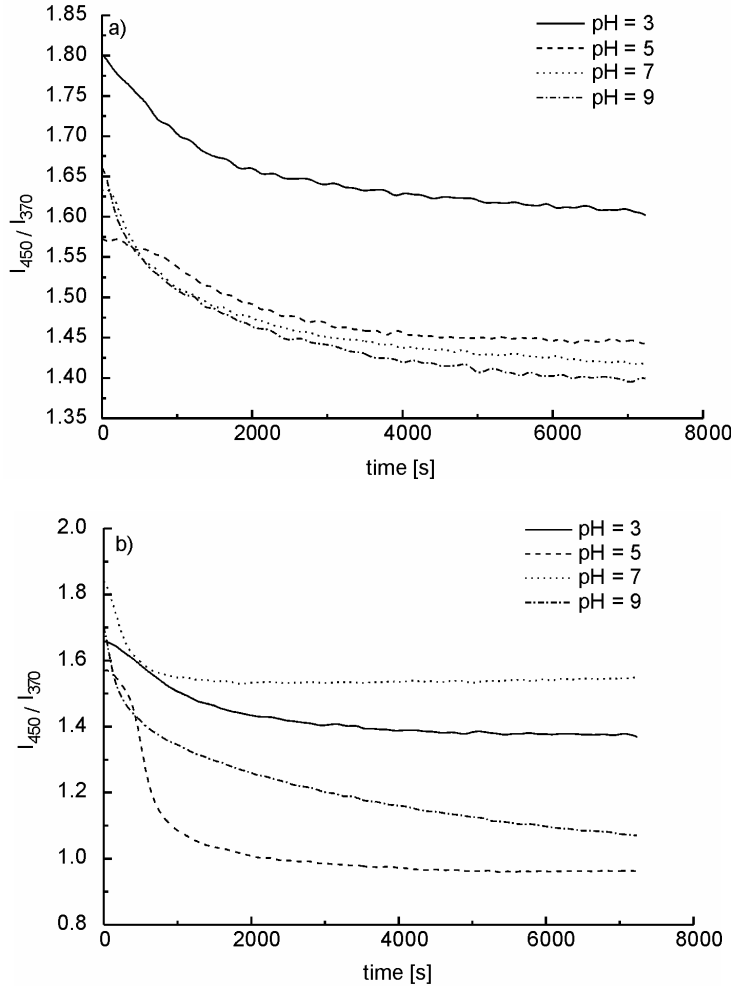

Fig. 4. Time dependences of I_{450}/I_{370} of FAD emission measured at 520 nm during the gel formation: a) oxidised enzyme, b) reduced enzyme

At all studied pH values, the fluorescence of reduced form of FAD decreases dramatically during first 10 min when excited at the wavelengths belonging to the band of HOMO-LUMO transition (450 and 467 nm). For the oxidised form of FAD the direction of changes depends on pH. At pH 3, the FAD fluorescence intensity increases, at pH 5 initially it increases then decreases, and at pH 7 and 9 it slowly decreases. When the fluorescence is excited at 370 nm, the changes are not so substantial and in some cases the direction of changes is different. Because of that the ratio of the emission excited at 450 nm and 370 nm (I_{450}/I_{370}) was taken into account

as the parameter characterising the FAD fluorescence. The changes of I_{450}/I_{370} during gel formation are shown in fig. 4. At every studied pH value and for both forms of enzyme (oxidised and reduced) this ratio is decreasing during gel formation. The rate of this decrease is the highest at the beginning (after mixing of all components) before gel is formed with some exception at pH 5. For the reduced form of FAD, the period of rapid decrease of I_{450}/I_{370} is well correlated with the gelling time.

The initial changes especially of FAD fluorescence during the gel formation can generally be attributed to the changes of the environment of a GOD molecule and the increase of ethanol concentration. These changes can alter the conformational motions of the whole molecule, the strength of FAD binding and thus its dynamics inside the GOD molecule [29].

3.3. Ageing of wet gels

Wet gels were prepared as described in the experimental part and kept in closed cuvettes, to prevent the gels from drying. During the ageing, a syneresis was observed. For every gel, the excitation and emission (excited at 370 nm and 450 nm) spectra of FAD and emission spectra of tryptophan were recorded. A characteristic example of the changes of FAD excitation spectra during ageing of gel is shown in Fig. 5.

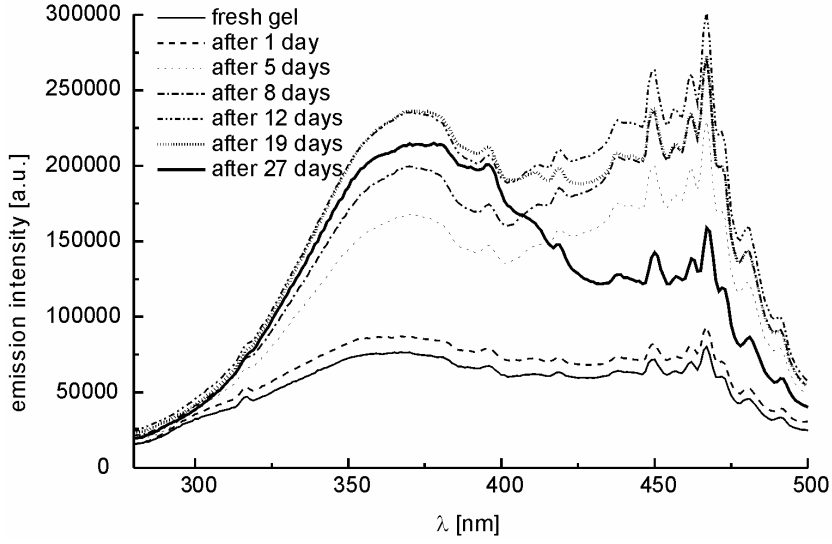

Fig. 5. Excitation spectra of FAD in reduced glucose oxidase during ageing of a wet gel prepared with the acetate buffer, pH 5

At all pH values studied, the intensity of FAD fluorescence initially increases (in the case of oxidised form only on the first day) and then decreases (Fig. 6). For freshly prepared gel, the intensity of FAD emission is much lower in the presence of

glucose (reduced form) as compared with the oxidised FAD. After 4 weeks of ageing the relation is quite opposite (with the exception of pH 3, at which the intensities tend to be equal).

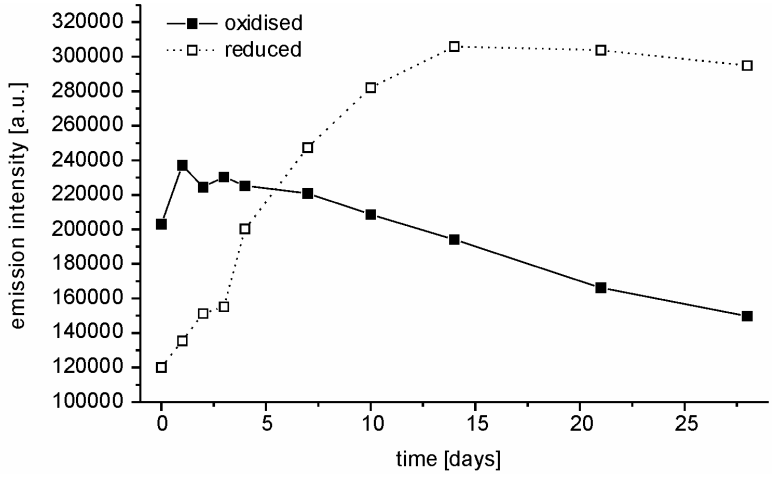

Fig. 6. Changes of FAD in glucose oxidase fluorescence intensity during ageing of a wet gel prepared with a phosphate buffer, pH 7, λ_{exc} = 450 nm, measured at the maximum of emission – 520 nm

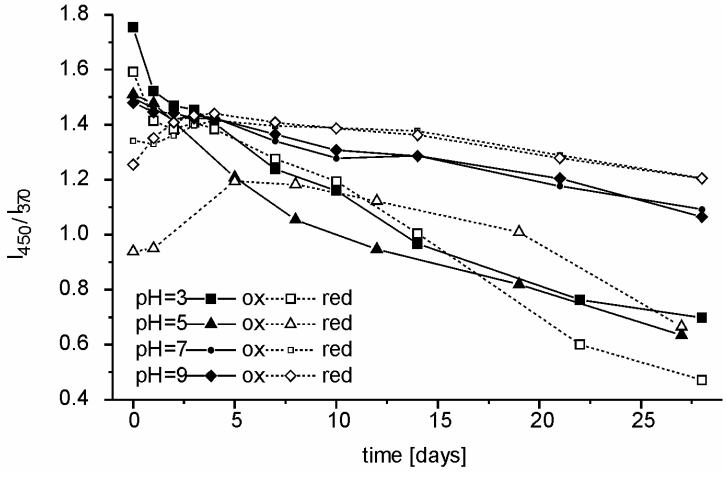

Fig. 7. Changes of I_{450}/I_{370} of FAD emission measured at 520 nm during wet gel ageing

The relative intensity of the band with its maximum intensity at 370 nm is higher as compared with the intensity of the HOMO-LUMO transition band (Fig. 7). Also the band at 370 nm is characteristically broadened after 3 weeks of ageing (Fig. 5). All these changes are less pronounced at pH 7 and 9. When the FAD emission was excited

at 450 nm, its maximum was situated at about 519–520 nm and showed no shift during ageing. The wavelength at the maximum is lower than that of the native enzyme in pure buffer but practically the same as for the enzyme in the presence of ethanol (Table 2). The FAD emission spectra show a blue shift when excited at 370 nm. At pH 3 and 5 the shift was about 20 nm. After 2 weeks the emission at the maximum disappeared and only a shoulder at 503 nm could be seen. At pH 7 and 9, the blue shift is less pronounced – only about 10 nm and the maximum of fluorescence does not vanish.

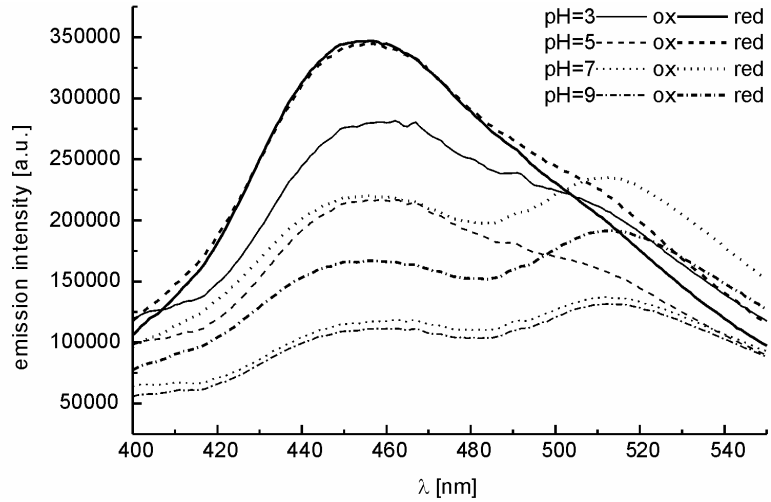

Fig. 8. Emission spectra of wet gels
after 4 weeks of ageing, excited at 360 nm

Such pronounced changes of the FAD fluorescence spectra during ageing of the gel cannot only be attributed to changes of the microenvironment and molecular dynamics but indicate that a new species is formed during the ageing. To recognise this unknown species, the emission spectra excited at 340, 350, 360, 370, 380 and 390 nm were recorded between 400 and 550 nm (Fig. 8). It could be seen that a new maximum appeared at about 460 nm for the oxidised GOD and at 456 nm for the reduced GOD. The wavelength of the maximum is independent of the excitation wavelength in the absence of glucose but shows a red shift (about 10 nm) when the excitation wavelength increases from 340 to 390 nm for gels with glucose added. The intensity of this maximum decreases with increasing pH. The second band with the maximum at 510 nm is visible only at pH 7 and 9. At pH 3, there is no evidence of this maximum and at pH 5 it is only a shoulder. Also the excitation spectra of the unknown species were recorded (λ_{em} 460 nm for the oxidised GOD; λ_{em} 455 nm for reduced GOD in the presence of glucose). They showed one maximum at about 355 nm, a shoulder at 380 nm and a second maximum at 396 nm. The fluorescence properties of the unknown species are very similar to those of alloxazine derivatives like lumichrome and 1-methyllumichrome in water [43]. It is well known that isoalloxazine derivatives like

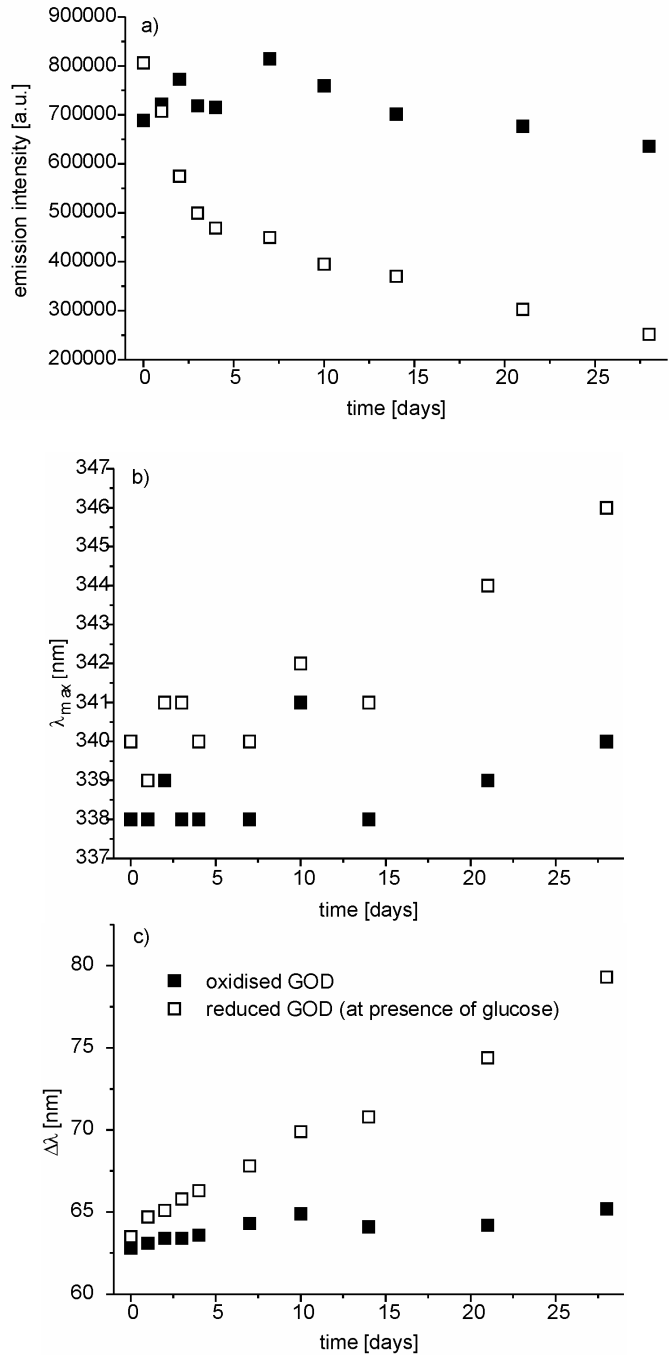

Fig. 9. Changes of tryptophan emission excited at 295 nm during ageing of wet gel prepared with a phosphate buffer, pH 7: a) intensity of the emission at the maximum, b) maximum wavelength, c) bandwidth at a half intensity of the maximum intensity; ■ – oxidised glucose oxidase; □ – reduced glucose oxidase (in the presence of glucose)

riboflavin, flavin mononucleotide (FMN) and FAD are not photostable and can undergo a photodegradadion [41, 44, 46]. The UV light irradiation caused first debranching of flavin derivative by removal of the ribityl moiety, then the reconfiguration of the ring structure, oxidation or reduction.

The mechanism of the photoreactions of flavins and detailed final products depend on the pH of the solution, the presence of oxygen and reducing species, temperature, environment, etc. [41]. The final products are: lumichrome (alloxazine derivative) in neutral and acidic solutions and lumiflavin (isoalloxazine derivative) in alkaline solutions [44]. It could be concluded that during ageing of gels the prosthetic group of glucose oxidase – FAD undergoes decomposition and as the result mainly alloxazine derivative is produced at pH 3 and 5, while at pH 7 and 9 both tautomeric forms are present. The ratio of the isoalloxazine form to alloxazine one increases with increasing pH (Fig. 8). The samples of hydrogel were not isolated from the daylight during ageing. Also the analysing light during the measurements could cause the FAD decomposition. The changes of tryptophan fluorescence are very similar at all pH studied but depend on the presence of glucose. The summary of fluorescence variation of tryptophane during ageing is shown in Fig. 9 (at pH 7 as an example).

For the oxidised form of enzyme, the intensity of fluorescence slightly increases during the first week and then decreases with a very small red shift of the maximum wavelength and some broadening of the emission band. Such changes of the tryptophane fluorescence are characteristic of conformational changes of the protein leading to unfolding and denaturation [47]. In the presence of glucose, the intensity of tryptophane emission decreases. At pH 3, after 4 weeks of ageing only 16.2% of initial intensity was retained, at pH 5, 7 and 9 – 18.9%, 31.2% and 37.7%, respectively. Also the red shift is more significant, after 4 weeks it amounts to 11 nm at pH 3 and 5 nm at other pH values. The emission band is broadened especially at the red edge of the spectrum. These changes indicate that the denaturation of glucose oxidase protein in the presence of glucose during ageing of the hydrogel is very pronounced. It could be supposed that the denaturation is not only caused by physical changes of the protein (apoenzyme) but also by some chemical changes. Aromatic amino acids, when irradiated with UV light in the presence of riboflavin or other flavin derivatives, undergo photodegradation and the rate constant of this reaction is greater in anaerobic conditions [46, 48–50]. The reaction is initialised by excited flavin in a triplet state [48, 49] and as the intermediate product the flavin semiquinones (radicals) are formed [49]. The photodegradation of tryptophane in enzyme protein molecules in the presence of riboflavin causes its deactivation [46].

3.4. Fluorescence of glucose oxidase in dried gels

Characteristics of fluorescence of glucose oxidase entrapped in silica gel dried in contact with the daylight is summarised in Table 4.

Table 4. Fluorescence properties of glucose oxidase entrapped in gels dried at the daylight,

Property	pH = 3		pH = 5		pH = 7		pH = 9	
	Ox	Red	Ox	Red	Ox	Red	Ox	Red
FAD λ_{max} (λ_{exc} = 450 nm) [nm]	511	509	516	516	524	515	521	517
I_{450}/I_{370}	0.614	0.209	0.596	0.289	0.596	0.325	1.116	0.330
Tryptophan λ_{max} (λ_{exc} = 295 nm) [nm]	344	441	338	348	339	433	342	433
$\lambda_{max\ exc}$ of unknown species [nm]	366	363	366	363	363	361	370	363
$\lambda_{max\ em}$ of unknown species (λ_{exc} = 360 nm) [nm]	467	461	467	461	460	460	467	462

As could be seen from Table 4, the fluorescence properties of GOD dried silica gel are very different from those of the native one, especially in the presence of glucose. Intensity of the HOMO-LUMO transition band in the excitation spectrum of FAD is very low as compared with that of the band peaking at 370 nm. In the presence of glucose, the value of I_{450}/I_{370} is extremely low; at pH 3 it is 9 times less than that for the native enzyme and at pH 9 – only 5 times. In the presence of glucose, the typical emission of tryptophan vanishes completely and a new maximum at 430 –440 nm can be observed. For gels without glucose this band can be observed as a shoulder. Also the new unknown species with fluorescence characteristics typical of alloxazine could be observed in dried gels, being the dominant fluorophore in the dried gel. These results indicate that in gels dried in the contact with the daylight, both the apoenzyme and prosthetic group – the FAD in glucose oxidase undergoe a photodestruction. The process is much more enhanced in the presence of glucose when there are practically anaerobic conditions inside the gel. This is in good agreement with the conditions of degradation of tryptophan photosensitized by riboflavin [46]. The degradation of glucose oxidase in gels depends also on pH and is the greatest at acidic environment.

When the gels were dried in darkness, the fluorescence properties of glucose oxidase were also changed as compared with those of the native enzyme but to a lesser extent. The direction of changes and the influence of pH as well as of the presence of glucose are comparable with those determined for wet gels and dried at the contact with the daylight. When the emission was excited at 370 nm, in the fluorescence spectrum of glucose oxidase a maximum at about 520 nm could be observed characteristic of FAD but also a little broad maximum or a shoulder at about 460 nm characteristic of alloxazine is present (Fig. 10).

Both types of dried gels were tested for leaching of the protein. They were soaked in the buffer as is described in the experimental part and then the buffers were tested for emission of FAD and tryptophane. The results are collected in Table 5.

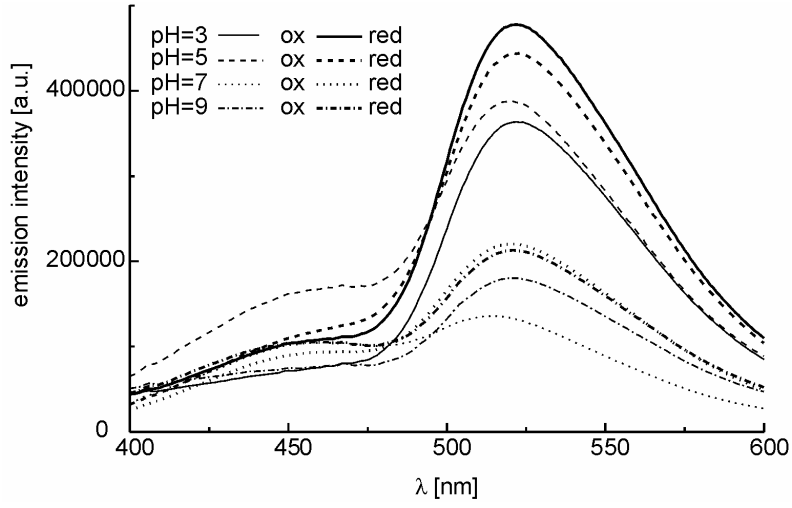

Fig. 10. Emission spectra of glucose oxidase entrapped in silica gels dried in darkness excited at 370 nm (The intensity of emission was corrected for a volume contraction of the gel after drying)

It could be seen that the species washed out from the dry gel have the fluorescence properties characteristic of the products of photodestruction of GOD. The emission spectra excited at 370 nm are similar to those of alloxazine derivatives [43].

Table 5. Characteristics of emission of buffers after soaking the dried silica gels in them

Property		pH = 3		pH = 5		pH = 7		pH = 9	
		Ox	Red	Ox	Red	Ox	Red	Ox	Red
λ_{max} [nm] (λ_{exc} = 450 nm)	a	530 (515^{s})	532	531	531	531	531	526	530
	b	502	509	496	504	494	506	500	505
λ_{max} [nm] (λ_{exc} = 370 nm)	a	466	465	–*	–*	459 (511^{s})	458	464 (506^{s})	456
	b	451	454	454	451	453	453	452	450
λ_{max} [nm] (λ_{exc} = 295 nm)	a	345 (419^{s})	409	343 (414^{s})	414	343 (406^{s})	409	409 (344^{s})	411
	b	429	431	443	443	441	447	434	429

a – gels dried in contact with the daylight, b – gels dried in darkness, s – shoulder, * – not measured.

In supernatants from soaking of gels dried in daylight, species with emission similar to isoalloxazine derivative with the maximum at 530–531 nm (λ_{exc} = 450 nm) can be observed, different from that of FAD. It could be 4′,5′-riboflavin cyclic phosphate which is known as the first intermediate product of FAD photolysis [45]. Also the spectra excited at 295 nm indicate that in supernatant the protein is in a denatured form (red shift of the maximum emission of tryptophan) or the products of oxidation of tryptophan photosensitized by FAD (species with the maximum of emission higher

than 400 nm) are present. This result is very important from the practical point of view. If the sol-gel process is applied to produce a glucose biosensor working *in vivo*, the products of photoreaction of flavins and tryptophan could be washed out. The final products of this reaction (especially lumiflavin and lumichrome) are toxic [48, 50].

3.5. Activity of glucose oxidase entrapped in gels

While the experiments with gels dried at the daylight indicated that the destruction of GOD occurred to a great extent, the activity was tested only for the gels dried in the darkness. The results are presented in Table 6. The greatest retention of activity was observed for the gel prepared with phosphate buffer, pH 9, in the absence of glucose. This result is in good agreement with those of fluorimetric measurements indicating the least degree of decomposition of glucose oxidase. When the gels were prepared with addition of glucose, only traces of activity in dried gels can be found.

Table 6. Retention of the glucose oxidase activity in gels dried in darkness and in buffer after soaking the gel

pH	Form	Retention of GOD activity in gel	% of GOD activity washed from gel
3	ox	13.2%	14.3%
	red	0.3%	0
5	ox	11.8%	32.4%
	red	0.2%	0
7	ox	15.0%	26.2%
	red	0.1%	~ 66%
9	ox	17.6%	> 100%
	red	0.3%	~ 48%

Although the fluorimetric measurements indicated that mainly the products of GOD destruction are washed out, the supernatants showed enzyme activity indicating that also GOD in a native form is washed out from the gel. The greatest leaching was obtained for the gel with the best retention – prepared with buffer at pH 9. The activity of the supernatant at pH 9 for oxidised GOD is higher than that of the gel (Table 6). The reason for this surprising result could be the inaccessibility of a part of the enzyme enclosed for example in closed pores to the substrate [6].

The problem is what is the reason for the decomposition of glucose oxidase in gels dried in darkness with the products similar to those obtained by photodestruction. It is known that the intermediate species produced during the photosensitised oxidation of tryptophan are free radicals [48, 49] and hydrogen atoms are involved in the reaction mechanism [48]. Recently, it was shown that various types of paramagnetic defects are formed in pure silica gels obtained in the sol-gel process from TEOS [51]. In silica gels there were identified entrapped electrons, protons in O^{2-} vacancies, peroxy centres and others. All these defects in the presence of water can produce free electrons

or hydrogen atoms – very reactive red-ox species causing cytotoxicity of some silica gels [51]. It could be supposed that these paramagnetic defects in a gel could initialize the reactions between FAD and tryptophan through formation of free radicals by addition of electrons or protons.

4. Conclusions

Changes of the fluorescence properties of glucose oxidase during ageing of gels indicate unfolding and a partial denaturation of the apoenzyme and a chemical decomposition of tryptophan in the apoenzyme and FAD. The decomposition of glucose oxidase is more pronounced in dried gels, at lower pH and in the presence of glucose. Among the products of the reaction, the alloxazine derivatives were identified. The destruction of the enzyme is caused by photooxidation of tryptophan by FAD. Also FAD itself undergoes a photoreaction leading to dealkylation and tautomerisation to alloxazine. In the darkness, the decomposition of GOD is probably initialised by the annihilation of the paramagnetic centres formed spontaneously during the sol-gel process with water.

The results obtained indicate that the optimum pH of gel production by two step procedure from TEOS is 7 (neutral environment). They also indicate that the main problems in application of the sol-gel process in fabricating an optical biosensor for glucose would be a decomposition of the enzyme enhanced by light and the presence of glucose. The products of the GOD decomposition are easily washed out from the gel and are (especially alloxazine) potentially toxic which could be a problem at applications *in vivo*. If glucose oxidase was used in optical biosensors, it would be advantageous to use fluorimetric indicators excited by the light with the wavelength greater than 500 nm to avoid photodestruction of the enzyme.

Acknowledgement

The author is grateful to the Polish Ministry of National Education and Sports for the financial support through the grant No. 4 T08E 00924.

References

[1] CLARK L.JR., LYONS C., Ann. N.Y. Acad. Sci., 102 (1962), 29.
[2] WILSON R., TURNER A.P.F., Biosens. Bioelectr., 7 (1992), 165.
[3] CASS A.E.G., DAVIS D., FRANCIS G.D., HILL H.A.O., ASTON W.J., HIGGINS I.J., PLOTKIN E.V., SCOTT L.D.L., TURNER A.P.F., Anal. Chem., 56 (1984), 667.
[4] ABEL P.U., VON WOEDTKE T., Biosens. Bioelectr., 17 (2002), 1059.
[5] BRAUN S., RAPPAPORT S., ZUSMAN R., AVNIR D., OTTOLENGHI M., Mater. Lett., 10 (1990), 1.
[6] JIN W., BRENNAN J.D., Anal. Chim. Acta, 461 (2002), 1.
[7] WANG J., Anal. Chim. Acta, 399 (1999), 21.
[8] GILL I., BALLESTEROS A., TIBTECH, 18 (2000), 282.
[9] GILL I., Chem. Mater., 13 (2001), 3404.
[10] TATSU Y., YAMASHITA K., YAMAGUCHI M., YAMAMURA M., YAMAMOTO H., YOSHIKAWA S., Chem., Lett. (1992), 1615.

[11] NARANG U., PRASAD P.N., BRIGHT F.V., RAMANATHAN K., KUMAR N.D., MALHOTRA B.D., KAMALASANAN M.N., CHANDRA S., Anal. Chem., 66 (1994), 3139.
[12] SAMPHAT S., LEV O., Anal. Chem., 68 (1996), 2015.
[13] WANG J., PAMIDI P.V.A., PARK D.S., Anal. Chem., 68 (1996), 2705.
[14] KÜNZELMANN U., BÖTTCHER U., Sensors Actuators B, 38-39 (1997), 222.
[15] YAO T., TAKASHIMA K., Biosens. Bioelectr., 13 (1998), 67.
[16] WU J., SULS J., SANSEN W., Anal. Sci., 15 (1999), 1029.
[17] COUTO C.M.C.M., ARAÚJO A.N., MONTENEGRO M.C.B.S.M., ROHWEDDER J., RAIMUNDO I., PASQUINI C., Talanta, 56 (2002), 997.
[18] TIAN F., ZHU G., Sensors Actuators B, 86 (2002), 266.
[19] SHANKARAN D.R., UEHARA N., KATO T., Biosens. Bioelectr., 18 (2003), 721.
[20] LI J., CHIA L.S., GOH N.K., TAN S.N., J. Electroanal. Chem., 460 (1990), 234.
[21] PANDEY P.C., UPADHYAY S., PATHAK H.C., Sensors Actuators B, 60 (1999), 83.
[22] PANDEY P.C., UPADHYAY S., Sensors Actuators B, 76 (2001), 193.
[23] YANG X., HUA L., GONG H., TAN S.N., Anal. Chim. Acta, 478 (2003), 67.
[24] PANDEY P.C., UPADHYAY S., SHUKLA N.K., SHARMA S., Biosens. Bioelectr., 18 (2003), 1257.
[25] DE MARCOS S., GALINDO J., SIERRA J.F., GALBÁN J., CASTILLO J.R., Sensors Actuators B, 57 (1999), 227.
[26] WOLFBEIS O.S., OEHME I., PAPKOVSKAYA N., KLIMANT I., Biosens. Bioelectr., 15 (2000), 69.
[27] WU X.J., CHOI M.M.F., XIAO D., Analyst, 125 (2000), 157.
[28] SHTELZER S., BRAUN S., Biotechnol. Appl. Biochem., 19 (1994), 293.
[29] HARTNETT A.M., INGERSOLL C.M., BAKER G.A., BRIGHT F.V., Anal. Chem., 71 (1999), 1215.
[30] RAMANATHAN K., JÖNSSON B.R., DANIELSSON B., Anal. Chim. Acta, 427 (2001), 1.
[31] QUINGWEN L., GUOAN L., YIMING W., XIGRONG Z., Mat. Sci. Engineer. C, 11 (2000), 67.
[32] ZHU L., LI Y., TIAN F. XU B., ZHU G., Sensors Actuators B, 84 (2002), 265.
[33] HECHT H.J., SCHOMBURG D., KALISZ H., SCHMID R.D., Biosens. Bioelectr., 8 (1993), 197.
[34] YAMANAKA S.A., NISHIDA F., ELLERBY L.M., NISHIDA C.R., DUNN B., VALENTINE J.S.,, ZINK J.I., Chem. Mat., 4 (1992), 495.
[35] AUDEBERT P., DEMAILLE C., SANCHES C., Chem. Mat., 5 (1993), 911.
[36] PRZYBYT M., BIAŁKOWSKA B., Mat. Sci., 20 (2002), 63.
[37] HAOUZ A., TWIST C., ZENTZ C., DE KERSABIEC A.-M., PIN S., ALPERT B., Chem. Phys. Lett., 294 (1998), 197.
[38] HAQ S.K., AHMAD MD.F., KHAN R.H., Biochem. Biophys. Res. Comm., 303 (2003), 685.
[39] GHISLA S., MASSEY V., LHOSTE J., MAYHEW S.G., Biochemistry, 13 (1974), 589.
[40] TRETTNAK W., WOLFBEIS O.S., Anal. Chim. Acta, 221 (1989), 195.
[41] HEELIS P.F., Chem. Soc. Rev., 112 (1982), 15.
[42] MILLER E., J. Photochem. Photobiol. A, 152 (2002), 249.
[43] SIKORSKI M., SIKORSKA E., KOZIOŁOWA A., GONZALES MORENO R., BOURDELANDE J.L., STEER R.P., WILKINSON F., J. Photochem. Photobiol. B, 60 (2001), 114.
[44] PAN Y.L., PINNICK R.G., HILLS S.C., NILES S., HOLLER S., BOTTIGER J.R., WOLF J.-P., CHANG R.K., Appl. Phys. B, 72 (2001), 449.
[45] GLISZCZYŃSKA A., KOZIOŁOWA A., J. Chrom. A, 822 (1998), 59.
[46] EDWARDS A.M., SIVA E., J. Photochem. Photobiol. B, 63 (2001), 126.
[47] ZHENG L., BRENNAN J.D., Analyst, 123 (1998),1735.
[48] BUENO C.A., SILVA E., EDWARDS A.M., J. Photochem. Photobiol. B, 52 (1999), 123.
[49] LU C.-Y., LIU Y.-Y., Biochim. Biophys. Acta, 1571 (2002), 71.
[50] EDWARDS A.M., BUENO C., SALDAÑO, SILVA E. KASSAB K., POLO L., JORI G., J. Photochem. Photobiol. B, 48 (1999), 36.
[51] ULATOWSKA-JARŻA A., KOMOROWSKA M., PODBIELSKA H., submitted for publication in Mat. Sci.

Received 27 July 2003
Revised 21 October 2003

Materials Science, *Vol. 21*, *No. 4*, *2003*

Potentiometric tungsten electrodes with enzymes immobilised by the sol-gel technique

MAŁGORZATA PRZYBYT*

Institute of General Food Chemistry, Department of Biochemistry and Food Science,
Technical University of Łódź, 90-924 Łódź, ul. Wólczańska 171/173, Poland

The application of sol-gel transitions in development of potentiometric enzyme electrodes with urease, glucose oxidase and tyrosinase is described. Urease and glucose oxidase electrodes showed features of typical potentiometric electrodes with the response modified by the change of pH. The slopes of calibration curves in semilogarithmic coordinates were lower than the Nernstian values and the dynamic ranges were narrow for both electrodes. The tyrosinase electrode shows response to mono- and *o*-diphenols. The response of this electrode is not connected with the pH changes. The mechanism of the response of the tyrosinase electrode is discussed; it is proposed that the potential changes reflect the redox state of the enzyme. The electrode responds to reactant concentration (phenol, catechol and some others) even at concentrations 2×10^{-6} M. Such a high sensitivity makes the electrode a promising candidate for application in detecting traces of phenols.

Key words: *sol-gel; potentiometric enzyme electrode; urease; tyrosinase; glucose oxidase*

1. Introduction

The method of the sol-gel entrapment of enzymes and other biologically active molecules is a widely used technique of immobilisation for construction of biosensors, because of its simplicity and flexibility as well as low temperature of the process. The method allows us also to immobilise large amounts of biological materials with a good retention of their activity and low leakage from the gel. Since 1990, when Braun et al. [1] reported for the first time immobilisation of the enzymes in silica gel obtained by the sol-gel method, it has been widely used in various types of biosensors (electrochemical and optical) [2–5].

Enzymatic reactions in which acids or bases are produced can be traced by appropriate pH sensors. pH transducers typically used in the construction of biosensors are

*E-mail: mprzybyt@snack.p.lodz.pl.

potentiometric electrodes: glass [6], metal–metal oxide [7–9] and chemically modified graphite [10, 11]. Other types of transducers with potentiometric response to pH used in biosensors are miniature semiconductor devices like field effect transistors (FET) [12, 13] or light addressable photodiodes (LAPs) [14]. Although the sol-gel method is widely used to immobilise enzymes in biosensors, its application in potentiometric biosensors is rare [15–17].

We developed potentiometric urea electrodes based on the tungsten–tungsten oxide system [8, 9]. We have also been involved in the application of the sol-gel method to the construction of amperometric enzyme electrodes based on enzymes of different types [18]. The aim of this work is to immobilise enzymes on the surface of tungsten –tungsten oxide pH-metric electrode in silica gel obtained by the sol-gel method. As the models, such enzymes as urease, glucose oxidase and tyrosinase were chosen. Tyrosinase, which oxidises phenols with consumption of two hydrogen ions leading to a local increase of pH [19, 20], was used in the construction of the enzyme FET selective for monophenols [20].

2. Experimental

2.1. Reagents

As the gel precursor, tetramethoxysilane (TMOS) (99+%, Aldrich) was used. It was chosen because the preliminary experiments with gels obtained from tetraethoxysilane showed lack of adhesion to the electrode surface. The enzymes used in experiments were: urease from Jack bean (type III, glycerol solution, 680 U/ml, Sigma), glucose oxidase from *Aspergillus niger* (solution, 5370 U/ml, Serva) and tyrosinase from mushroom (solid, 6050 U/mg, Sigma). Urease and glucose oxidase were used as delivered, tyrosinase was dissolved in 0.1 M phosphate buffer, pH 7 (1 mg per 1 ml). All other reagents were of analytical grade. Twice-distilled water was used throughout.

2.2. Apparatus

Potentiometric measurements were done with a microcomputer pH/oxygen meter CPO-551 (Elmetron, Zabrze, Poland). Saturated calomel electrode (SCE) OH-962 P (Radelkis, Budapest, Hungary) was used as a reference electrode. The measurements were done at the ambient room temperature. A magnetic stirrer BMM 21 maintained a constant stirring rate of the solutions.

2.3. Preparation of electrodes and enzyme immobilisation

Tungsten electrodes were prepared from tungsten rods, 3 mm in diameter and 70 mm long. After polishing, the electrodes were flame oxidised [8]. Then the central

part of the electrode was covered with lacquer leaving 1.5 cm of free surface at each end. Prior to use, the electrodes were soaked in water overnight.

The stock solution of the silica sol was prepared as follows: 5 ml of TMOS, 1 ml of water and 0.05 ml of 0.1 M HCl [21] were stirred vigorously at room temperature until a transparent homogenous solution was obtained (15 min) and stored in a refrigerator.

The casting solution was prepared by mixing 0.5 ml of the sol solution with 0.1 M phosphate buffer, pH 7, and the enzyme solution: 0.25 ml of buffer with 0.25 ml of urease solution, or 0.5 ml of buffer with 0.05 ml of glucose oxidase or tyrosinase were added. The casting solutions were used immediately after mixing and the electrodes were covered with the gel layer by dip coating. After formation of hydrogel (about 1 min), the electrode was dipped in 0.005 M phosphate buffer, pH 6.

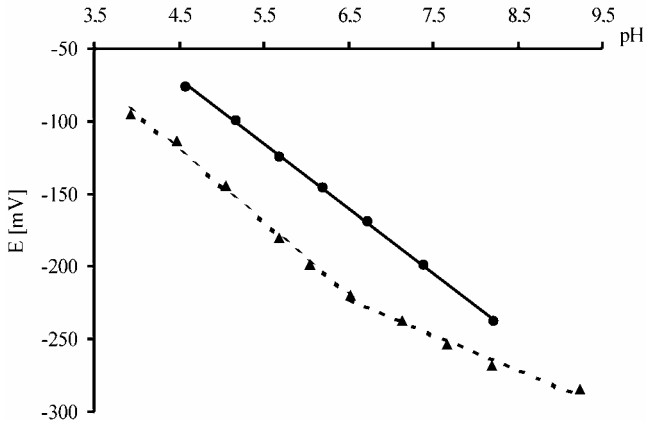

Fig. 1. pH response of the tungsten–tungsten oxide electrode:
● – uncovered electrode; ▲ – covered electrode

The electrodes were tested in a series of buffers for their pH response before and after covering with silica gel (Fig. 1).

2.4. Measurement procedure

The substrate water solutions of the concentration of 0.1 M were prepared freshly every day except glucose. Solution of this substrate was prepared one day before use to allow mutarotation. Solutions of gallic acid were adjusted to pH 6 by addition of NaOH.

The enzyme electrode and reference SCE connected with a voltmeter were dipped in 50 ml of 0.005 M phosphate buffer, pH 6, (if not stated otherwise), stirred with magnetic stirrer (at the rate of 500 rpm) at ambient temperature. In the case of urease, buffers were added with 0.002 M EDTA to avoid inactivation of the enzyme by heavy metal ions. When the potential of the electrode became stable, the desired amount of

0.1 M solution of the substrate was added. The electrode potential was measured and collected every 1 s by a PC computer until no changes were observed during 30 s (typically 5 min were enough for the whole measurement, in the case of urease this time was longer). From the obtained dependencies of the electrode potential vs. time (Fig. 2), the differences of initial and final potentials ΔE (steady-state method) and initial rates of potential change dE/dt (kinetic method) were found.

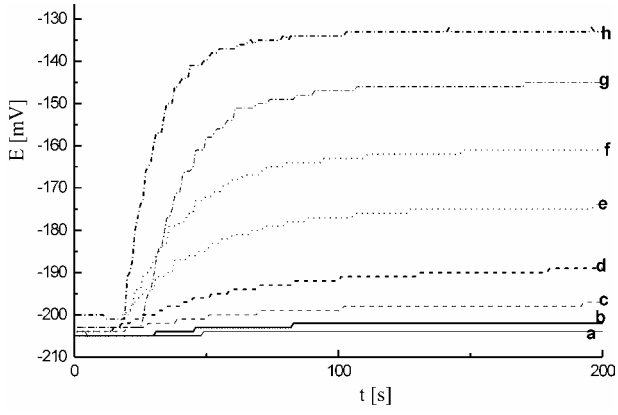

Fig. 2. Example of the potentiometric enzyme electrode response: enzyme–glucose electrode at pH 6; volume of added 0.1 M glucose solution: a) 10 μl, b) 25 μl, c) 50 μl, d) 100 μl, e) 250 μl, f) 500 μl, g) 1000 μl, h) 2500 μl

Calibrations curves of the electrodes were plotted as the dependencies of the electrode response (ΔE or dE/dt) on decimal logarithm of the substrate concentration. From these curves, dynamic range (linear parts of the calibration curves) and the slopes of the linear parts were read.

3. Results and discussion

3.1. pH response of the electrode

Figure 1 shows the dependence of the electrode potential on pH. For a bare tungsten–tungsten oxide electrode its potential decreases linearly with the increase of pH. The slope of the straight line is –44.5 mV/decade (r = 0.999). For the electrode covered with silica gel, the potential of the electrode is lower than for the bare electrode. Its potential also decreases with increasing pH but one can recognise two regions with different slopes: first at the pH range from 4 to 6.5 (slope –49.9 mV/decade, r = 0.997), the other – between 6.5 and 9.5 (slope –24.3 mV/decade, r = 0.989). In each case, the slope is lower than the Nernstian value –59 mV/decade. The deviations from linearity for the electrode covered with silica gel and the sub-Nernstian values of

the slopes are probably connected with the reaction of neutralisation of hydrogen ions with silanol groups on the surface of silica [15].

The enzymes studied in this work are the catalysts of the following reactions:

• Urease:

$$CO(NH_2)_2 + 3H_2O \xrightarrow{\text{urease}} 2NH_4^+ + OH^- + HCO_3^- \quad (1)$$

The products of this reaction form a self-buffering mixture with pK_a = 8.83 [22]. When the pH of the environment of the reaction is less than pK_a value, the pH increases. Thus the potential of the urease electrode would decrease.

• Glucose oxidase:

$$\beta\text{-D-glucose} + O_2 \xrightarrow{\text{glucose oxidase}} \text{gluconic acid} + H_2O_2 \quad (2)$$

As the product of this reaction is an acid, the potential of the glucose oxidase electrode is predicted to increase after addition of the substrate.

• Tyrosinase:

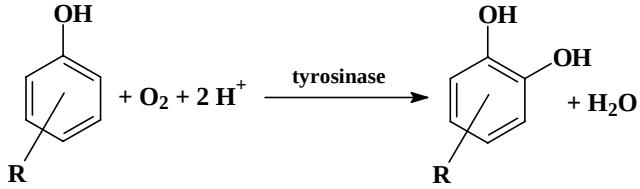

(3)

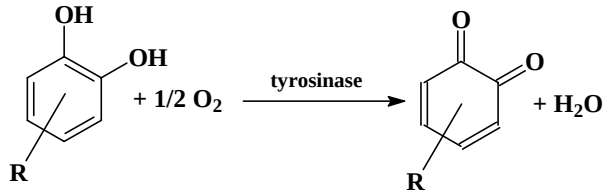

(4)

Tyrosinase oxidises differently substituted mono- and *o*-diphenols with different rates of reactions (3) and (4). In reaction (3), the pH value increases, while in reaction (4) it remains constant. Thus by immobilisation of tyrosinase on a pH-transducer, a biosensor selective for phenols can be constructed [20].

3.2. Urease electrode

As predicted, after addition of urea the potential of the electrode decreases. The rate of the decrease is low and thus it cannot be the measure of the changes in urea concentration. Thus to obtain calibration curves for urea only the steady-state method was used. Figure 3 shows the calibration curves of the electrode with urease immobilised in silica gel.

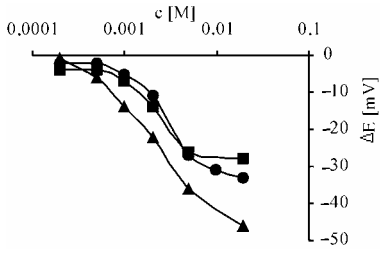

Fig. 3. Calibration curves for the urease electrode in 0.005 M buffers (steady -state method): ● – acetate, pH 5; ■ – phosphate, pH 6; ▲ – alanine, pH 6

The dynamic range of this sensor in acetate and phosphate buffers is very narrow; only about one decade. The result is similar to the results obtained with the tungsten–tungsten oxide electrode with urease covalently bound to the surface [9] and entrapped in gelatine gel [8]. The response time is rather long – about 6–7 min. Only when alanine buffer was used, the dynamic range of the electrode was broader (2×10^{-4}–2×10^{-2} M of urea) with the slope of –24.2 V/decade ($r = 0.991$), which is much less than for the tungsten electrode with urease covalently bound [9].

These preliminary measurements indicate that entrapment of urease in silica gel on the surface of the tungsten–tungsten oxide electrode is not a promising way to construct the urease electrode with properties allowing its practical use. But the results of Ogura et al. [15] and Pandey and Singh [17] indicate that using a different pH sensor would improve the properties of the urea sensor.

3.3. Glucose oxidase electrode

Figure 2 shows typical changes of the glucose oxidase electrode after addition of glucose. As predicted, the electrode potential increases after addition of the substrate. The increase of the potential is quick and the response time of the electrode is shorter than 3 min. Only at a very low concentration of the buffer and at high concentration of the substrate it is longer (about 4 min).

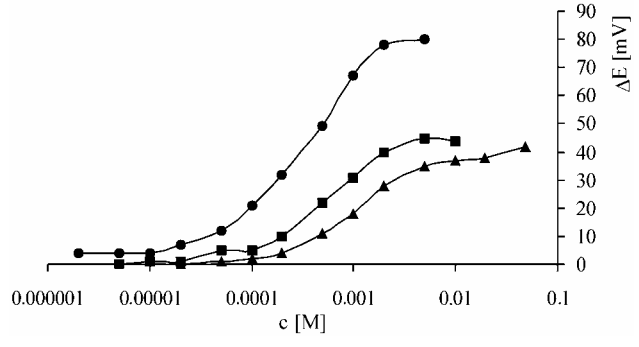

Fig. 4. Calibration curves for the glucose oxidase electrode at pH 6 (steady-state method) at different concentrations of the buffer: ● – 0,001 M; ■ – 0,005 M; ▲ – 0,02 M

Figure 4 shows the calibrations curves of the glucose oxidase electrode at pH 6 at different concentrations of the buffer. When the buffer concentration increases, the dynamic range of the curve is moving to higher substrate concentrations and the slope

of the linear part of calibration curve is decreasing (Table 1). This is a typical behaviour of the pH-based potentiometric enzyme electrodes, connected with increasing buffer capacity at higher concentrations [8–10]. The kinetic response of the electrode is practically independent of the buffer concentration.

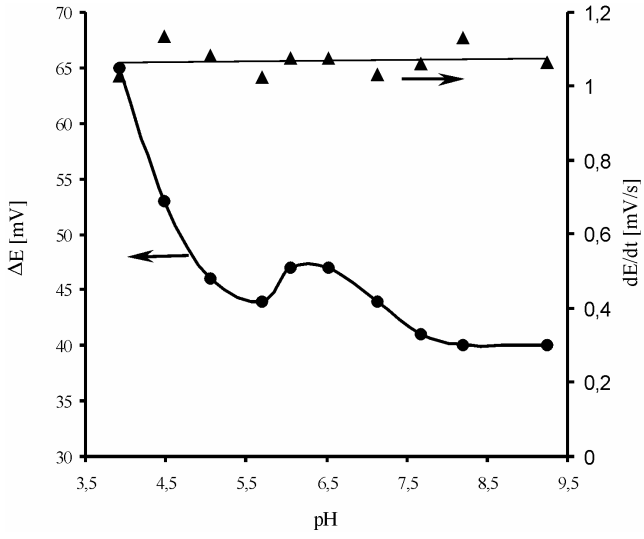

Fig. 5. Dependence of the glucose oxidase electrode response on pH (0.005 M buffers, for pH less then 5.5 – acetate, higher – phosphate, glucose concentration 5×10^{-4} M): ● – steady-state method; ▲ – kinetic method

Table 1. Characteristics of glucose oxidase electrode (steady-state method)

pH	Buffer concentration [M]	Dynamic range [M]	Slope [mV/decade]	*r*
5	0.005	10^{-4}–5×10^{-3}	46.3	0.998
6	0.001	5×10^{-5} – 2×10^{-3}	42.6	0.995
	0.005	10^{-4}–5×10^{-3}	37.7	0.995
	0.02	2×10^{-4} – 5×10^{-3}	23.2	0.994
7	0.005	10^{-3}–2×10^{-2}	31.2	0.998

The response of the glucose oxidase electrode depends on pH (Fig. 5 and Table 1). Figure 5 shows the variation of the electrode response at different pH values. It can be seen that the response in the steady-state method depends significantly on pH with local maximum at pH about 6 and sharp increase for decreasing pH values. The local maximum well corresponds with the optimum value of pH of a free enzyme [23] and those immobilised on platinum in bovine serum albumin [24]. The increase of the response with decreasing pH for the values less than 5.5 when acetate buffers were used is most probably connected with decreasing buffer capacity. In the kinetic method, the electrode response is practically independent of pH. When the rates of the

initial changes of the electrode potential are taken into account as the glucose concentration measures, the beginning of the linear part of the calibration curves passes to higher values and the slope of the linear part is practically the same for pH 5, 6 and 7. The slopes of calibration curves in the steady-state method are less than the Nernstian value for all pH values tested and all buffer concentrations (Table 1).

The results obtained indicate that the glucose electrode potential is altered by the hydrogen ion concentration (pH). The sub-Nerstian slopes of the calibration curves in the steady-state method and independence of the rate of the potential changes (kinetic method) of pH and buffer capacity indicate, however, that there could also be other sources of potentiometric response like red-ox state of the enzyme [24] or reactions of hydrogen peroxide produced in reaction (2) [25].

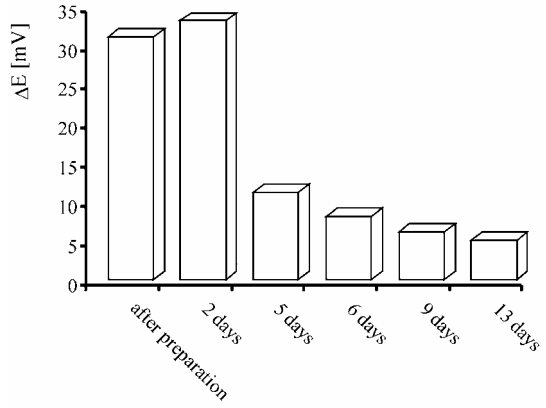

Fig. 6. Stability of the glucose oxidase electrode (tested for 0.005 M phosphate buffer, pH 6, glucose concentration 5×10^{-4} M)

The potentiometric glucose oxidase electrode is very unstable (Fig. 6). Glucose oxidase is a very stable enzyme as its molecule is a glycoprotein [23] and many of the biosensors for glucose are also very stable allowing practical use. But some data indicate that glucose oxidase immobilised in silica gel is unstable [18, 26]. This instability is partially caused by the leakage of the enzyme from the silica gel [18].

3.4. Tyrosinase electrode

For the tyrosinase electrode, the results were surprising. The predicted response was: a decrease of the electrode potential for phenol as substrate and no change for *o*-diphenol (catechol). The electrode studied showed an increase of the potential after addition of both substrates. The example of the electrode response for catechol is shown in Fig. 7.

The potential increase is quick and very significant even for very low concentrations of catechol (compare curve a in Fig. 7 – $c_{\text{catechol}} = 2\times10^{-6}$ M). For an amperometric electrode constructed on the basis of oxygen electrode there would be practically no response for such a concentration [18]. For higher concentrations of the substrate, after initial quick increase of the electrode potential a slow decrease is observed

(curves f, g and h in Fig. 7). Thus, in the case of tyrosinase electrode, ΔE was calculated as a response in the steady-state method i.e., as a difference between initial value and the maximum one after addition of the substrate. Also the initial rate of the potential increase *dE/dt* is lower for high concentrations of the substrate. This effect is connected with the properties of tyrosinase which undergoes a suicide auto-inhibition by the substrate [27, 28]. This inactivation is irreversible and because of that many biosensors with tyrosinase have very low operational stability [20, 29].

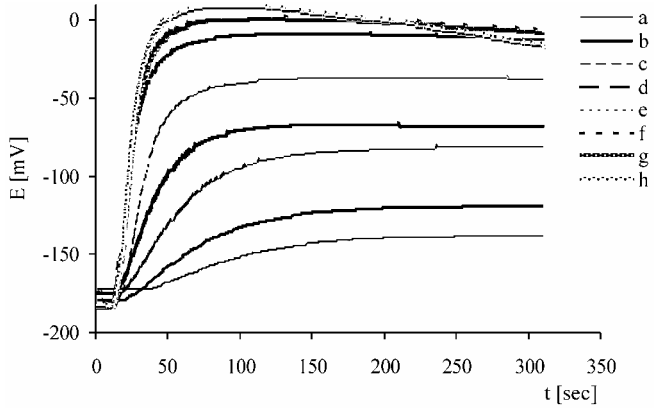

Fig. 7. Potentiometric tyrosinase electrode response to catechol at pH 6;
volume of 0.1 M substrate solution added:
a) 1 µl, b) 2.5 µl, c) 5 µl, d) 10 µl, e) 25 µl, f) 50 µl, g) 100 µl, h) 250 µl

The influence of the buffer pH and concentration was tested for a model substrate – catechol. For the catechol concentration equal to 2×10^{-5} M, the maximum response in a steady-state and kinetic methods was observed at pH = 6 (Fig. 8).

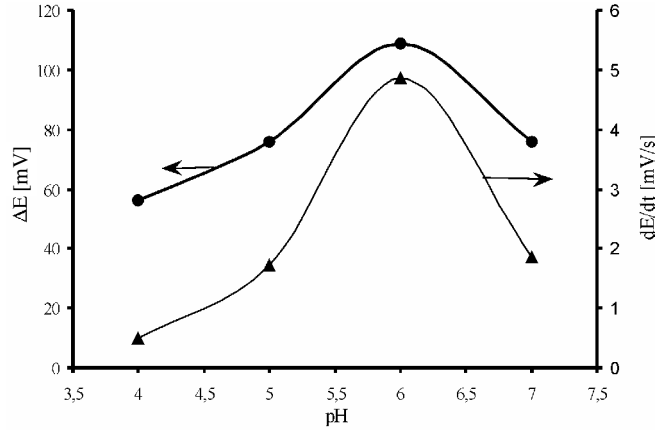

Fig. 8. Dependence of the tyrosinase electrode response on pH (0.005 M buffers,
for pH 4 and 5 – acetate, higher – phosphate, catechol concentration 2×10^{-5} M):
● – steady-state method; ▲ – kinetic method

This optimum of the sensor response is in good agreement with the results obtained by other authors [20, 30, 31]. The slopes of linear parts of the calibration curves vary slightly with pH with a minimum at pH 5 (Table 2). The response time of the electrode to catechol is practically about 3 min, only at pH 4 it is longer. The inhibition effect of the substrate is enhanced at higher pH. At pH 7 this effect is visible for catechol concentration 5×10^{-5} M (compare the results in Fig. 7 at pH 6). At pH 4 for all catechol concentrations tested no effect of auto-inhibition was evident. The buffer concentration was tested at pH 6 (Table 2) and practically no influence was found.

At pH 6, the tyrosinase electrode was tested for catechol in a buffer containing 10% of isopropanol. This was done because tyrosinase activity can be modulated by addition of organic solvents [32]. Addition of isopropanol causes the increase of the electrode response, especially of *dE*/*dt*. Also the slope of the linear part of the calibration curve in the steady-state method is increased and is higher than the Nernstian value (Table 2). These results indicate that addition of isopropanol activates tyrosinase.

Table 2. Characteristics of tyrosinase electrode (steady-state method) for catechol as a substrate

pH	Buffer concentration [M]	Dynamic range [M]	Slope [mV/decade]	*r*
4	0.005	5×10^{-6}–2×10^{-4}	60.2	0.992
5	0.005	2×10^{-6}–10^{-4}	51.1	0.992
6	0.001	2×10^{-6}–10^{-4}	62.6	0.988
	0.005	2×10^{-6}–10^{-4}	58.4	0.992
	0.02	2×10^{-6}–10^{-4}	56.5	0.997
6	0.005 with 10% of isopropanol	2×10^{-6}–10^{-4}	79.3	0.999
7	0.005	2×10^{-6}–5×10^{-5}	57.9	0.992

The source of the tyrosinase electrode response is unknown. It is of course not the change of pH because the results are completely different to those obtained for pH sensitive FET with immobilised tyrosinase [19, 20]. It was checked that similar response was obtained when tyrosinase was immobilised in albumin gel on the surface of tungsten–tungsten oxide electrode. When tyrosinase is immobilised on the surface of a glass pH-metric electrode in silica gel, no response to catechol was observed.

There could be two other sources of the potentiometric response of the electrode. The first – the potential of the electrode is altered by the local oxygen concentration near the electrode surface. Preliminary experiments indicate that the tungsten –tungsten oxide electrode is also sensitive to oxygen. The second – the potential variation is caused by the red-ox state of the enzyme. Tyrosinase belongs to the class of copper enzymes. The active centre of tyrosinase contains two copper atoms (Cu^{2+}) which are reduced to Cu^{+} when the substrate molecule (monophenol or *o*-diphenol) is oxidised, and reduced form of the enzyme is formed [28]. In the next step, the enzyme is reoxidised by oxygen. A similar copper-containing enzyme – ascorbate oxidase was used to construct the potentiometric electrode for ascorbate [33]. The potential varia-

tion of such an electrode was attributed by the authors to a change of the electron density on the electrode surface caused by the reduction of Cu^{2+} to Cu^{+} by the substrate. The characteristics of that electrode was also similar to that of the tyrosinase electrode studied in this work: very low concentrations detected and similar dynamic ranges, no influence of the buffer concentration. Because of that it is supposed that the source of potential variation for tyrosinase electrode is most probably the red-ox state of the enzyme.

Tyrosinase oxidises variously substituted mono- and *o*-diphenols at different rates. Thus the biosensors with immobilised tyrosinase show the response to many substrates [18]. The selectivity spectrum of a biosensor could depend on the source of the enzyme, method of immobilisation, transducer and composition of environment in which it is used [18, 20, 34]. The studied electrode was tested for various substrates. The results are collected in Table 3.

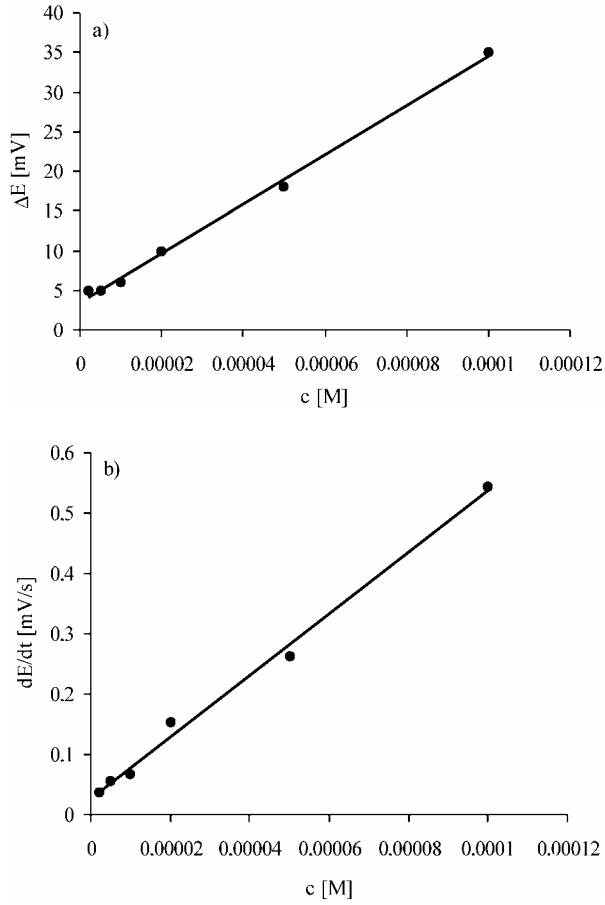

Fig. 9. Calibration curve of the tyrosinase electrode for phenol in 0.005 M phosphate buffer, pH 6:
a) steady-state method – equation of the straight line is $\Delta E = 3010390c + 3.5$ ($r = 0.998$);
b) kinetic method – equation of the straight line is $dE/dt = 5114c + 0.027$ ($r = 0.997$)

Table 3. Analytical characteristics of tyrosinase electrode at pH 6 (0.005 M phosphate buffer) for different substrates

Substrate	Dynamic range [M]	Slope [mV/decade]	r
Catechol	2×10^{-6}–10^{-4}	58.4	0.992
Phenol	2×10^{-5}–10^{-3}	40.7	0.990
p-Cresol	2×10^{-6}–10^{-4}	24.5	0.982
m-Cresol	5×10^{-6}–5×10^{-4}	28.2	0.989
p-Chlorophenol	2×10^{-6}–10^{-4}	18.7	0.999
Pirogallol	2×10^{-4}–10^{-3}	13.4	0.996
Gallic acid	10^{-4}–10^{-2}	14.8	0.985
Dopamine	10^{-5}–5×10^{-4}	91.9	0.990

As can be seen from Table 3, the potentiometric tyrosinase electrode is most sensitive to dopamine, catechol and phenol. For other substrates tested, the sensitivity is much lower. For pirogallol and gallic acid the dynamic range is shifted to higher concentrations. There were no response for *o*-cresol, *o*-chlorophenol, *o*-aminophenol, *p*-aminophenol and tyrosine.

If the response of the electrode to phenol is plotted against concentration (Fig. 9), the straight line is obtained for both methods: the steady-state- and the kinetic one, and the fit is better than for the logarithmic dependence (see Table 3).

These results suggest that tyrosinase electrode based on metal–metal oxide with enzyme immobilised in silica gel could be used to assay traces of phenol, for example, in water. Such an application needs an optimisation of the biosensor construction and operation conditions. Because of properties of tyrosinase (autoinhibition) such a biosensor ought to be used rather as a disposable one.

4. Conclusions

The results presented in this work indicate that entrapment of the enzymes in silica gel obtained by the sol-gel method is suitable in construction of potentiometric biosensors. The layer of silica gel changes the potentiometric response of the tungsten –tungsten oxide electrode to pH. The urease and glucose oxidase electrodes showed behaviour as predicted but their properties are too poor for practical use. The results indicate also that glucose oxidase is instable in silica gel.

The most promising results were obtained for tyrosinase electrode. It is very sensitive to phenol, catechol and dopamine. The direction of changes of the electrode potential in this case is completely different to the predicted one, indicating that the the electrode potential does not depend on the concentration of hydrogen ions. A reasonable explanation is that the potential of the electrode reflects the red-ox state of the active centre of tyrosinase.

A practical use of tyrosinase electrode needs an improvement of its construction and optimisation of the operation conditions.

References

[1] BRAUN S., RAPPAPORT S., ZUSMAN R., AVNIR D., OTTOLENGHI M., Mater. Lett., 10 (1990), 1.
[2] JIN W., BRENNAN J.D., Anal. Chim. Acta, 461 (2002), 1.
[3] WANG J., Anal. Chim. Acta, 399 (1999), 21.
[4] GILL I., BALLESTEROS A., TIBTECH, 18 (2000), 282.
[5] GILL I., Chem. Mater., 13 (2001), 3404.
[6] NILSSON H., ÅKERLUND A.-CH., MOSBACH K., Biochim. Biophys. Acta, 320 (1973), 529.
[7] ROBERTS D.C., OSBORN J.A., YACYNYCH A.M., Anal. Chem., 58 (1986), 140.
[8] PRZYBYT M., SUGIER H., Anal. Chim. Acta, 237 (1990), 399.
[9] PRZYBYT M., SUGIER H., Anal. Chim. Acta, 239 (1990), 269.
[10] KARYAKIN A.A., BOBROVA O.A., LUKACHOVA L.V., KARYAKINA E.E., Sens. Actuators B, 33 (1996), 34.
[11] TINKILIC N., CUBUK O., ISILDAK I., Anal. Chim. Acta, 452 (2002), 29.
[12] BOUBRIAK O.A., SOLDATKIN A.P., STARODUB N.F., SANDROVSKY A.K., EL'SKAYA A.K., Sens. Actuators B, 26, 27 (1995), 429.
[13] SINGH A.K., FLOUNDERS A.W., VOLPONI J.V., ASHLEY C.S., WALLY K., SCOENIGER J.S., Biosens. Bioelectr., 14 (1999), 703.
[14] SEKI A., IKEDA S., KUBO I., KARUBE I., Anal. Chim. Acta, 373 (1998), 9.
[15] OGURA K. NAKAOKA K., NAKAYAMA M., KOBAYASHI M., FUJII A., Anal. Chim. Acta, 384 (1999), 219.
[16] FLOUNDERS A.W., SINGH A.K., VOLPONI J.V., CARICHNER S.C., WALLY K., SIMONIAN A.S., WILD J.R., SCHOENIGER J.S., Biosens. Bioelectr., 14 (1999), 715.
[17] PANDEY P.C., SINGH G., TALANTA, 55 (2001), 773.
[18] PRZYBYT M., BIAŁKOWSKA B., *Enzyme Electrodes with Enzyme Immobilised by Sol-Gel Technique*, [in:] E. Buzaneva and P. Scharff (Eds.), *Frontiers of Multifunctional Nanosystems*, Kluwer Academic Publishers, Amsterdam, 2002, p. 91.
[19] DZYADEVYCH S.V., ANH T.M., SOLDATKIN A.P., CHIEN N.D., JAFFREZIC-RENAULT N., CHOVELON J.-M., Bioelectrochemistry, 55 (2002), 79.
[20] ANH T.M., DZYADEVYCH S.V., SOLDATKIN A.P., CHIEN N.D., JAFFREZIC-RENAULT N., CHOVELON J.-M., Talanta, 56 (2002), 627.
[21] LEE W.Y., KIM S.-R., KIM T.-H., LEE K.S., SHIN M.-C., PARK J.-K., Anal. Chim. Acta, 404 (2000), 195.
[22] SZUMINSKY N.J., CHEN A.K., LUI C.C., Biotechnol. Bioeng., 26 (1984), 642.
[23] WILSON R., TURNER A.P.F., Biosens. Bioelectr., 7 (1992), 165.
[24] ALVA S., GUPTA S.S., PHADKE R.S., GOVIL G., Biosens. Bioelectr., 6 (1991), 663.
[25] CASTNER J.F., WINGARD L.B.JR., Anal. Chem., 56 (1984) 2891.
[26] YAO T., TAKASHIMA K., Biosens. Bioelectr., 13 (1998), 67.
[27] CÉNOVAS F.G., TUDELA J., MADRID C.M., VARÊN R., CARMONA F.G., LOZANO J.A., Biochim. Biophys. Acta, 912 (1987), 417.
[28] SÁNCHEZ-FERRER Á., RODRÍGUEZ-LÓPEZ J.N., GARCÍA-CÁNOVAS F., GARCÍA-CARMONA F., Biochim. Biophys. Acta, 1247 (1995), 1.
[29] FUHRMANN B., SPOHN U., Biosens. Bioelectr., 13 (1998), 895.
[30] ORTEGA F., DOMINGUEZ E., JONSSON-PETERSSON G., GORTON L., J. Biotechnol., 31 (1993), 289.
[31] WANG J. FANG L., LOPEZ D., Analyst, 119 (1194), 455.
[32] MOORE B.M., FLURKEY W.H., J. Biol. Chem., 265 (1990), 4982.
[33] FERNANDES J.C.B., KUBOTA L.T., DE OLIVEIRA NETO G., Anal. Chim. Acta, 385 (1999), 3.
[34] CHEN Y., TAN T.C., Talanta, 42 (1995), 1181.

Received 17 July 2003
Revised 5 August 2003

Materials Science, *Vol. 21*, *No. 4*, *2003*

Application of the sol-gel method to the synthesis of ferroelectric nanopowders $(Pb_{1-x}La_x)(Zr_{0.65}Ti_{0.35})_{1-0.25x}O_3$, $0.06 \leq x \leq 0.1$

MAŁGORZATA PŁOŃSKA*, DIONIZY CZEKAJ, ZYGMUNT SUROWIAK

University of Silesia, Faculty of Engineering, Department of Materials Science,
ul. Śnieżna 2, 41-200 Sosnowiec, Poland

The aim of this study was to prepare pure, dense and transparent lead–lanthanum zirconate–titanate (PLZT) ceramics. The PLZT ceramics was sintered by the hot-pressing method from sol-gel derived powders. The samples obtained exhibited lack of voids, and the density close to the theoretical X-ray values. They were homogeneous from the chemical and physical points of view and exhibited stoichiometric chemical compositions. Dimensions of the crystallites depended on the temperature of sintering of the amorphous nanopowders. Dielectric and ferroelectric properties of the nanocrystalline PLZT ceramics were studied and relationships between their properties and processing conditions were revealed.

Key words: *sol-gel method; nanopowders; ceramics; PLZT; ferroelectric properties*

1. Introduction

Application of proper technological methods to the fabrication of ceramic powders is one of the factors improving the control of the stoichiometry of materials, influencing the properties of ferroelectric ceramic materials. The sol-gel method is a low-temperature process, which utilizes chemical precursors and makes it possible to obtain fine powders that exhibit high chemical reactivity, as well as better purity, homogeneity and physical properties than those fabricated by conventional high-temperature processes.

The lead–lanthanum zirconate–titanate (PLZT) ceramics is one of the ferroelectric materials, which is successfully obtained by the sol-gel method. The chemical composition of PLZT is given by the formula [1]:

*Corresponding author, e-mail: mplonska@ultra.cto.us.edu.pl.

$$(Pb_{1-x}La_x)(Zr_{1-y}Ti_y)_{1-0.25x}V_{0.25x}O_3 \quad (1)$$

The formula takes into account the charge compensation, assuming that the electrical neutrality is maintained by the creation of (Zr, Ti) vacancies (*V*). The concentration of La, x = La/(La + Pb), may vary from 0.02 to 0.3. The ratio y of Zr/(Zr + Ti) may take any value from 0 to 1. The composition of PLZT is usually represented by the notation $x/(1-y)/y$, which denotes the amounts of La/Zr/Ti, given in mole fractions or mole per cent (i.e. mole fraction multiplied by 100). For instance, the notation 8/65/35 represents PLZT with the chemical composition $(Pb_{0.92}La_{0.08})(Zr_{0.65}Ti_{0.35})_{0.98}O_3$ [2].

Lanthanum-doped lead zirconate–titanate ceramics, with variable dopant concentration and the ratio of Zr/Ti exhibit a variety of phases such as ferroelectric (FE), antiferroelectric (AFE), paraelectric (PE) and mixed (MPh) phases, shown in the room temperature phase diagram in Fig. 1 [3, 4].

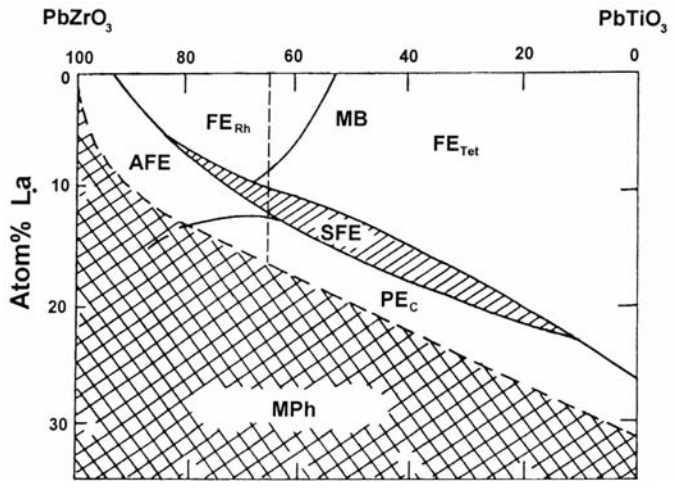

Fig. 1. Phase diagram of the PLZT system at room temperature [3]

The doping of La to the basic PZT system results in many effects such as enhanced dielectric and piezoelectric properties, increased squareness of the *P–E* hysteresis loops, decreased coercive field (E_c) and transparency [5].

The advantages of this material include not only the optical transparency, but also a fast response, multicolour capability and electrooptic properties. Solid-state nature of the material is based on the simple $PbZrO_3$–$PbTiO_3$ (PZT) solid solution system, the function of the La concentration as well as the Zr/Ti ratio, i.e., the *x*/65/35 composition yields the most transparent ceramics for La concentrations in the range of 8–16 mole per cent [2].

Nanocrystalline PLZT materials obtained from the sol-gel derived powders exhibit some features substantially increasing possibilities of their application in electronic and opto-electronic devices such as: segment displays, light shutters, coherent modu-

lators, colour filters, linear gate arrays and image storages. As a result, they have been widely investigated [6].

The goal of this study was: (i) to utilise a modified sol-gel method for obtaining amorphous PLZT nanopowders with the chemical composition corresponding to the *x*/65/35 ratio, where x = 6–10 mole per cent of La, (ii) to obtain transparent ceramics by the hot-pressing method, and (iii) to study their structure and basic dielectric properties.

2. Experimental

The technological process of fabrication of the PLZT ceramics included two basic stages. In the first stage, a modified sol-gel process was employed to obtain amorphous nanopowders of the ferroelectric PLZT ceramics with the following chemical compositions:

- $(Pb_{0.94}La_{0.06})(Zr_{0.65}Ti_{0.35})_{0.985}O_3$, 6/65/35 PLZT,
- $(Pb_{0.93}La_{0.07})(Zr_{0.65}Ti_{0.35})_{0.9825}O_3$, 7/65/35 PLZT,
- $(Pb_{0.92}La_{0.08})(Zr_{0.65}Ti_{035})_{0.98}O_3$, 8/65/35 PLZT,
- $(Pb_{0.91}La_{0.09})(Zr_{0.65}Ti_{0.35})_{0.9775}O_3$, 9/65/35 PLZT,
- $(Pb_{0.9}La_{0.1})(Zr_{0.65}Ti_{0.35})_{0.975}O_3$, 10/65/35 PLZT.

The second stage involved consolidation of the prepared powders and obtaining fine-grained PLZT ceramics by the hot-pressing method.

As the initial materials, the following high-purity organometallic salts of precursors were chosen:

- lead(II) acetate trihydrate, $Pb(COOCH_3)_2{\cdot}3\ H_2O$,
- lanthanum acetate hydrate, $La(COOCH_3)_3{\cdot}H_2O$,
- zirconium(IV) propoxide, $Zr(OCH_2CH_2CH_3)_4$,
- titanium(IV) propoxide, $Ti(OCH_2CH_2CH_3)_4$,
- *n*-propyl alcohol as a solvent,
- acatyloacetone as a stabilizing agent.

The processes used for preparation of PLZT are presented in the flow chart (Fig. 2).

The stoichiometric mixture of the components was disolved in *n*-propyl alcohol and then heated for 2 h below the boiling point of the solution. As a result of the reaction the alkoxide complexes and an organic ester were formed. The by-product of the synthesis (the ester – propyl acetate) was removed by simple distillation. The condensed form of the by-product needed an addition of the solvent and the stabiliser to form a sol. Distilled water was used to activate the reaction of hydrolysis. A gradual colloidal gel formation was then observed. The colloidal sol-gel system was IR -dried and calcined at T = 873 K. The calcined powders (i.e., the powders without organic components) consisted of small particles and agglomerates of nanoparticles. The powders were ground, mixed and sintered by the hot-pressing method at the temperature verified experimentally, T_s = 1473 K for 2 h.

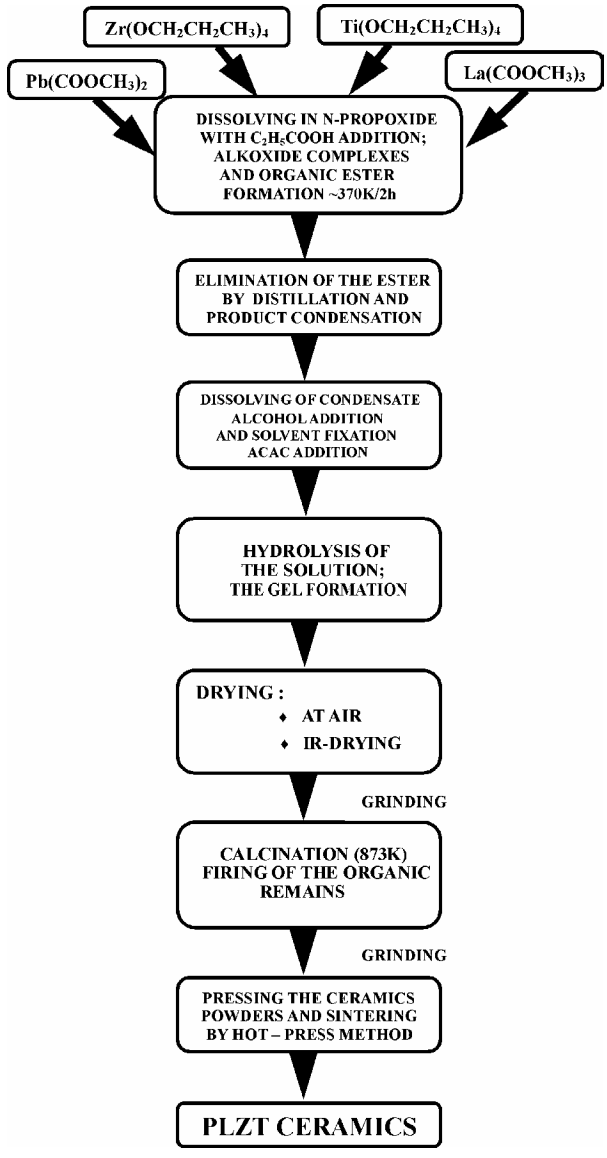

Fig. 2. Flow chart of the preparation of PLZT ceramics

X-ray analysis (Philips PW 3710 diffractometer, Θ–2Θ geometry, $CuK_{\alpha 1}$ radiation) was used to characterise the structure of the PLZT samples (the calcined powders and the hot-pressed ceramics were studied). Electrodes were formed with a silver paste on disk-shaped ceramic samples. A Tesla BM 595 RLCG meter was used to perform measurements of temperature dependences of the electric permittivity ε and the dielectric loss tangent $\tan\delta$. The dielectric hysteresis loops were recorded with the Sawyer–Tower method.

3. Results and discussion

X-ray spectra were recorded for the powdered gel, the calcined powder (i.e., the powder devoid of organic remains) and the powdered PLZT ceramics obtained by the hot-pressing method. Figure 3 presents the thermal evolution of the crystal structure of the 8/65/35 PLZT material. The X-ray pattern of the IR-dried powdered gel indicates the presence of the diffraction lines originating from the organic remains. Their calcination (T = 873K) leads to the crystallisation of PLZT in the rhombohedral symmetry. The crystal structure was identified as a rhombohedral one with the space group $R3m$ and the parameters of the unit cell equal to a_h = 0,5745 nm and c_h = 0,7060 nm (the hexagonal setting was used for the indexing).

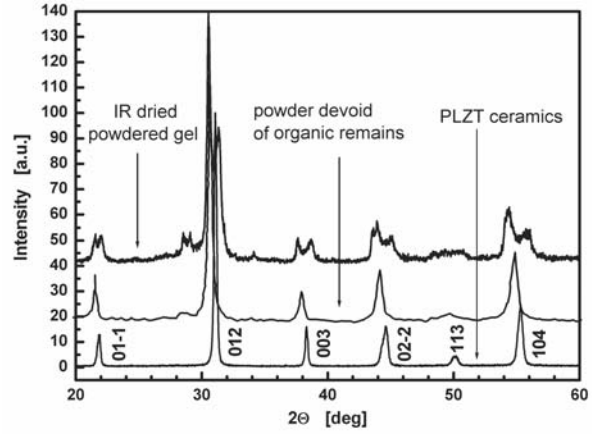

Fig. 3. X-ray powders diffraction diagrams of 8/65/35 PLZT at 3 stages of the ceramics preparation

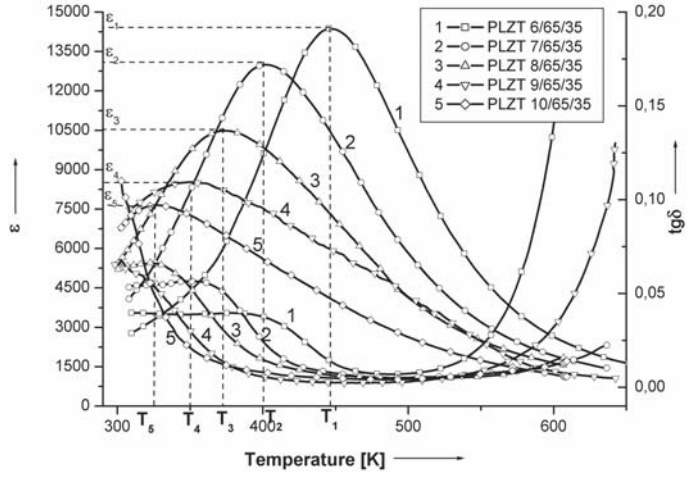

Fig. 4. Temperature dependence of the relative electric permittivity ε and the dielectric loss tangent $\tan\delta$ for the selected PLZT compositions with Zr/Ti = 65/35

The dielectric parameters (the electric permittivity ε and the dielectric loss tangent $\tan\delta$ were measured by the bridge method. The results are shown in Fig. 4.

As can be seen in Fig. 4, the increase of the La content reduces the height of the dielectric constant peak and makes it more diffuse. A significant change in the maximal temperature of the peak (the table) is also observed. The loss tangent increases with the increase of the La content. It reaches the maximum values of $\tan\delta = 0.02$ and $\tan\delta = 0.06$ for $x = 0{,}06$ and $x = 0.10$, respectively. The results obtained are typical of materials exhibiting diffuse phase transitions.

Table. Selected properties of the PLZT ceramics

Composition	Density [g/cm^3]	T_0 [C°]	T_m [°C]	ε_m
PLZT 6/65/35	7.715	222	189	13570
PLZT 7/65/35	7.705	168	143	12590
PLZT 8/65/35	7.660	120	108	9980
PLZT 9/65/35	7.630	64	83	8550
PLZT 10/65/35	7.550	16	60	7370

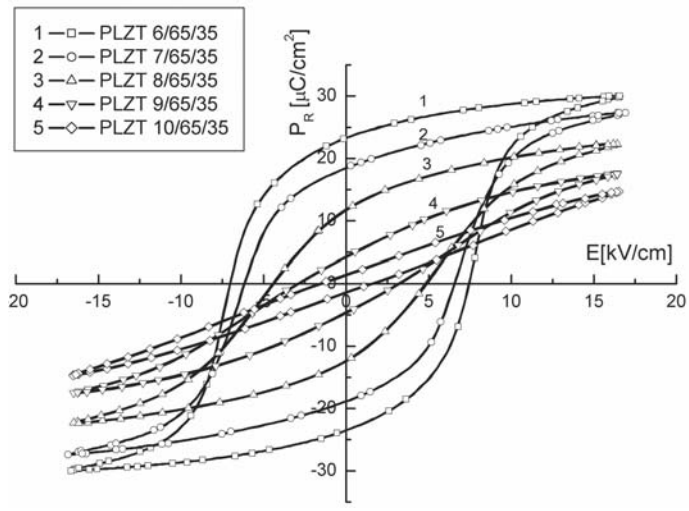

Fig. 5. *P–E* hysteresis loops of the PLZT *x*/65/35 ceramics (for x = 6–10 La mole per cent) measured for 1 Hz at room temperature

Ferroelectric properties of PLZT ceramics obtained by the hot-pressing method from the sol-gel derived powders have been proved by the ferroelectric hysteresis loops. The results of these investigations are presented in Fig. 5. Remanent polarization and coercive field have been measured at the frequency of $\nu = 1$ Hz at room temperature. Figure 5 shows that the increase in the La mole fraction from 0.06 to 0.1

(for the constant Zr/Ti ratio) results in disappearance of the hysteresis loop. Our investtigations showed that the application of the hot-pressing method to consolidation of sol-gel derived powders and sintering of ceramics makes it possible to prepare transparent PLZT materials. Figure 6 shows a selected sample of PLZT 10/65/35 material exhibiting a good optical transparency.

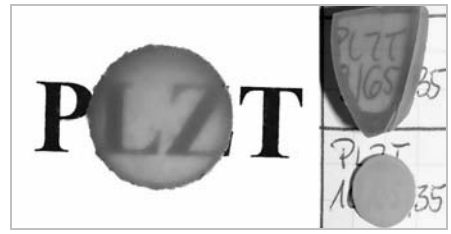

Fig. 6. Optical transparency of the PLZT 10/65/35 ceramics

4. Conclusions

By employing the sol-gel method, amorphous nano-powders of PLZT ceramics were obtained. Transparent PLZT ceramics, exhibiting rhombohedral symmetry, have been obtained by means of the hot-pressing method. The ferroelectric properties of the sintered ceramics have been proved by measurements of the ferroelectric hysteresis loop. Dielectric, ferroelectric and optical properties (i.e., transparency in the visible region) of PLZT ceramics prove high quality of the obtained ceramics.

Acknowledgements

Investigation was partly financed within the confines of the grant No. 4T08 D 020 24 supported by the State Committee for Scientific Research.

References

[1] PEREIRA M., MANTAS P.Q., Key Eng. Materials, 132–136 (1997), 1123.
[2] XU Y., *Ferroelectric Materials and Their Applications*, Elsevier, Amsterdam, 1991.
[3] HAERTLING G.H., Ferroelectrics, 75 (1987), 25.
[4] HAERTLIG G.H., *Piezoelectric and Electrooptic Ceramics,* [in:] *Ceramic Materials for Electronics. Processing, Properties, and Applications*, R.C. Buchanan (Ed.), Marcel Dekker, New York, 1986, pp. 139–225.
[5] JIANG Q. Y., SUBBARAO E.C., CROSS L.E., J. Appl. Phys., 75, 11 (1994), 7433.
[6] HAERTLING G.H., J.Am. Ceram. Soc., 82, 1 (1999), 797.

Received 22 July 2003
Revised 21 October 2003

Materials Science, Vol. 21, No. 4, 2003

Application of the sol-gel method to deposition of thin films

ALDONA ZARYCKA*, JAN ILCZUK, DIONIZY CZEKAJ

University of Silesia, Faculty of Engineering, Department of Materials Science,
ul. Żeromskiego 3, 41-200 Sosnowiec, Poland

A method for synthesizing ferroelectric thin films of lead zirconate-titanate (PZT) and lead-lanthanum zirconate-titanate (PLZT) by a modified sol-gel technique is reported. The following chemical compositions with the Zr/Ti ratio were obtained: PZT 65/35 and PLZT 6.5/65/35. Thin films, prepared from acetate and alkoxide precursors of La, Pb, Zr and Ti, were deposited on stainless steel and MgO substrates by spin coating. Crystallization of PZT-based electroceramic thin films was performed by thermal annealing at the temperature range of 550–700 °C. The structure of the thin films was investigated by X-ray diffraction. The formation of the perovskite-type structure was confirmed. Microstructure was investigated by the optical microscopy. Technological conditions of the preparation of thin films were optimized.

Key words: *sol-gel method; ferroelectric ceramics; PLZT; PZT*

1. Introduction

Metal oxides with the perovskite structure are very important materials for technological applications due to their ferroelectric properties. An increasing interest in lead zirconate-titanate $Pb(Zr_x Ti_{1-x})O_3$ (PZT) thin films has been observed for such applications as nonvolatile ferroelectric memory elements, sensors and optical devices. These applications are possible due to a high capacity of load storage, low coercive field and large thermal stability of PZT with compositions near the morphotrophic phase boundary (MPB). In practice, the MPB of PZT ceramics exists over a defined range of x ($x \sim 0.53$) and involves a coexistence of the tetragonal and rhombohedral phases due to variations of the composition. These variations give rise to local differences in the lattice parameters, which have a strong influence on the ferroelectric properties [1].

*Corresponding author, e-mail: azarycka@us.edu.pl.

The method of the sol-gel fabrication of ferroelectric thin films gained much interest because of its simplicity, low processing temperature, stoichiometry control and its ability to produce uniform, chemically homogenous films over large areas that can provide integration with other circuit elements. The sol-gel method can be successfully used for preparation of pure oxides applied in electronics, optics, as ceramics for utilization of radioactive wastes as well as filters in chemical and food industries. During the last few years, this method has also been applied to the synthesis of high-temperature superconductors (HTSC). Lead zirconate-titanate films have a wide range of applications, which include pyroelectric sensors [1, 2] and infrared thermal imaging devices, micro-electromechanical devices and ferroelectric random-access memories (FeRAM). Thin films for these applications must have a reproducible stoichiometry, fine homogeneity of compact structures and good electric properties. Moreover, processing of thin films must be compatible with the planar technology of semiconductors. These properties can be obtained for ferroelectric thin films deposited by the sol-gel technique [3].

The purpose of the research presented in this paper was to grow perovskite-type PZT and PLZT thin films on both, metal and single crystal substrates by the modified sol-gel technique, as well as to identify their crystal structures and microstructures.

2. Experimental

For the preparation of PZT material, metal organic precursors such as lead(II) acetate $Pb(CH_3COO)_2{\cdot}3H_2O$, zirconium(IV) propoxide, $Zr(OCH_2CH_2CH_3)_4$, titanium(IV) propoxide, $Ti(OCH_2CH_2CH_3)_4$ were used. For the preparation of PLZT material, a lanthanum containing metal-organic precursor, lanthanum(III) acetate, $La(CH_3COO)_3{\cdot}H_2O$, was also used. In the latter case, the chemical reaction can be written as:

$$(1-x)\mathrm{Pb(OAc)_2} + x\mathrm{La(OAc)_3} + (1-0.25x)[(1-y)\mathrm{Ti(O\text{–}}n\mathrm{Pr)_4}] \rightarrow (\mathrm{Pb_{(1-x)}La_x(Zr_yTi_{(1-y)})_{(1-0.25x)}} + n\mathrm{PrOOAc} \quad (1)$$

where the coefficient $0.25x$ comes from the demand for the electrical neutrality of PLZT. The electrical neutrality is maintained by the creation of $0.25x$ of (Zr, Ti) vacancies (x is the mole fraction of La used for ceramic preparation). The ratio y of Zr/(Zr + Ti) may take any value from 0 to 1 (y is the mole fraction of Zr used for ceramic preparation).

n-Propanol was used to dissolve all compounds and to form a solution. The synthesis was carried out in the argon atmosphere by heating the solution for 2 h below the solvent boiling point to form alkoxide complexes. The by-product obtained (propyl acetate ester) was removed from the solution by distillation. After cooling the reaction mixture to room temperature, *n*-propanol and acetyloacetone were added. The mixture was then hydrolysed (distilled water was used to activate the hydrolysis

reaction) and a colloid solution was formed. In few minutes, the sol-gel system was formed. The PZT and PLZT thin films were deposited on stainless steel and MgO substrates by spin coating. Crystallization of PZT- and PLZT-based ceramics thin films was performed by thermal annealing at temperatures ranging between 550 and 700 °C [4–6]. The whole process is presented in Fig. 1.

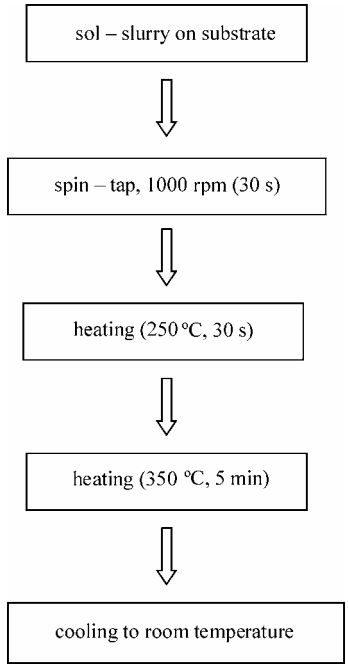

Fig. 1. Flow chart of preparation of PZT and PLZT thin films

2. Results

The crystal structure of the thin films was investigated by the X-ray diffraction method (X′ Pert Philips PW 3710 diffractometer, Θ–2Θ geometry, CuK_α radiation). Figure 2 shows the X-ray diffraction pattern recorded for a PLZT thin film grown on an MgO substrate. The strong line at $2\Theta = 43°$ originates from the MgO substrate. The other experimental diffraction lines correspond well to the assumed *R*3*m* space group. Parameters of the unit cell have been found as follows: $a_h = 0.5781$ nm, $c_h = 0.7081$ nm.

In Figure 3, the XRD pattern of the PZT thin film deposited on a stainless steel substrate is presented. The pattern was identified as a mixture of the rhombohedral *R*3*m* phase with the following parameters of the elementary cell: $a_h = 0.5802$ nm, $c_h = 0.7085$ nm and the tetragonal *P*4*mm* (group No. 99) unit cell with: $a_t = 0.4047$ nm, $c_t = 0.4132$ nm.

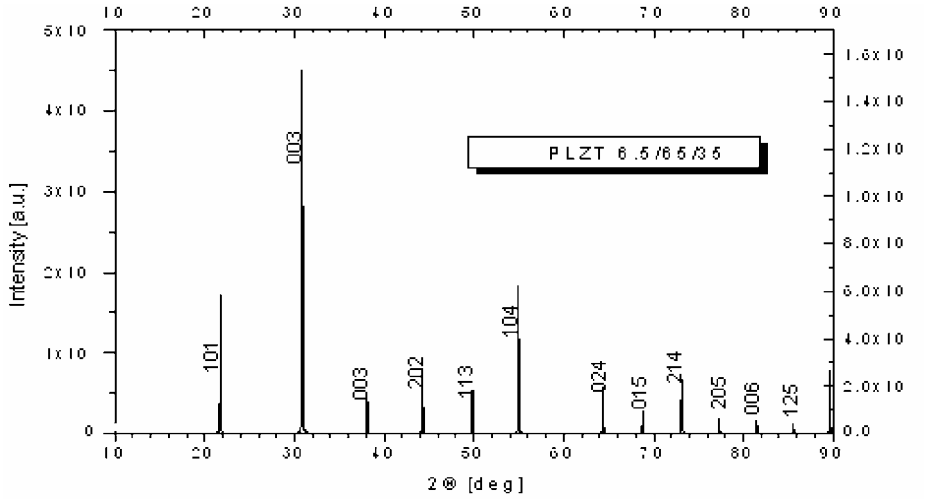

Fig. 2. X-ray diffraction pattern of PLZT on MgO

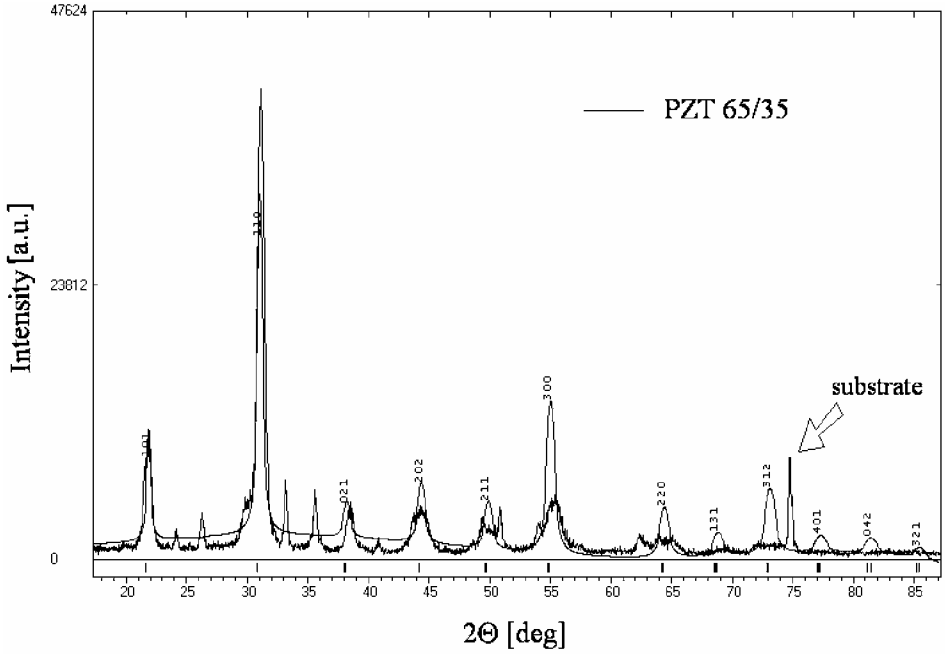

Fig. 3. X-ray diffraction pattern of PZT on stainless steel

The structure was identified as a mixture of the tetragonal and rhombohedral phases, their amounts depending on the technology of fabrication. The rhombohedral (101) (110) peaks were detected in the PLZT and PZT thin films. This indicates that the morphotropic phase boundary moved toward the Ti-rich composition and the PZT 65/35 film contained only the rhombohedral structure [5].

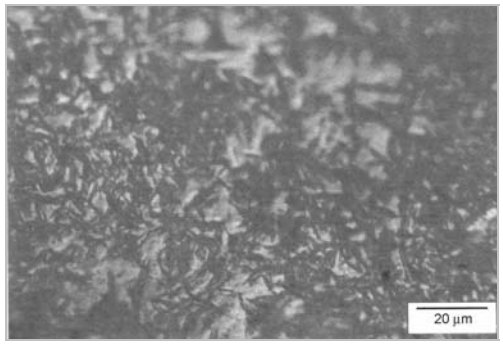

Fig. 4. Microstructure of PLZT film on MgO

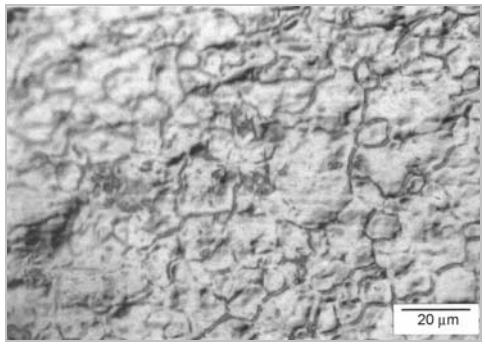

Fig. 5. Microstructure of PZT film surface on stainless steel

Both films exhibit a dense microstructure with no cracks (Figs. 4 and 5). The results of the investigations suggest that our modified sol-gel technique can prevent the formation of cracks and yield dense microstructures of the perovskite type for both PZT and PLZT thin films on metal and single-crystal substrates [7].

3. Conclusions

The purpose of the present research was to grow perovskite-type PZT and PLZT thin films on both metal and single-crystal substrates by a modified sol-gel technique, as well as to investigate their crystal structures and microstructures.

All the preparation steps, including the coating procedure, are relatively simple and can be carried out in the air. The fabricated films are dense and crack-free. The crystal structures of PZT and PLZT depend on the process of fabrication. A mixture of tetragonal and rhombohedral structures was identified for PLZT, whereas PZT thin films contained only the rhombohedral phase.

References

[1] SUROWIAK, Z., Mol. Quant. Acoust., 21 (2000), 267.
[2] SUROWIAK Z., DUDKEVICH V. P., *Cienkie warstwy ferroelektryczne* (*Thin Ferroelectric Films*, in Polish), Wyd. Uniw. Śl., Katowice, 1996.
[3] CZEKAJ D., *Technology, Properties and Applications of PZT Thin Films*, Wyd. Uniw. Śl., Katowice, 2002.
[4] MATTHES B., TOMANDL G., WERNER G., J. Ceram. Soc., 19 (1999), 1387.
[5] PAIK D.S., KOMARNENI S., Mat. Res. Bull., 32, 8 (1997), 1091.
[6] CARUSO R., DE SANCTIS O., FRATTINI A., STEREN C., GIL R., Surface and Coatings Techn., 122 (1999), 44.
[7] MENG X. J., CHENG J.G., LI B., GUO S.L., YE H.J., CHU J.H., J. Cryst. Growth, 208 (2000), 541.

Received 15 June 2003
Revised 14 October 2003

Materials Science, Vol. 21, No. 4, 2003

Crystallization of TiC and TiN from a colloidal system

ANNA BIEDUNKIEWICZ*

Institute of Materials Engineering, Technical University of Szczecin,
al. Piastów 19, 70-310 Szczecin, Poland

The sol-gel processing of materials offers several potential advantages over conventional methods. The most important are improved properties thanks to the specific microstructural features. The paper presents the synthesis of TiC and TiN powders and coatings by the sol-gel method. Parameters of the processes were found to influence the structures, chemical compositions and morphologies of TiC and TiN, which were examined using the following analytical techniques: SEM, TEM, XRD, EDX and WDS.

Key words: *titanium carbide; titanium nitride; sol-gel method; composites; coatings*

1. Introduction

The utilization of 'soft' chemical methods of activation of chemical reactions in liquids or in sol-gel precursors are modern directions of material engineering. These methods enable the design of materials starting from well-defined clusters or molecules to complex architectures of final products [1, 2]. Reactions proceed in such systems at lower temperatures in comparison to conventional methods (such as syntheses in gas phases or those based on solid-state reactions) and require lower energies.

Carbides, nitrides and carbonitrides are materials that have properties desirable for a variety of applications. Their key properties are high hardness and strength along with resistance to heat, corrosion and wear. A common feature of the methods already developed for the preparation of titanium carbide in the form of powders, fibres and coatings is the application of energy to activate the chemical processes. Thermal energy, low-temperature plasma and ionizing radiation are, for instance, utilized in the CVD, PACVD and PAPVD processes [3, 4].

The sol-gel based processes utilize chemical methods of activation yielding continuous forms of matter organization. Organotitanium compounds containing a carbon-titanium bonds are characterized by a low durability and an extreme sensitivity to

*E-mail: Anna.Biedunkiewicz@ps.pl.

the air and humidity [5–7]. Higher stability of the Ti–O–C bonds makes it easier to prepare, store and use such compounds than compounds containing only the Ti–C bonds. A higher affinity of titanium towards oxygen at temperatures below 1000 K prevents their conversion to titanium carbide and nitride. The conversion of titanium oxides or the systems with Ti–O–C bonds to carbide and titanium nitride proceeds under conditions of the carbothermal reduction at elevated temperatures [8]. Thin films of titanium carbide have been obtained by the polymerization process using transesterification of titanium tetraizopropylate with α,α′-diacetateorthoxylene, followed by thermal conversion of the polymer obtained [9]. With regard to the systems with Ti–O–C bonds, the conversion of these precursors to titanium carbide proceeds under conditions of the carbothermal reduction, i.e. above 1073 K. Similar compounds have been obtained as a result of the polymerization of titanium alcoholates with polyalcohols, hydroxylated polymers, resins and cellulose as well as with dicarboxylic acids [10–13].

In the present work, mixtures of polyacrylonitrile, dimethylformamide and titanium chlorides were used to form gels containing Ti–C bonds and being precursors for the synthesis of titanium carbide as well as titanium nitride. According to the hypothesis formulated in [14], the dispersed phase of the gel is formed by polymerizing polyacrylonitrile crosslinked with titanium chlorides, which initially form connections with the polymer chains as a result of intermolecular interactions and chemical bonds. Dimethylformamide acts as the dispersing agent in the system.

2. Experimental

The preparation of the organotitanium precursor was described in the previous papers [14, 15]. All the operations were carried out in a glove box in the protective atmosphere of argon using the Schlenk technique. The gel was applied onto substrates based on sintered aluminum oxide and on nitrided Armco iron surfaces. Before the coating, the substrates were polished and washed with an organic solvent. Armco iron samples were nitrided at 843 K in the ammonia atmosphere for 1h. The dissociation degree of ammonia was equal to 49%. The samples covered then with the gel and the gel samples were heated in a furnace in inert and/or reactive atmospheres depending on the desired products. The heating was carried out in gas atmospheres which contained argon and/or nitrogen, hydrogen and ammonia, under the atmospheric pressure at temperatures ranging from 293 to 1273 K. The reactions of TiC and TiN phases proceeded at temperatures lower than 800 K. The parameters of manufacturing of TiC and TiN with or without carbon as coatings and powders are subjected to the patenting procedure.

The following techniques were applied for the sample characterization: scanning electron microscopy (JEOL JSM 6100), X-ray diffraction (PHILIPS X'PERT), transmission electron microscopy and electron diffraction (JEOL JEM 1200EX). The TiC/C and TiN powders, Ti–C coatings, and the TiN/C pumice were additionally

characterized by the microanalysis (wavelength dispersive and energy dispersive spectroscopies) using an IBEX System Noran Instruments and an Oxford ISIS 300.

3. Results and discussion

Organotitanium compounds being the key precursors for obtaining the TiC and TiN materials have already been described in the literature, e.g. $Ti[N(C_2H_5)_2]_4$ [16, 17], $Ti(bipy)_3$ [5], $Ti[CH_2C(CH_3)_3]_4$ [6] and others. They all allow us to lower the temperature of the TiC and TiN syntheses in comparison to temperatures of conventional syntheses and also enable the achievement of unique microstructural properties. The compounds containing carbon-titanium bonds are characterized by a low durability and an extreme sensitivity to the air and humidity.

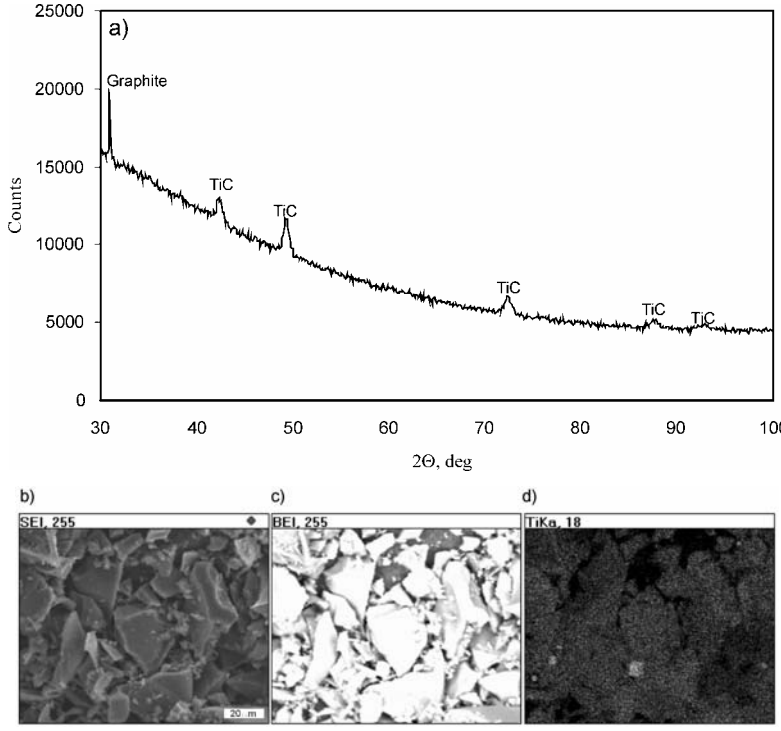

Fig. 1. X-Ray powder diagram (CoK_α) of the TiC/C powder (a), SEI image (b), BEI image (c), and mapping of the Ti distribution in the powder (d)

Similarly to the above-mentioned organotitanium compounds, the gel precursors which were synthesized from mixtures of polyacrylonitrile, dimethylformamide and titanium chlorides contain the Ti–C bonds and allow to synthesize titanium carbide as well as titanium nitride at lower temperatures, i.e. below 800 K. The advantages of the gel precursors include their higher durability in the air as well as all the common benefits of the sol-gel method.

The X-Ray powder diagram and the SEM images of the TiC/C composite powder prepared by the sol-gel method are presented in Fig. 1. As can be clearly seen, the powder contains two crystalline phases: graphite and titanium carbide. The microscopic and microanalysis results suggest that TiC is homogeneously dispersed in a carbon matrix (Fig. 1b, c, d). The same results have been obtained for the TiN/C system (Fig. 2). Saturation of the solution influenced the rate of the nucleation of TiC and TiN (Fig. 3). The TEM investigations of the TiC and TiN particles showed that they were formed with the average grain size below 100 nm.

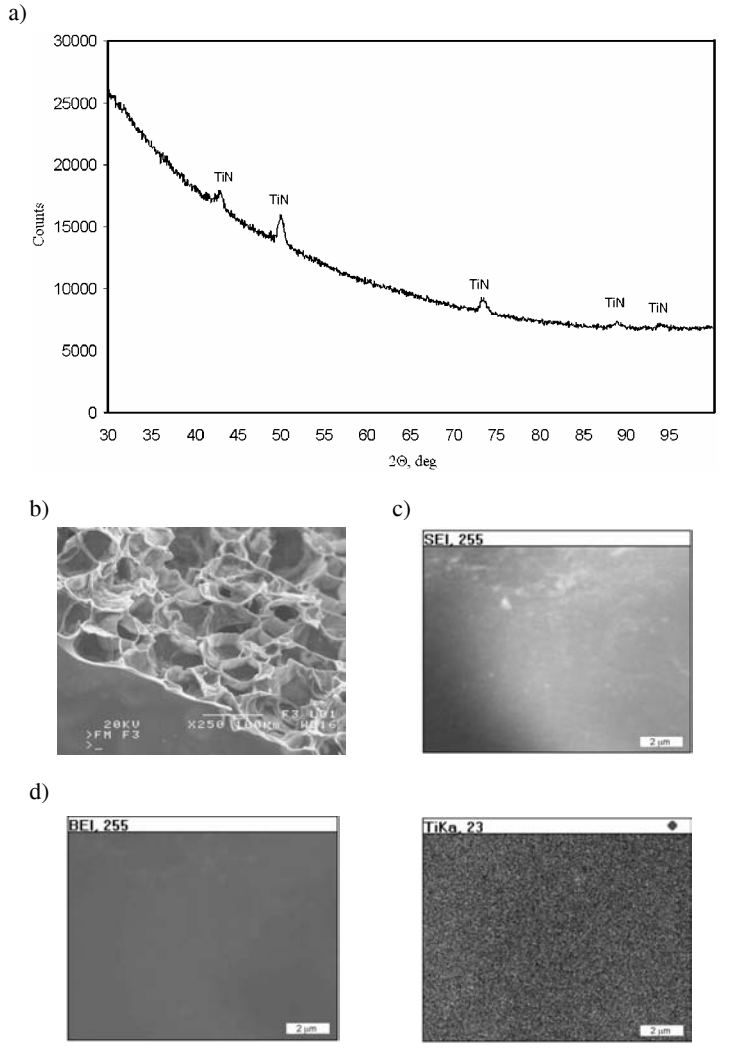

Fig. 2. X-Ray powder diagram (CoK_α) of the TiN\C pumice (a), SEM image of TiN\C (×250) (b) and EDS images: SEI (c), BEI (d) and mapping of the Ti distribution in the TiN-amorphous carbon pumice (×10 000)

Two competitive reactions ran during the syntheses of the Ti–C–N materials, i.e. the synthesis of titanium carbide or nitride and the formation of carbon, as becomes evident upon comparing Figs. 1 and 4. Figure 1 shows the X-Ray diagram of the crystalline TiC/graphite powder and Fig. 4 shows the crystalline TiC/amorphous carbon powder. They were obtained under various heating conditions. The conditions such as the temperature, time, heating rate and chemical composition of the gaseous atmosphere influence the form (powder or pumice) and the phase compositions of the products (Figs. 1, 2, 5).

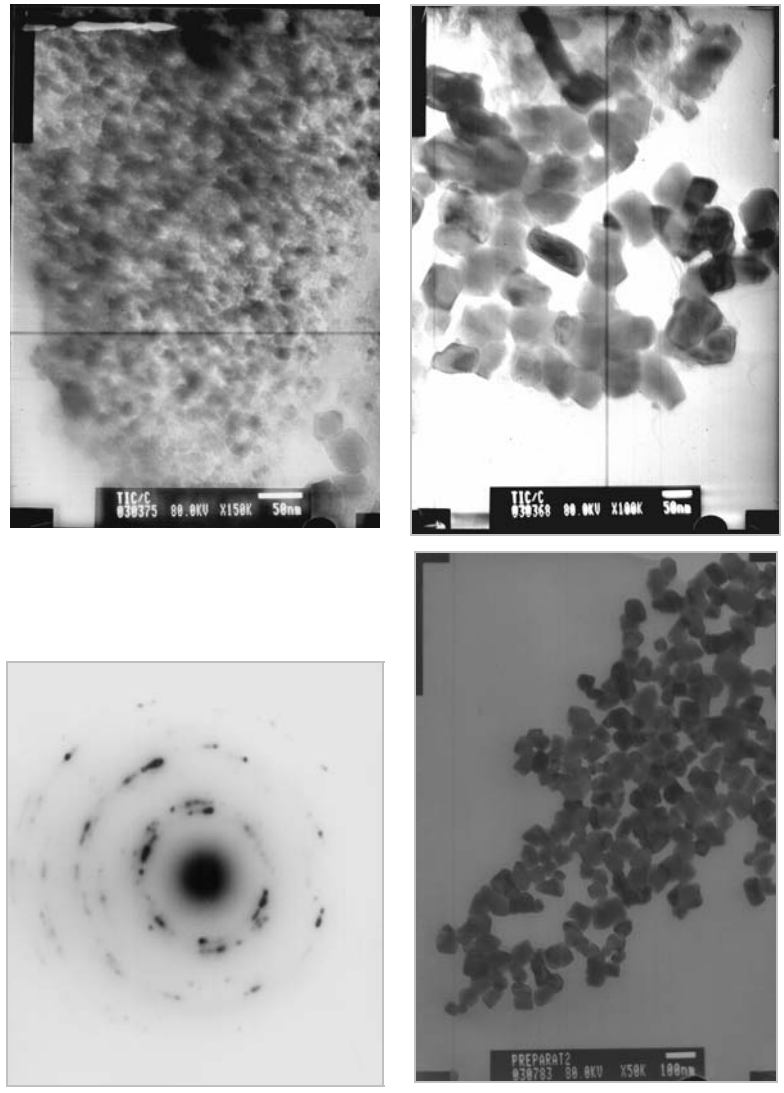

Fig. 3. Transmission electron micrographs and electron diffraction pattern of the nanocrystalline TiC particles obtained from differently saturated precursors

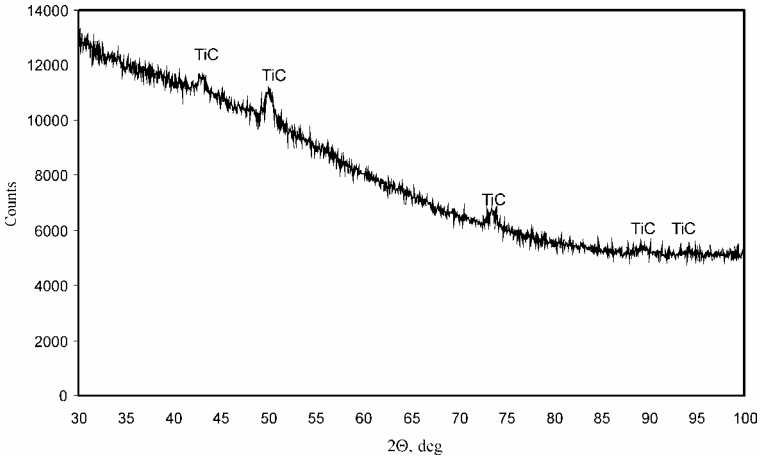

Fig. 4. X-Ray powder diagrams of the products obtained during the synthesis of the TiC/C powders (CoK_α)

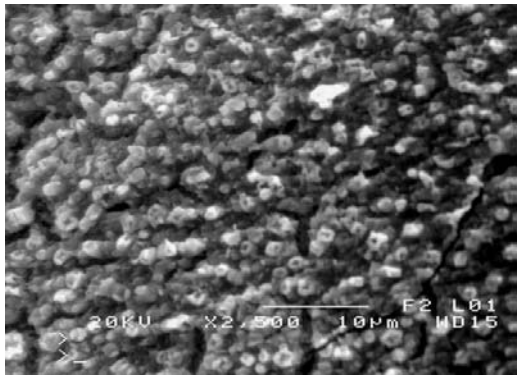

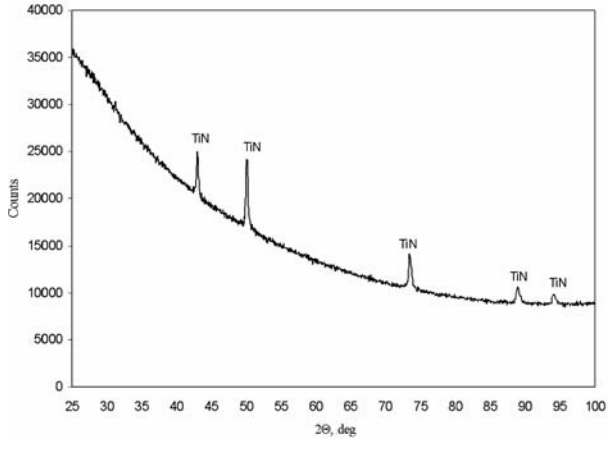

Fig. 5. SEM image and X-Ray powder diagram (CoK_α) of the TiN powder

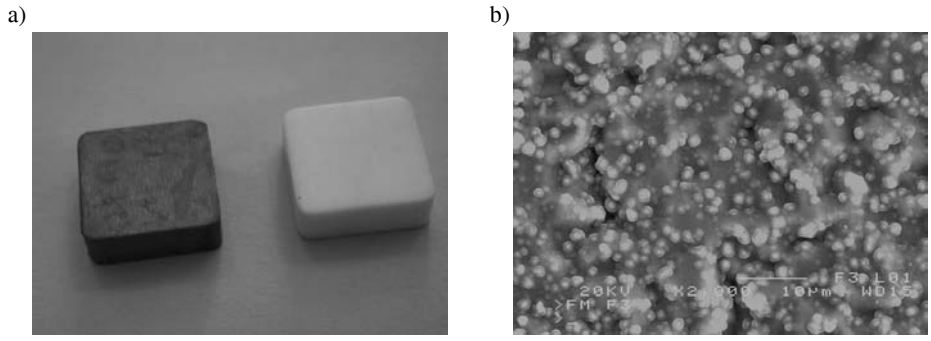

Fig. 6. Photographs of the cutting tools: a) sintered aluminium oxide with the Ti–C coatings, and without the coating (white), b) SEM image of the surface of the Ti–C coating

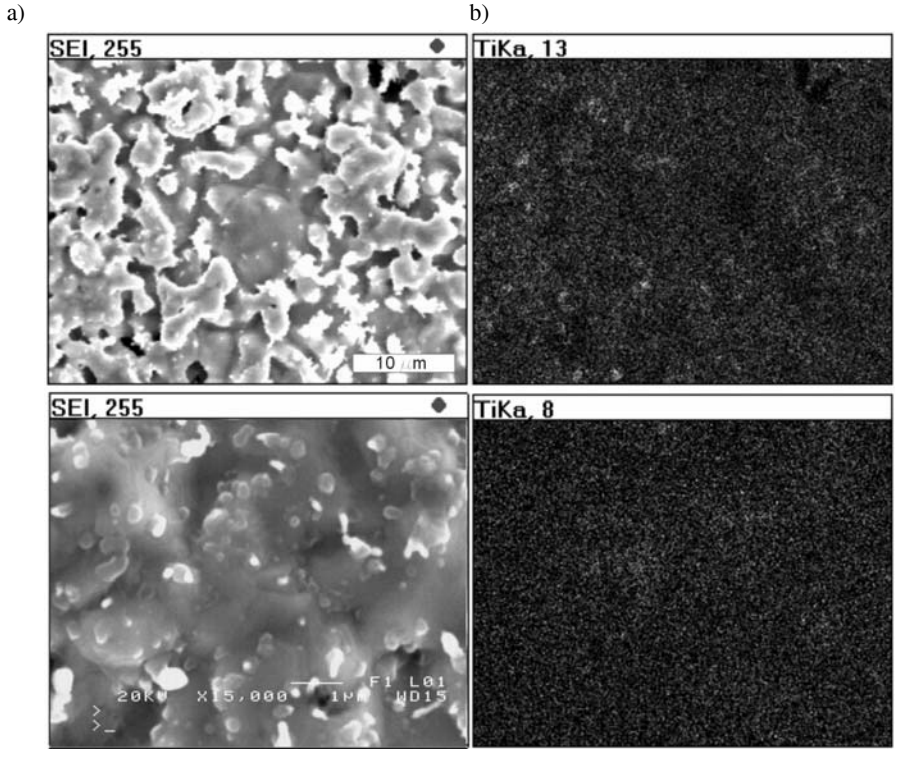

Fig. 7. SEM images of the surface of the Ti–C coatings on nitrided Armco iron surface (a) compared with mappings of the Ti distribution (b)

It has been observed that the substrate altered the conditions of the crystallization and the nucleation rates during the processes of coating production in which the gel precursor was used. The Ti–C coatings were deposited on the sintered aluminum oxide (Fig. 6) and nitrided Armco iron (Fig. 7a) substrates using the same parameters as those applied during of the process of the TiC/graphite composite synthesis. The

WDS chemical analysis indicated the ratio of C : Ti > 1. These coatings are amorphous, with titanium being homogenously dispersed in the carbon matrix as is illustrated in Fig. 7b.

4. Conclusions

The results of the investigations of the titanium carbide and nitride nanocomposites are presented. The materials were fabricated using organotitanium precursors. During the synthesis of Ti–C–N materials, two competitive reactions take place, i.e. the synthesis of titanium carbide or nitride and the formation of carbon. Saturation of the solution influences the size of the crystallites of TiC and TiN. The parameters of the TiC and TiN manufacturing with or without carbon as powders, pumice and coatings are subjected to patenting procedure. The sol-gel synthesis of the Ti–C–N materials may be an attractive starting point for low-temperature Ti–C–N coating technologies.

Acknowledgements

Financial support of the project No. 4 TO8C 00924 by the State Committee for Scientific Research, 2003–2006 is gratefully acknowledged.

References

[1] SANCHEZ C., SOLLER-ILLIA G.J. DE A.A., RIBOT F., LALOT T., MAYER C.R., CABUIL V., Chem. Mater., 13 (2001), 3061.
[2] CARUSO R.A., ANTONIETTI M., Chem. Mater., 13 (2001), 3272.
[3] SOKOŁOWSKA A., *Niekonwencjonalne środki syntezy materiałów* (*Unconventional Means for Materials Synthesis*, in Polish), WNT, Warszawa, 1991.
[4] OHRING M., *The Materials Science of Thin Films*, Academic Press, New York, 1992.
[5] KALOYEROS A.E., HOFFMAN M., WILLIAMS W.S., Thin Solid Films, 141 (1986), 231.
[6] GIROLAMI G.S., JENSEN J.A., KALOYEROS A.E., WILLIAMS W.S., ALLOCCA C.M., POLLINA D.M., J. Am. Chem. Soc., 109 (1987), 1579.
[7] DAVIDSON P.J., LAPPERT M.F., PEARCE P., Chem. Rev., 76 (1976), 219.
[8] WHITE G.V., MACKENZIE K.J.D., J. Mater. Sci., 27 (1992), 4294.
[9] GALLO T., GRECO C., SIMMS B., CAMBRIA F., *Covalent Ceramics*, [in:] *Extension to Proceedings of Symposium N. 1990 Fall Meeting of the Materials Research Society*, G.S. Fischman, R.M. Spriggs (Eds.), Materials Research Society, Boston, 1990, pp. 29–32.
[10] JIANG Z., RHINE W.E., Chem. Mater., 3 (1991), 1232.
[11] KRUMBE W., LAUBACK B., FRANZ G., U.S. Patent 4 948 762, 1990.
[12] JANEY M.A., U.S. Patent 4 622 215, 1986.
[13] GALLO T., GRECO C., PETERSON C. CAMBRIA F., BURK J., Mater. Res. Soc., 271 (1992), 887.
[14] BIEDUNKIEWICZ A., Thesis, Technical University of Szczecin, Poland, 1996.
[15] BIEDUNKIEWICZ A., JASIŃSKI W., LENART S., Vacuum, 50 (1998), 65.
[16] GONSALVES K.E., KEMAIYAN K.T., Solid State Ionics, 32/33 (1989), 661.
[17] CHIU H-T., HUARG C-C., Mater. Lett., 16 (1993), 194.

Received 15 June 2003
Revised 14 October 2003

Materials Science, Vol. 21, No. 4, 2003

Silicate solvated by an organic solvent as electrolyte or electrode material

MARCIN OPALLO*

Institute of Physical Chemistry, Polish Academy of Sciences,
ul. Kasprzaka 44/52, 01-224 Warszawa, Poland

Preparation and properties of silicate gels solvated by organic solvents as electrolytes or electrode materials were summarised. A silicate matrix based on tetraalkoxysilane, trialkoxysilane modified with organic groups or a mixture of these two, modified by organic solvents or solutions is the principal component of all the systems studied. The material used as the electrolyte is filled with a salt solution in an organic polar solvent or in the case of hybrid organic-inorganic silicate matrix it is functionalised with tetraalkylammonium groups with a pure solvent. The electrodes are made of a composite material consisting of graphite particles, silicate matrix functionalised with methyl groups and filled with a pure or diluted redox liquid.

Key words: *sol-gel; solid electrolyte; electrode; silicate; redox liquid; ion transfer*

1. Introduction

Typically, the synthesis of silicate glass based on the sol-gel process and performed at ambient conditions is aimed at preparation of xerogels with the amount of liquid left reduced to minimum [1]. However, the impregnation of a silicate matrix or composite material with silicate glass as one of the components, with carefully selected organic liquid, may result in a solid material having some properties of the latter. Among them is high mobility of molecules or ions dissolved in impregnating liquid. This is because the pore diameter of sol-gel silicate glass is in the range of several to several hundred nanometres [1]. Its comparison with the size of typical molecules or ions shows that at least a single molecule or ion with its solvation shell is able to move along the pores.

*E-mail: mopallo@ichf.edu.pl.

In the paper, the results of the research on preparation and properties of solid electrolytes or modified electrodes based on this concept are summarised, also in relation to those already published. The paper is restricted to silicate matrices solvated by solutions of substances in organic solvents or pure organic solvents. This approach can be considered as a variant of the popular modification of glass by organic substances by sol doping [2] or covalent bonding [3]. It has to be emphasized that it is not restricted to electrochemistry. Silica sol-gel glasses with embedded organic liquids can be used as containers for oil solutions of flavours or fragrances [4]. This is because encapsulated substances offer greater convenience, improved storage stability and possibility of their controlled release [4]. Electrochemical redox reactions in solid electrolytes based on the solvated silica sol-gel glass were recently reviewed [5].

2. Solid electrolytes based on solvated silicate gels

Solvated gels acting as solid electrolytes consist of silicate matrices impregnated by ionic solutions in organic solvents. They are based on unmodified or modified silicates. Tetramethoxysilicate (TMOS) or tetraethoxysilicate (TEOS)-based matrix solvated by salt solutions in viscous organic polar solvents like ethylene carbonate (EC), propylene carbonate (PC) or sulpholane (TMS) [6–16] belong to the first group. Other are based on hybrid organic-inorganic matrices [17–19].

The matrix composed of silicate and hydrocarbon-based chain elements and filled with Li^+ solution in a polar organic solvent mixture [17] was applied as the electrolyte in lithium secondary batteries [18]. The presence of short alkyl chains makes the matrix flexible and reduces the number of unreacted hydrophilic groups OH bonded to Si atoms. Recently, our group prepared a solid electrolyte consisting of a hybrid organic-inorganic silicate matrix functionalised with tetraalkylammonium groups solvated by a viscous organic polar solvent [19]. It was obtained from the mixture of trimethoxysilane functionalised with alkyl-N,N,N,-trialkylammonium group and TMOS with the excess of the latter component. It has to be emphasized that analogous matrices based on unmodified or modified alkoxysilanes filled with an aqueous solution of a salt were also proposed as media for electrode reactions [20–22].

There are two strategies for silicate matrix modification by organic solution. It may be added directly to the sol before the sol-gel transition occurs [7, 11–19] or exchanged with the liquid left after the sol-gel process [6, 8–10]. The loss of mass accompanying gelation and ageing during the first procedure indicates that almost all alcohol produced during hydrolysis of tetraalkoxysilane is removed [16]. If the sol-gel process is not carried out in a humidity-free environment [6], some amount of water is left in organic solvent-modified silicate as is confirmed by differential scanning calorimetry, thermogravimetry, IR spectroscopy [16, 19] and electrochemical experiments [13].

The time of gelation (t_{gel}) of the sol-gel electrolyte impregnated with organic solution in an acid-catalysed process depends on the precursor, the solvent and the salt dissolved [13, 16, 19]. t_{gel} is always longer than that of the material prepared in the

absence of organic solvent. Obviously, the presence of organic solvent decreases water activity in all systems leading to slower hydrolysis. Typically, t_{gel} of a PC -solvated TMOS-based gel equals 1–4 days, whereas the formation of an analogous TEOS-based material occurs after 25–30 days [13]. The addition of more viscous solvents extends the time of gelation because higher viscosity is expected to slow down all steps of the sol-gel process. The replacement of 'structure making' Li^+ ions by 'structure breaking' tetraalkylammonium cations also slows down the sol-gel formation. This can be explained by their influence on the structure of hydrogen bonds and thereby affecting pH of the sol. The rate of formation of a solid electrolyte functionalised with tetraalkylammonium groups depends on the ratio of precursors [19].

The structure of a wet gel seems to be dramatically affected by the presence of an organic solvent. It shrinks by about 10–20% in comparison to 80–90% observed for the unmodified material. Interestingly, the syneresis of an analogous TMOS-based silicate matrix filled with an aqueous salt solution is larger being equal to about 40% [21]. As revealed by IR spectra, some OH groups of the TMOS-based gel solvated by the tetraalkylammonium (TAA^+) salt solution in PC or TMS remain unreacted [16]. For a TAA^+ functionalised material, the number of these groups is much lower [19]. The formation of this electrolyte seems to be complete, because no NMR signal of organic substituent can be found in the solution used for the extraction of crushed material [19].

Unfortunately, no convenient method for determination of the porosity and internal area of wet gels is available. However, it is reasonable to assume that the size of pores is larger than in dry or calcined material. The results based on the BET method indicate that the pore size depends on the organic modifier and precursor being in the range of 5–15 nm [16, 19].

The electrical conductivity (σ) of TMOS-based solvated gels is typically one order of magnitude smaller than that of an analogous liquid electrolyte [7–10, 16]. For the material solvated by PC solution, it is close to 10^{-3} $S \times cm^{-1}$ [16]. The value of σ of the electrolyte functionalised with tetraalkylammonium groups is at least one order of magnitude smaller [19, 20], yet still larger than that of the silicate matrix modified with the pure solvent [16]. The value of this parameter depends on the time elapsed after gelation. A most substantial decrease is observed during first 10 days after gelation correlating with the mass loss [16, 19]. A similar dependence is observed for the diffusion coefficients of neutral or ionic species obtained from the voltammetric and chronoamperometric experiments [11–15, 19]. This is connected with the development of the silicate network, affecting the mobility of ions. Interestingly, the temperature dependence and thereby activation energy of the conductivity and diffusion coefficients are not much affected by the presence of the silicate matrix [15, 16]. This indicates weak interactions between neutral or ionic species and the silicate matrix. It has to be emphasized that a similar temporal dependence of the diffusion coefficients of the redox probes was observed in the silicate matrix solvated by an aqueous salt solution [20–22].

3. Composite electrodes based on solvated gels

Despite its insulating properties, the silicate matrix can be used as a component for the composite electrode preparation. Lev et al. opened the way to a new family of electrode materials showing that a conductive porous material can be obtained by the sol-gel method from the mixture of carbon (graphite) particles and an alkoxysilane-based sol [24, 25]. The ratio of these two components affects both the electrical conductivity and mechanical stability of carbon ceramic electrodes (CCE) [25]. The optimised amount of carbon particles depends also on the their type and size [25].

Typical application of modified electrodes requires the presence of a redox component which is absent in unmodified material except some amount of quinone functionalities present on the graphite particle surface. The redox active groups can be introduced by (i) sol doping, (ii) covalent bonding to the silicate matrix (iii) covalent bonding to the surface of graphite particles and (iv) adsorption on the electrode surface (see ref. [25] for a recent review on CCE).

Recently, our group put forward another method of modification of CCE [26, 27]. This approach was inspired by the electroactivity of redox molecules dissolved in a drop or a thin film of a hydrophobic polar solvent like nitrobenzene (NB) or benzonitrile (BN) placed on the surface of the electrode made of hydrophobised graphite, pyrolytic graphite or glassy carbon [28–31]. An analogous approach was used for the modification of the electrode with droplets of the so-called redox liquid. It can be defined as a redox active compound being liquid at ambient conditions [32]. Tetraalkyl-*p*-phenylenediamines or butyloferrocene are the examples reported in the literature [33, 34]. One can manipulate the hydrophobic properties of such molecules by changing the number, length and shape of alkyl substituents connected to the redox active core. The mechanism of the electrode processes on the electrodes described above, immersed into an aqueous electrolyte which does not contain any redox active compounds involves electron transfer from/to the redox probe followed by a counter-ion transfer from the aqueous phase or a charged product ejection to the aqueous phase [31, 33, 34].

Our strategy was based on a strong affinity of hydrophobic organic solvents towards the hydrophobic silicate matrix. We have shown that CCE obtained from the organically modified precursor methyltrimethoxysilane (MTMOS) can be impregnated with the redox probe solution in a hydrophobic solvent or a pure redox liquid. The properties of these electrodes made of hydrophobic matrices are similar to those of redox polymer electrodes [35, 36] in the sense that the electron exchange between highly concentrated redox centres dissolved in a hydrophobic solvent and an electronic conductor is the source of the measured current. However, they exhibit some specific features, which are connected with the anion transfer through the hydrophobic sol-gel glass-supported liquid–liquid interface.

The following solvents were used for the CCE modification: chain hydrocarbons, toluene, nitrobenzene and *o*-nitrophenylether [14, 26, 27, 37–39]. The electrodes

modified with a hydrophobic redox probe solution – decamethyloferrocene in hydrocarbons resemble electroactive carbon paste electrodes, having been widely used for almost 40 years [40–42]. These are made of a mixture of graphite particles with the redox probe solution in a viscous oil like Nujol, silicone oil or hexadecane. The use of rigid silicate matrix extends the range of solvents to less viscous ones, enhancing the mobility of the redox probe and leading to the increase of the current. Even redox probe solution in a solvent as volatile as hexane can be used for electrode modification [37].

Electrochemical studies of CCE electrodes modified with organic solvents were performed with an aqueous salt solution without any redox probe dissolved. The shape of the voltammogram and the current magnitude observed under linear polarisation conditions is proportional to the concentration of the redox probe in the modifying solution with the largest value for the pure redox liquid [37–39]. In the latter case, the current density is similar to that observed with the redox polymer-modified electrodes [35–36]. This is not surprising since in a redox liquid, the concentration of redox groups is equal to about 4 $mol \times dm^{-3}$. Interestingly, the dependence of current vs. redox probe concentration indicates some matrix effect.

The linear relationship between the current and the concentration of ions is a specific feature of the CCE modified with organic liquid containing redox active molecules [37–39]. This is observed for the electrodes modified with a pure redox liquid – *t*-butyloferrocene (BuFc) or its solution in nitrobenzene. This effect is absent in the electrodes modified with the redox probe solution in hydrocarbons. Like in the case of the redox liquid-modified electrodes this can be explained by the participation of counterions in the electrode process – insertion in an organic solvent or ejection of the charged redox probe to aqueous solution in order to provide the charge balance for electrogenerated ions. Despite some loss of the electroactive substance, a stable electrode response can be maintained [39]. This is because the hydrophobic silicate matrix serves as a reservoir of the redox liquid enabling its continuous supply to the organic aqueous interface.

The effect of the ion concentration on the amperometric response of CCE modified with undiluted or diluted redox liquid is quite unusual and almost not observed for the electrodes modified with thin films of redox or other conductive polymers [43–45]. This is probably because the polymer films are porous and ions can interact with charged redox groups without transfer to a different phase. On the other hand, the current proportional to nonelectroactive ion concentration can be generated at unsupported or supported liquid–liquid interface where ion transfer is generated by applying a potential difference [47–49]. After optimisation, the CCE-modified with organic liquids can be eventually applied as amperometric nonelectroactive anion sensors based on different phenomena – electrogeneration of ions near the liquid –liquid interface.

We were also able to observe the effect of electrode morphology on the amperometric response. One can imagine a composite material as interconnected network of large (diameter equal to tens of micrometers) conducting particles immersed in a porous matrix with the pore size of about three orders of magnitude

smaller [46]. Hydrophobic liquid fills the matrix pores and they can be easily penetrated by individual redox molecules or $tBuFc^+$ cations having the size smaller than 1 nm. Eventually, the hydrophobic liquid covers the rough surface of the sol-gel material facing the aqueous phase as well as the surface of the most outer graphite particles not covered by the silicate matrix. We proved that the electrode process occurs at a three-phase junction formed by the wall of graphite particles, organic solvent and aqueous phase [37–39].

Although we did not yet study systematically the effect of the silicate matrix on the electrochemical behaviour of the CCE-modified organic liquid it is clear that some interactions with reactant of the electrode process exist. We have shown a stabilising effect of the matrix towards formation of butyloferrocene cation within CCE body [38]. This was explained by a likely coordination of electrogenerated cation to oxygens bridging silicon atoms.

4. Conclusions

The modification of silicate or silicate-based composites by selected organic liquids enables us to obtain solid materials while preserving some properties of liquids. Their electrochemical properties are sometimes unusual, like these of impregnated carbon ceramic electrodes because of the ability of hydrophobic silicate-based material to support liquid–liquid interface. One can envisage their future use in electrochemical devices after optimisation and improvement of their long-term stability.

Acknowledgements

The author is greatly indebted to all co-workers who contributed to the work reviewed above: Joanna Kukulka-Walkiewicz, Monika Saczek-Maj, Joanna Niedziolka and Galyna Shul from our group, dr Ewa Utzig from the Institute of Physical Chemistry of Polish Academy of Sciences, dr Julita Mrowiec-Bialon from the Institute of Chemical Engineering of Polish Academy of Sciences, dr Grazyna Zukowska, Jacek Stygar and prof. Wladyslaw Wieczorek from the Chemical Department of the Warsaw University of Technology.

Most of the work reviewed in this paper was supported by the funds of the Institute of Physical Chemistry of Polish Academy of Sciences and by the grant No. 3T09A 07419 from the State Committee for Scientific Research (KBN).

References

[1] BRINKER C.J., SCHERER G.W., *Sol-Gel Science: The Physics and Chemistry of Sol-Gel Processing*, 1990, San Diego, Academic Press.
[2] AVNIR D., LEVY D., REISFELD R., J. Phys. Chem., 88 (1984), 5956.
[3] PHILIPP G., SCHMIDT H., J. Non-Crystal. Solids, 63 (1984), 283.
[4] BOTTCHER H.K., KALLIES H., HAUFE H., SEIDEL J., Adv. Mater., 11 (1999), 138.
[5] OPALLO M., Mat. Sci., 20 (2002), 7.
[6] DURAKPASA, H. BREITER M.W., DUNN B., Electrochim. Acta, 38 (1993), 371.

[7] WU P-W., HOLM S.R., DUONG A.T., DUNN B., KANER R.B., Chem. Mater., 9 (1997), 1004.
[8] WASIUCIONEK M., BREITER M.W., J. Applied Electrochem., 27 (1997), 1106.
[9] WASIUCIONEK M., BREITER M.W., J. Electroanal. Chem., 443 (1998), 117.
[10] WASIUCIONEK M., BREITER M.W., J. Sol-Gel Sci. Technol., 11 (1998), 17.
[11] OPALLO M., KUKULKA J., Electrochem. Commun., 2 (2000), 394.
[12] KUKULKA-WALKIEWICZ J., OPALLO M., J. New Mater. Electrochem. Sci., 4 (2001), 155.
[13] OPALLO M., KUKULKA-WALKIEWICZ J., Electrochim. Acta, 46 (2001), 4235.
[14] OPALLO M., KUKULKA-WALKIEWICZ J., SACZEK-MAJ M., J. Sol-Gel Sci. Technol., 26 (2003), 1045.
[15] OPALLO M., KUKULKA-WALKIEWICZ J., Solid State Ionics, 157 (2003), 263.
[16] OPALLO M., KUKULKA-WALKIEWICZ J., UTZIG E., MROWIEC-BIALON J., ZUKOWSKA G. WIECZOREK W., Electrochim. Acta, 48 (2003), 799.
[17] POPALL M., ANDREI M., KAPPEL J., KRON J., OLMA K., OLSOWSKI B., Electrochim. Acta, 43 (1998), 1155.
[18] POPALL M., BUESTRICH R., SEMRAU G., EICHINGER G., ANDREI M., PARKER W.O., SKAARUP S., WEST K., Electrochim. Acta, 46 (2001), 1499.
[19] OPALLO M., NIEDZIOLKA J., SACZEK-MAJ M., SHUL G., UTZIG E., MROWIEC-BIALON J., STYGAR J., WIECZOREK W., Electrochim. Acta, 48 (2003), 4149.
[20] COLLINSON M.M., ZAMBRANO P., WANG H., TAUSSIG J.R., Langmuir, 15 (1999), 662.
[21] COLLINSON M.M., HOWELLS A.R., Anal. Chem., 72 (2000), 702.
[22] COLLINSON M.M., NOVAK B., J. Sol-Gel Sci. Technol., 23 (2002), 215.
[23] TSIONSKY M., GUN G., GLEZER V., LEV O., Anal. Chem., 66 (1994), 1747.
[24] GUN J., LEV O., Anal. Chim. Acta, 336 (1996), 95.
[25] RABINOVICH L., LEV O., Electroanalysis, 13 (2001), 265.
[26] OPALLO M., SACZEK-MAJ M., Electrochem. Commun., 3 (2001), 306.
[27] OPALLO M., SACZEK-MAJ M., Chem. Commun., (2002), 448.
[28] NAKATANI K., UCHIDA T., MISAWA H., KITAMURA N., MASUHARA H., J. Phys. Chem., 97 (1993), 5197.
[29] SHI C., ANSON F.C., Anal. Chem., 70 (1998), 3114.
[30] SHAFER H.O., DERBACK T., KOVAL C.A., J. Phys. Chem., 104 (2000), 1025.
[31] SCHOLZ F., KOMORSKY-LOVRIC S., LOVRIC M., Electrochem. Commun., 3 (2001), 112.
[32] MARKEN F., WEBSTER R.D., BULL S.D., DAVIES S.G., J. Electroanal. Chem., 437 (1997), 209.
[33] SCHRODER U., COMPTON R.G., MARKEN F., BULL S.D., DAVIES S.G., GILMOUR S., J. Phys. Chem. B, 105 (2001), 1344.
[34] WADHAVAN J.D., EVANS N.C., COMPTON R.G., J. Electroanal. Chem., 533 (2002), 71.
[35] MURRAY R.W., *Chemically Modified* Electrodes, [in:] *Electroanalytical Chemistry*, Vol. 13, A.J. Bard (Ed.), Marcel Dekker, New York, 1987, p. 191 and refs. therein.
[36] INZELT G., *Mechanism of Charge Transfer in Polymer-Modified Electrodes*, [in:] *Electroanalytical Chemistry*, Vol. 18, A.J. Bard (Ed.), Marcel Dekker, New York, 1994, p. 90, and refs. therein.
[37] SACZEK-Maj M., OPALLO M., Electroanalysis, 14 (2002), 605.
[38] SACZEK-MAJ M., OPALLO M., Electroanalysis, 15 (2003), 566.
[39] SHUL G., SACZEK-MAJ M., OPALLO M., Electroanalysis, in press.
[40] KUWANA T., FRENCH W.G., Anal. Chem. 36, (1964), 95.
[41] KALCHER K., Electroanalysis, 2 (1990), 419.
[42] KALCHER K., KAUFFMAN J-M., WANG J., SVANCARA I., VYTRAS K., NEUHOLD C., YANG Z., Electroanalysis, 7 (1995), 5.
[43] IKARIYAMA Y., HEINEMAN W.R., Anal. Chem., 58 (1986), 1803.
[44] MICHALSKA A., WALKIEWICZ S., MAKSYMIUK K., Electrochem. Soc. Proc., 18 (2001), 42.
[45] MARIAULLE P., SINAPI F., LAMBERTS L., WALCARIUS A., Electrochim. Acta, 46 (2003), 3543.
[46] OSKAM G., SEARSON P.C., J. Phys. Chem. B, 102 (1998), 2464.

[47] SCHIFFRIN D., GIRAULT H.H., *Electrochemistry of Liquid–Liquid Interfaces*, [in:] *Electroanalytical Chemistry*, Vol.15, A.J. Bard (Ed.), Marcel Dekker, New York, 1989, p. 1.
[48] GIRAULT H.H., *Charge Transfer Across Liquid–Liquid Interfaces*, [in:] *Modern Aspects of Electrochemistry*, J. O'M Bockris, B. Conway, R. White (Eds.), Plenum Press, New York, 1993, p. 1.
[49] REYMOND F., FERMIN D., YEE H.J., GIRAULT H.H., Electrochim. Acta, 45 (2001), 2647.

Received 12 June 2003
Revised 23 July 2003

Materials Science, Vol. 21, No. 4, 2003

Synthesis of nanosilica by the sol-gel method and its activity toward polymers

JERZY CHRUŚCIEL*, LUDOMIR ŚLUSARSKI

Institute of Polymers, Technical University of Łódź, 90-924 Łódź, Poland

Applicability of the sol-gel method to fabricate polymer-silica composites has been briefly reviewed. The sol-gel method has been applied for synthesis of nanosilica in mineral and naphthenic oils and also in latexes of diene copolymers. A new silane precursor of nanosilica was prepared by transesterification of tetraethoxysilane with *n*-decyl alcohol and (aminopropyl)trimethoxysilane, in the presence of an emulsifier and a stabilizer. Transparent sols of nanosilica in oils were obtained as the main product, accompanied by few % of dispersions of SiO_2. Microscope and AFM studies confirmed the presence of particles of nanometric size. The studies are continued in order to optimize reaction conditions and minimize the size of SiO_2 particles. Nanosilica sols are applied for modification of properties of elastomers and other polymers. New hybrid modifiers of general formula $X(Me_2SiO)_4R$ have been prepared. Their chemical structures were confirmed by spectroscopic methods: FT-IR and NMR (^1H, ^{29}Si-). These new products have been applied for synthesis of modified silica nanoparticles in elastomers matrices (*in situ*).

Key words: *sol-gel; nanosilica; modification of polymers*

1. Introduction

A quickly growing range of applications of nanomaterials in many fields has been observed in recent years [1, 2], nanosilica being often used in these studies [3]. Graft polymerization of vinyl monomers onto nanoalumina was accomplished through the free radical polymerization with the participation of double bonds at the particle surfaces, preintroduced by a silane coupling agent modification of the alumina [4]. An advantageous effect of nanoparticles on the properties of nanocomposites has been presented in the literature [5].

Colloidal silica, so-called 'white carbon black' is frequently used as an active filler in many polymer systems. Primary particles of silica are nanosized. However, their high surface energy and particularly the ability to form interparticle hydrogen

* Corresponding autor, e-mail: jchrusci@p.lodz.pl.

bonds causes an aggregation or even agglomeration of silica in a polymer matrix. Many attempts have been made to prepare polymer nanocomposites filled with nanosilica. It is impossible to cause deaggregation of secondary particles with a high shear stress. To solve the problem, the method of nanosilica synthesis in a polymer matrix (*in situ*) was elaborated [6]. Tetraethoxysilane (TEOS) as a precursor is usually used [7]. To fasten the hydrolysis reaction, basic as well as acidic, catalytic systems could be added [8]. The first step of the process is the preparation of a TEOS–polymer mix. It is not so easy to prepare homogeneous mix because of a difference in solubilities of both components. As a consequence, a coalescence of TEOS molecules and formation of its droplets is often observed. After hydrolysis, micro- or mesoparticles of silica are formed. To avoid this detrimental effect, other precursors, reactive toward the polymeric matrix, are added to TEOS [9]. However, a full hydrolysis of precursors in polymer matrices is rather difficult. The same concerns the necessary separation of the hydrolysis product (e.g. ethyl alcohol) and residues of the catalytic systems applied. Therefore, in our opinion, the synthesis of nanosilica *in situ* is not a perspective method from the technological point of view.

Nanosilica could also be produced in a form of a dry powder via pyrolysis of tetraalkoxysilanes or tetrachlorosilane in the presence of water as well as by direct hydrolysis of sodium methasilicate or tetraalkoxysilanes. Stabilization of nanoparticles is needed to avoid their aggregation. Such products are already offered on the market, although their application in the polymer technology has been restricted so far because they aggregate during processing.

2. Preparation of silica from alkoxysilanes

Many important scientific and commercial applications of the sol-gel chemistry have already been developed [10]. Most sol-gel syntheses of silica are based on the hydrolysis of tetraalkoxysilanes, $Si(OR)_4$, according to the following equation, e.g.:

$$Si(OC_2H_5)_4 + 4H_2O \xrightarrow{\text{catalyst}} SiO_2 + 4C_2H_5OH$$

Gelation of silicon alkoxide solutions takes place as a result of the hydrolysis of the silicone alkoxides $Si(OR)_4$ and subsequent polycondensation (*dehydration*) leading to the formation of polymers and particles with siloxane bonds. The reaction can be expressed by the following formulae [11]:

$$Si(OC_2H_5)_4 + 4H_2O \xrightarrow{\text{catalyst}} Si(OH)_4 + 4C_2H_5OH$$

$$Si(OH)_4 \longrightarrow SiO_2 + 2H_2O$$

However, the mechanisms of these reactions are unknown because of the complexity of the gelation process. Theoretical reaction pathways are presented in Scheme 1, illustrating the competition between the hydrolysis and the condensation steps of

some species, the number of which increases as the reactions proceeds [12]. Cyclic structures can be formed as well. The condensation between this kind of intermediate polyhydroxylated species may be responsible for the gel formation. The above reactions are catalyzed by acids or bases and are accompanied by the redistribution reactions:

$$2(RO)_3SiOH \rightleftharpoons (RO)_2Si(OH)_2 + (RO)_4Si$$

$$(RO)_2Si(OH)_2 \rightleftharpoons (RO)_3SiOH + ROSi(OH)_3$$

Thus, the proportions of Si–OH, $Si(OH)_2$, and $Si(OH)_3$ change during the process, which first gives a swollen gel. It is then dried, heated, and densified into the final monolithic piece of silica. The gelation may correspond to a crosslinking process taking place between macromolecular species of polysiloxanes containing free Si–OH bonds.

In the presence of acids, the probability of formation of $Si(OH)_4$, which is produced by the hydrolysis of all four OR groups of an alkoxide molecule, is small and condensation reactions start before the complete hydrolysis of $Si(OR)_4$ to $Si(OH)_4$ can occur. Under basic conditions $Si(OH)_4$ is easily formed by the preferential hydrolysis of the rest of the OR groups belonging to a partially hydrolyzed $Si(OR)_4$ molecule, and some silicon alkoxide molecules tend to remain non-hydrolized [11].

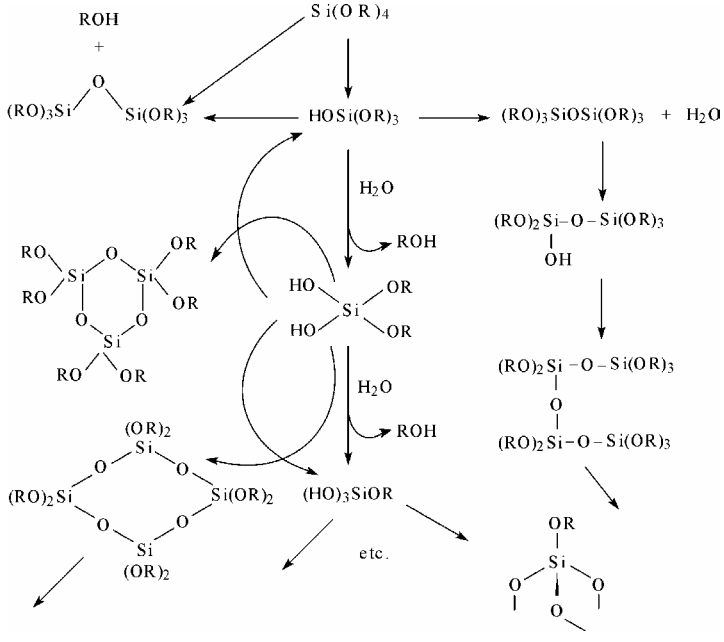

Scheme 1. Possible reactions of tetraalkoxysilanes

The determination of the overall mechanism of the chemical steps leading to gelation needs:

• information on the kinetics of all reactions involved at the beginning of the process [12];

• a better knowledge of the nature of 'building blocks' formed during the first steps.

The hydrolysis and condensation reactions involve a nucleophilic attack on the electrophilic silicon atom both in acid and basic catalysis, through the mechanisms depicted in Schemes 2 and 3 [13].

The catalyst and pH value of the solution, water concentration, silicon alkoxide concentration, the type of alkoxysilane and of solvent [11] affect the reaction rates, the reaction mechanism of the sol-gel transition, the gelation time, the nature of polymerized species formed in the sol, and the bulk nature of the gel.

The sol-gel process was also applied to two-phase systems, and thin films of uniform porous silica were successfuly made. Their structures depend on the precursor structure and deposition conditions [14]. It is possible to initiate the hydrolysis of TEOS without alcohol solvent by exposing TEOS and water to ultrasounds in the presence of an acid catalyst. The gelling time of the 'sonogel' was 115–200 min for different ratios of water per 1 mole of TEOS, while for classic gels, made by the dilution of 3 moles of alcohol per 1 mole of TEOS, the gelation may require several days [15].

Hydrolysis

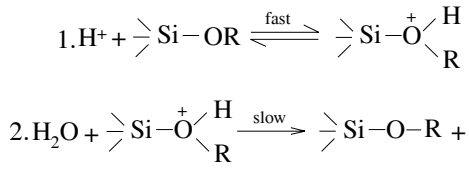

Condensation

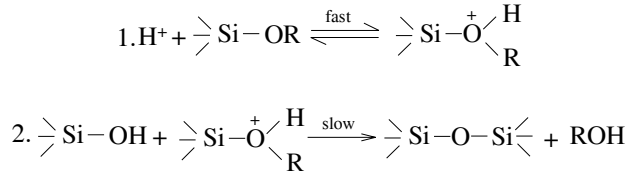

Scheme 2. Acid catalysis

The combination of emulsion techniques with alkoxide hydrolysis offers a more versatile approach to preparing multicomponent oxide powders. Three general approaches can be applied. The first one involves preparation of water-in-oil emulsions, followed by the reaction of water droplets with alkoxide. In the second method, an aqueous sol is emulsified in an organic liquid and the sol droplets are then gelled. The third one involves emulsification of the alkoxide with an appropriate immiscible solvent, followed by addition of water to hydrolyze the alkoxide droplets [16].

Hydrolysis

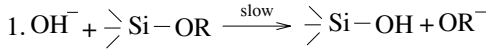

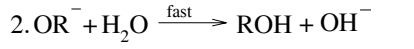

Condensation

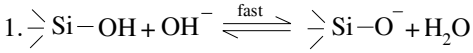

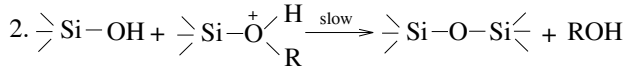

Scheme 3. Basic catalysis

To form a stable emulsion, an addition of a surfactant is necessary in order to lower the interfacial energy and minimize the surface energy between two liquids. Emulsions formed with a solution consisting of 60% of mineral oil and 40% of heptane were stable with respect to alcohol generation, and powder formed without separation of the emulsion. After heating to 450 °C, residual mineral oil and unreacted alkoxide groups were burned off and the surface area increased from 2–8 m^2/g to 220 –390 m^2/g. Densities of the silica particles (1.7 g/cm^3) were smaller than the theoretical ones also confirming a porous structure of SiO_2 [16].

The hydrolysis and polymerization of TEOS in ethanol solution containing water and ammonia allows preparation of monodispersed silica powders. The final particle size *d* was determined as a function of initial reagent concentrations over the range studied: 0.17–0.5 M TEOS, 0.5–3 M NH_3, 0.5–14 M H_2O (at 25 °C). It was possible to obtain SiO_2 particles with average diameters between 15 and 700 nm [17].

The sol-gel method provides means for modifying glasses and crystalline ceramics with organic polymers [18–20], promising materials displaying unique and varied mechanical, electrical and optical properties. A wide variety of coatings compositions were produced by varying the ratio of PVDF-PTFE copolymer to TEOS and by varying the partial hydrolysis conditions of TEOS. The results of DSC indicated that polymer modified glasses contained regions of unrestricted polymer and regions in which the polymer and the glass were intimately mixed. Additions of relatively small amounts of TEOS to the copolymer increased the temperature of the onset of thermal decomposition – in some cases by as much as 40 °C. Similar unexpected increases in the temperature of thermal decomposition were observed in the previously studied PDMS-modified glasses. SEM studies of monoliths and coatings revealed variety of material microstructures. In many of the coatings, the honeycomb structures were observed [21]. SEM studies of PTFE–silicate composites showed that PTFE particles were wetted by TEOS, suggesting potential applications as adherent low-coefficient-

of-friction coatings. The coefficient of sliding friction was reduced by incorporating PTFE into TEOS coatings, and heating was shown to improve the coating's resistance to wear [22].

Properties of the sol-gel glasses composed of SiO_2 [10] and SiO_2–TiO_2 [23] were also modified by addition of difunctional polydimethylsiloxane elastomeric oligomers in order to improve the fracture toughness [10]. Alternatively, the hydrolysis and polycondensation reactions of TEOS were carried out within a polymeric matrix, with the silica generated in the form of very small, well-dispersed particles. When the matrix is an elastomer, these particles provide the same highly desirable reinforcing effects obtained by the usual blending of a filler (such as carbon black) and polymer (such as natural rubber) prior to their being crosslinking or curing into tough elastomers of commercial importance. Various filling sequencies were applied, i.e. filler precipitation before or after curing [24].

3. Results and discussion

Based on the sources published as well as on our experience in the synthesis and application of conventional fillers, we came to the conclusion that there are three possible routes to avoid aggregation and agglomeration of primary nanosized silica particles:

- Synthesis of nanosilica in an oil or an oligomer liquid (using precursors with appropriately chosen substituents), which suppresses the process of grains enlargement because of a steric hindrance and lowers the tension at the interface. In such a case separation of reactions products is much easier as compared to the *in situ* method of synthesis. Also mixing of the nanosilica suspension in an oil or oligomer with a polymer could easily be performed.
- Synthesis of nanosilica in polymer latexes or during emulsion polymerization process. If the coprecipitation is carefully stirred, a uniform distribution of nanosilica in a polymer matrix can be achieved. A great advantage of the method is the possibility to obtain the dispersion of nanosilica in a powdered polymer system. The usage of filled polymer powders will increase due to more common application of extruders for the preparation of mixes instead of internal mixers.
- Synthesis of nanosilica functionalized on the surface. If appropriate precursors are used, functional groups cover the nanograins. In such a case, functional groups may be introduced into the top layer of nanograins, thus increasing the wettability of nanosilica by a polymer and also allowing their grafting by the matrix. In this article, some results of our experiments in this field are presented.

The syntheses of nanosilica in aliphatic or naphthenic oils and also in latexes of diene copolymers have been studied. We applied the sol-gel method and a new silane precursor of nanosilica, which was prepared by transesterification of tetraethoxysilane and (aminopropyl)trimethoxysilane with *n*-decyl alcohol in the presence of an emulsifier and a stabilizer.

Table 1. Reaction conditions and some results of nanosilica preparation

Substrates [ml]	Synthesis				
	A	B	I	II	III
'Precursor'[a] (or TEOS)	1.76	1.8	16.5	(35.15)	16.5
Naphtenic oil (Nyfleks 221)	–	–	16.5	10.0	5.5
Aliphatic oil	(1.88)	(1.0)	–	–	–
Emulsifier (Rokanol)	–	–	1.65	1.0	0.55
'Nanosilica stabilizing agent' (and as a second catalyst)	–	–	0.20	0.20	0.20
H_2O	0.04	0.02	0.85	11.35	0.85
Temperature [°C]	~ 25–30	~ 25–30	~ 25–80	~ 25–80	~ 25–30
wt. % of SiO_2[b]	15.9	26.2	14.6	37.4	33.3

[a]'Nanosilica precursor' was prepared by transesterification of TEOS and 5 mol. % of (aminopropyl)trimethoxysilane with *n*-decyl alcohol.

[b]With respect to the substrate.

The goal of our studies was:

- Improvement of mechanical properties of elastomers (and other polymers) by decrease of the size of silica particles (as a filler) and formation of unconventional networks in an elastomer matrix or chemical bonding of silica with a polymer.
- Simultaneous improvement of surface properties of elastomers and other polymers (e.g., tribological properties, thermal stability) and decreasing their flammability.

The following assumptions were taken into consideration:

- Assurance of good homogeneity of the reagent system by chemical modification of TEOS, i.e. by substitution of one ethoxyl group with a group of fatty alcohol and synthesis of the so-called 'modified nanosilica precursor'.
- Regulation of sizes of molecules and particles of 'SiO_2' by appropriate choice of the [H_2O]/['precursor'] stoichiometry and of the reaction conditions.
- Stabilization of silanol groups Si–OH by hydrogen bonds (using a stabilizing agent).
- Application of adhesion promoters.

As the main product we obtained transparent gels of nanosilica in oils with small amounts (a few per cent) of SiO_2 dispersions. The microscope and AFM studies confirmed the presence of particles of nanometric size. The nanosilica sols are currently applied to modification of properties of elastomers.

Our studies are continued in order to optimize reaction conditions and minimize the size of SiO_2 particles. Moreover, new hybrid modifiers of general formula $X(Me_2SiO)_4R$, where Me is the methyl group, and R a fatty alcohol radical ((1) X = H, R = *n*-$C_{10}H_{21}$; (2) X = RO = *n*-$C_{10}H_{21}$; (3) X = RO = *n*-$C_{18}H_{37}$) have been prepared. We have also prepared novel hybrid polymer modifiers containing polysiloxane units as side or terminal groups: trimethylsilylamino- functions and long chains of *n*-alkoxy- side groups (prepared by derivatization of polymethylhydrosiloxanes with fatty alcohols):

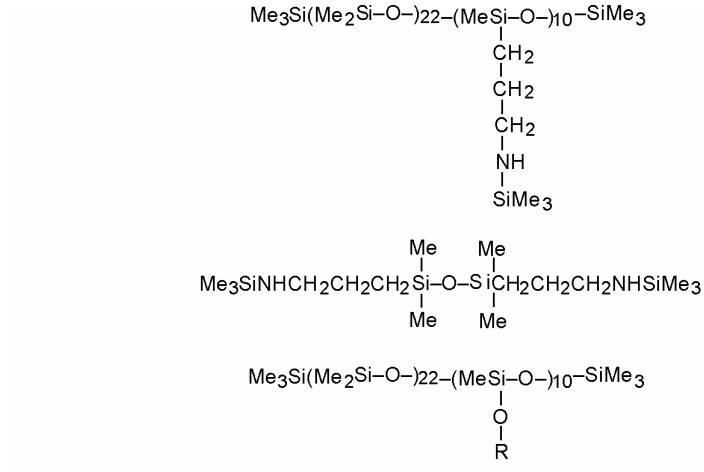

where: R = *n*-$C_{10}H_{21}$, *n*-$C_{14}H_{29}$, *n*-$C_{16}H_{33}$, *n*-$C_{18}H_{37}$

The chemical structures of new hybrid polysiloxanes were confirmed by spectroscopic methods: FT-IR and NMR (^{1}H-, ^{29}Si-). Synthetic procedures will be published in a separate paper. These new products have been applied for the synthesis of modified silica nanoparticles in elastomers matrices (*in situ*). This way it is possible to modify surface and bulk properties of rubber vulcanizates. The studies of physical properties of rubbers obtained are in progress and will be published elsewhere.

References

[1] *Organic-Inorganic Nanocomposite Materials*, [in:] Chem. Mater., 13 (2001), No. 10.
[2] PUT J., *e-Polymers*, T_001[2002].
[3] FURUKAWA M., YASHIKAI K., Proceedings of the International Rubber Conference, Prague, July 2002.
[4] RONG M.Z., JI Q.L., ZHANG M.Q., FRIEDRICH K., Eur. Polymer J., 38 (2002), 1573.
[5] (a) ALEXANDRE M., DUBOIS P., Mater. Sci. Eng., Reports, 28 (2000), 1.
(b) KANG S., HONG S.I., CHOE C.R., PARK M., RIM S., KIM J., Polymer, 42 (2001), 879.
[6] (a) MARK J.E., NING Y.-P., JIANG C.Y., TANG M.-Y., ROTH W.C., Polymer, 26 (1985), 2069.
(b) MARK J.E., Heteroorg. Chem. Rev., 3 (1996), 307.
[7] ILER R.K., *The Chemistry of Silica*, Wiley, New York, 1979.
[8] STOEBER W., FINK A., BOHN E., J. Colloid Interface Sci., 26 (1968), 62.
[9] SCHARTL W., GOHR K., GRAF C., LINDENBLATT G., ROSS C., SCMID M., *Extended Abstracts of the Silica '98* Conference, Mulhouse, 1998, p. 427.
[10] MCGRATH J.E., PULLOCKAREN J.P., RIFFLE J.S., KILIC S., ELSBERND C.S., [in:] *Ultrastructure Processing of Advanced Ceramics*, J.D. Mackenzie, D.R. Ulrich (Eds.), Wiley, 1984, Chapter 3, pp. 55–75.
[11] SAKKA S., KOZUKA H., Kim S.-H., [in:] *Ultrastructure Processing of Advanced Ceramics*, J.D. Mackenzie, D.R. Ulrich (Eds.), Wiley, 1984, Chapter 10, pp. 113–126.
[12] KAŹMIERSKI K., Ph. D. Thesis, Łódź, 1996.
[13] CORRIU R.J.P., LECLERQ D., VIOUX A., PAUTHE M., PHALIPPOU J., [in:] *Ultrastructure Processing of Advanced Ceramics*, J.D. Mackenzie, D.R. Ulrich (Eds.), Wiley, 1984, Chapter 7, pp. 113–126.
[14] BRINKER C.J., HURD A.J., Ward K.J., [in:] *Ultrastructure Processing of Advanced Ceramics*, J.D. Mackenzie, D.R. Ulrich (Eds.), Wiley, 1984, Chapter 15, pp. 223–239.

[15] ELSQUIAS L., ZARZYCKI J., [in:] *Ultrastructure Processing of Advanced Ceramics*, J.D. Mackenzie, D.R. Ulrich (Eds.), Wiley, 1984, Chapter 17, pp. 255–270.
[16] HARDY A.B., GOWDA G., MCMAHON T.J., RIMAN R.E., RHINE W.EBOWEN., H.K., *Ultrastructure Processing of Advanced Ceramics*, J.D. Mackenzie, D.R. Ulrich (Eds.), Wiley, 1984, Chapter 30, pp. 407–428.
[17] BOGUSH G.H., ZKOSKI C.F., [in:] *Ultrastructure Processing of Advanced Ceramics*, J.D. Mackenzie, D.R. Ulrich (Eds.), Wiley, 1984, Chapter 35, pp. 477–486.
[18] SCHMIDT H., U.S. Patent 4 374 696.
[19] MARK J.E., JIANG C.Y., TANG M.-Y., Macromolecules, 17, (1984), 2613.
[20] HUANG H.H., ORLER B., WILKES G.L., Polym. Bull., 14 (1985), 557.
[21] DOYLE W.F., FABES B.D., ROOT J.C., SIMMONS K.D., CHIANG Y.M., UHLMANN D.R., [in:] *Ultrastructure Processing of Advanced Ceramics*, J.D. Mackenzie, D.R. Ulrich (Eds.), Wiley, 1984, Chapter 61, pp. 795–805.
[22] DOYLE W.F., UHLMANN D.R., [in:] *Ultrastructure Processing of Advanced Ceramics*, J.D. Mackenzie, D.R. Ulrich (Eds.), Wiley, 1984, Chapter 78, pp. 953–962.
[23] PARKHURST C.S., DOYLE W.F., SILVERMAN L.A., SINGH S., ANDERSEN M.P., MCCLURG D., WNEK G.E., UHLMANN D.R., [in:] *Better Ceramics Through Chemistry*, C.J. Brinker, D.E. Clark, D.R. Ulrich (Eds.), Materials Research Society Symposium Proceedings, Pittsburgh (PA), 1986, Vol. 73, pp. 769.
[24] MARK J.E., [in:] *Ultrastructure Processing of Advanced Ceramics*, J.D. Mackenzie, D.R. Ulrich (Eds.), Wiley, 1984, Chapter 46, pp. 623–633.

Received 12 June 2003
Revised 23 July 2003

Materials Science, Vol. 21, No. 4, 2003

Microstructure and optical properties of methylmethacrylate-modified silica hybrid glasses and thin films

M. NOCUŃ[1*], E. LEJA[2], W. BUGAJSKI[1]

[1]AGH University of Science and Technology, Faculty of Materials Science and Ceramics, al. Mickiewicza 30, 30-059 Kraków, Poland

[2]AGH University of Science and Technology, Faculty of Electrical Engineering, Automatics, Computer Science and Electronics, al. Mickiewicza 30, 30-059 Kraków, Poland

Silica glasses modified with organic materials offer many new, easily tailorable properties that can lead to various applications. In this work, silica–methylmethacrylate hybrid glasses have been studied. Transparent gels in the form of bulk glass and thin layers were prepared by a one-step sol-gel process. Thermal decomposition of the gels was studied by differential thermal analysis (DTA) and infrared spectroscopy (IR). Microstructure and optical properties of the glasses with different content of methacrylate were established by means of scanning electron microscopy (SEM), photoelectron spectroscopy (XPS) and UV-VIS spectroscopy.

Key words: *hybrid glasses; inorganic-organic glasses; optical properties; thin layers; microstructure*

1. Introduction

In recent years, organically modified silicates (hybrid glasses) have attracted much attention being considered as promising materials with easily tailorable new properties. The sol-gel process is a convenient method for preparation of bulk glasses as well as of films and layers. The main advantage of the sol-gel technique is a high homogeneity and purity of synthesized materials. The sol-gel is the only method enabling to introduce organic molecules into an inorganic network. Since its implementation, many hybrid glasses and ceramics have been synthesized [1–6]. Generally, hybrid materials can be classified into two classes: molecules, oligomers or polymers belonging to class I are entrapped or encapsulated within the network of base materi-

[*]Corresponding author, e-mail: nocun@uci.agh.edu.pl.

als (usually silica network). In such a case only week interactions between networks and entrapped material exist, based on hydrogen bonding or van der Waals forces. Hybrid materials with chemical bonds between host network and entrapped molecules belong to class II. Some of materials cannot be easily classified into one of the classes mentioned as they contain molecules bonded to the network by strong covalent or ion-covalent bonds but some molecules are simultaneously weekly bonded.

Methylmethacrylate is often used to modify the structure of silica glasses [7–10]. The bonds between an inorganic network and organic filler can be of chemical and/or physical nature and depend mainly on the composition and preparation procedures [11]. In this study, we present selected properties of hybrid materials obtained in the form of bulks and thin layers and based on the system TEOS/MMA.

2. Preparation

All hybrid glasses were prepared from pure reagents: tetraethyloorthosilicate 98% (TEOS), methylmethacrylate monomer (MMA) (Sigma-Aldrich) HCl and ethyl alcohol (Polish Chemicals). The chemicals are listed in Table 1.

Table 1. Materials used

Properties	TEOS $Si(OC_2H_5)_4$	Organic component methyl metacrylate, MMA	Catalyst HCl	Water H_2O	Solvent C_2H_5OH
Molecular weight	208.3	100.1	36.46	18.0	46.02
Composition [mol]	1	0.1–1	0.05	2.5	2.0

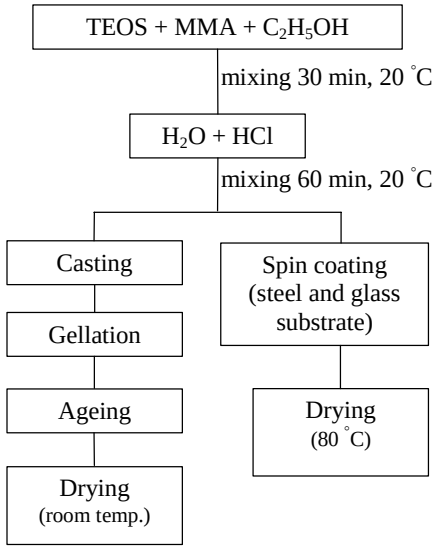

Fig. 1. Preparation scheme for silica–MMA hybrid materials

Glasses were prepared with molar ratios of TEOS to MMA ranging from 1:1 to 1:0.1. Molar ratio of TEOS:C_2H_5OH:H_2O:HCl was always 1:2:2.5:0.05. The preparation route is shown in Fig. 1. Thin layers were prepared by the spin coating technique (5000 rpm) on steel and glass substrates (microscope slides).

3. Results

3.1. Thermal stability of hybrid glasses

Thermal stability of hybrid glasses was established on the basis of DTA analysis (Q1500, Hungary). Powdered samples were heated at a rate of 10 °C/min. Selected results are shown in Fig. 2. The endothermal peak at 140 °C is due to water and remaining solvent evaporation from the porous gel. The hybrids of SiO_2/MMA glasses are stable up to 280 °C, when the decomposition begins. The first exothermal peak at 330 °C is sensitive to the MMA content in the glass (Fig. 2).

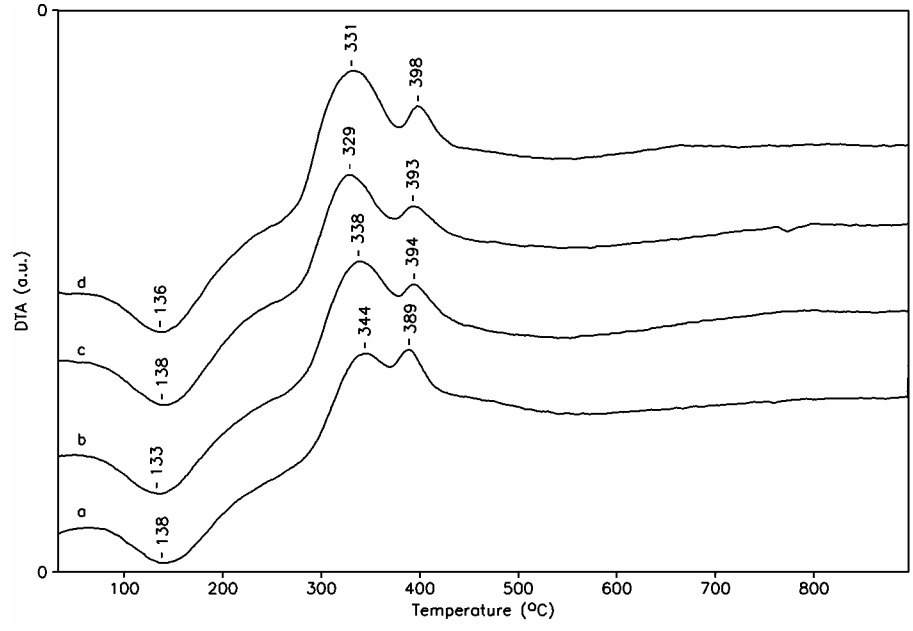

Fig. 2. DTA curves of the samples with different molar ratios of TEOS to MMA: a) 1:0.2, b) 1:0.5, c) 1:0.7, d) 1:1

This indicates that the effect is connected with the MMA decomposition. However, the exothermal peak at this position is also observed in pure silica gel prepared with a high alcohol content [12], so this exothermal effect is assumed to be due to combustion of non-hydrolyzed $–OC_2H_5$ and $–OCH_3$ groups [13,14]. Loss of –OH

groups chemically bonded to the silica is also possible [15]. The second exothermal peak, which appears at 400 °C, is connected with a further combustion of organic compounds (mainly $–OC_2H_5$ groups) [16].

3.2. FTIR results

To reveal structural evolution during thermal decomposition of hybrid glasses, IR spectra in a MIR region were recorded for samples thermally treated at 900, 350, 150 °C. FTIR analyses were carried out with a BIO-RAD FTS-6000 spectrometer. Absorption spectra were measured from 400 to 4000 cm^{-1} in KBr wafers with the resolution of 1 cm^{-1}. The results of the IR analysis are shown in Fig. 3. The broad band with a maximum at 3440 cm^{-1} is due to a superposition of the following stretching vibration bands [17]:

- isolated SiO–H – 3750 cm^{-1},
- internal SiO–H – 3660 cm^{-1},
- SiO–H of surface silanols bonded to molecular water – 3540 cm^{-1},
- O–H streching of hydrogen bonded molecular water – 3400–3500 cm^{-1}.

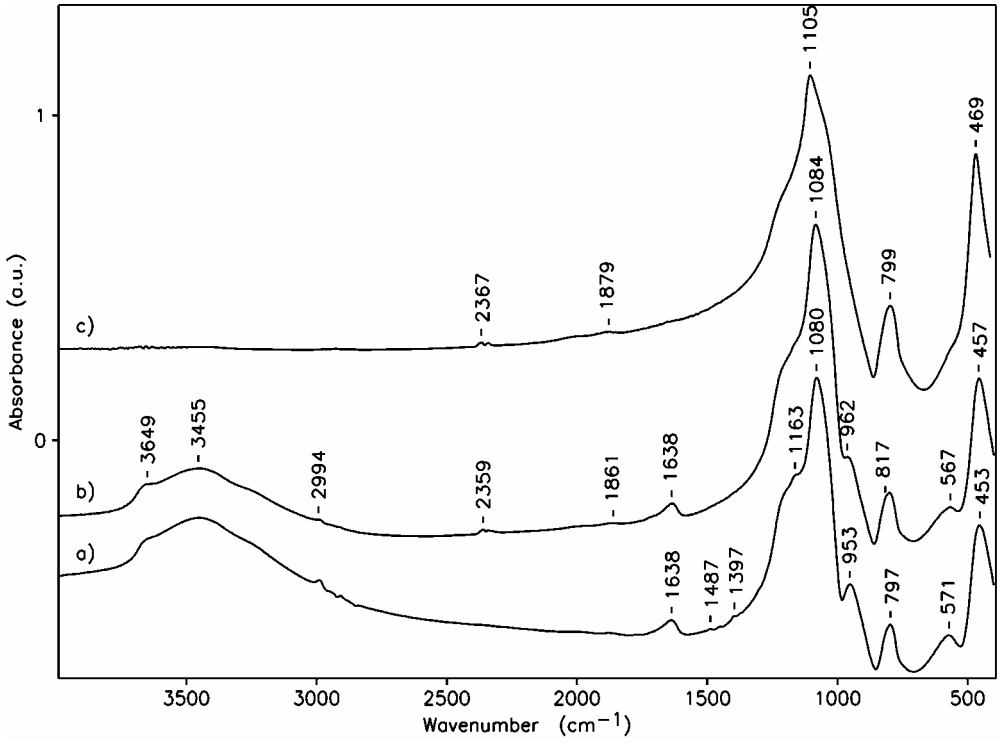

Fig. 3. MIR spectra of the samples after thermal treatment at: a) 150 °C, b) 350 °C, c) 900 °C

In addition to the vibrations corresponding to O–H bonds, the band at 1640 cm^{-1} is assigned to the deformation mode of adsorbed molecular water. All main vibration frequencies related to molecular water present in the gel are observed up to 350 °C (Fig. 3c). The narrow, low-intensity bands at 2990 and 1400–1490 cm^{-1} correspond to the C–H stretching vibrations (H_2C=O, H_3C–O–). These bands indicate the presence of unhydrolyzed methoxy groups from methylmethacrylate. A significant decrease of their intensities at 350 °C confirms that the first exothermal effect observed on DTA curve is due to combustion of $–OCH_3$ and the unreacted $–OC_2H_5$ groups. The bands at 950 and 570 cm^{-1} are attributed to silanol groups in the glass. They correspond to Si–O(H) stretching and bending vibrations, respectively. The absorption band at 950 cm^{-1} is connected with hydrogen bonding; it is present in hydrated glasses and microporous gels [17, 18]. Some contribution from the C–C stretching vibration has also been suggested [19, 20]. This band is shifted to higher frequencies as temperature increases and eventually disappears at 900 °C (Fig. 3c). The most intensive band at 1080 cm^{-1} is attributed to the stretching asymmetric Si–O–Si mode, while the symmetric band of this mode is observed at 800 cm^{-1}. Bending vibrations of Si–O–Si bridges give rise to the absorption band at 460 cm^{-1}. Increase in the intensity of the bands at 800 and 460 cm^{-1} is interpreted as the formation of new Si–O–Si bridges. The band corresponding to the C=C vibration usually observed at 1700 cm^{-1} is very weak even in the gel with 1:1 TEOS to MMA molar ratio. It indicates that the C=C double bonds break during the gel formation.

3.3. Photoelectron spectroscopy

XPS spectra were recorded with a VSW spectrometer equipped with a hemispherical analyzer. Data were collected in the resolution mode FAT 22. Al K_α X-ray (200 W) was used as the excitation source. The spectra were adjusted to the main carbon C1s peak at the position of 284.6 eV. The results are summarized in Table 2.

Table 2. Results of XPS analysis for the sample with the composition 1:1 TEOS to MMA

Core level	Bond	Binding energy peak [eV]	Peak area [a.u.]	FWHM [eV]
C1s	C–Si	283.1	1199.4	1.35
	C–C, C–H	284.6	5206.1	1.95
	C–O	285.7	2175.8	1.95
	C=O	287.3	923.6	3.0
O1s		533.1	75224.0	2.4
Si2p		103.9	6983.4	2.4

The carbon 1s region of the samples with different contents of MMA is shown in Fig. 4. The C1s peak at 283.1 eV, visible in the spectra of the samples with high con-

tent of MMA (1:1), indicates the existence of C–Si bonds [21]. It is not observed in the samples with low content of MMA (TEOS to MMA 1:0.5 or less) (Fig. 4a). The

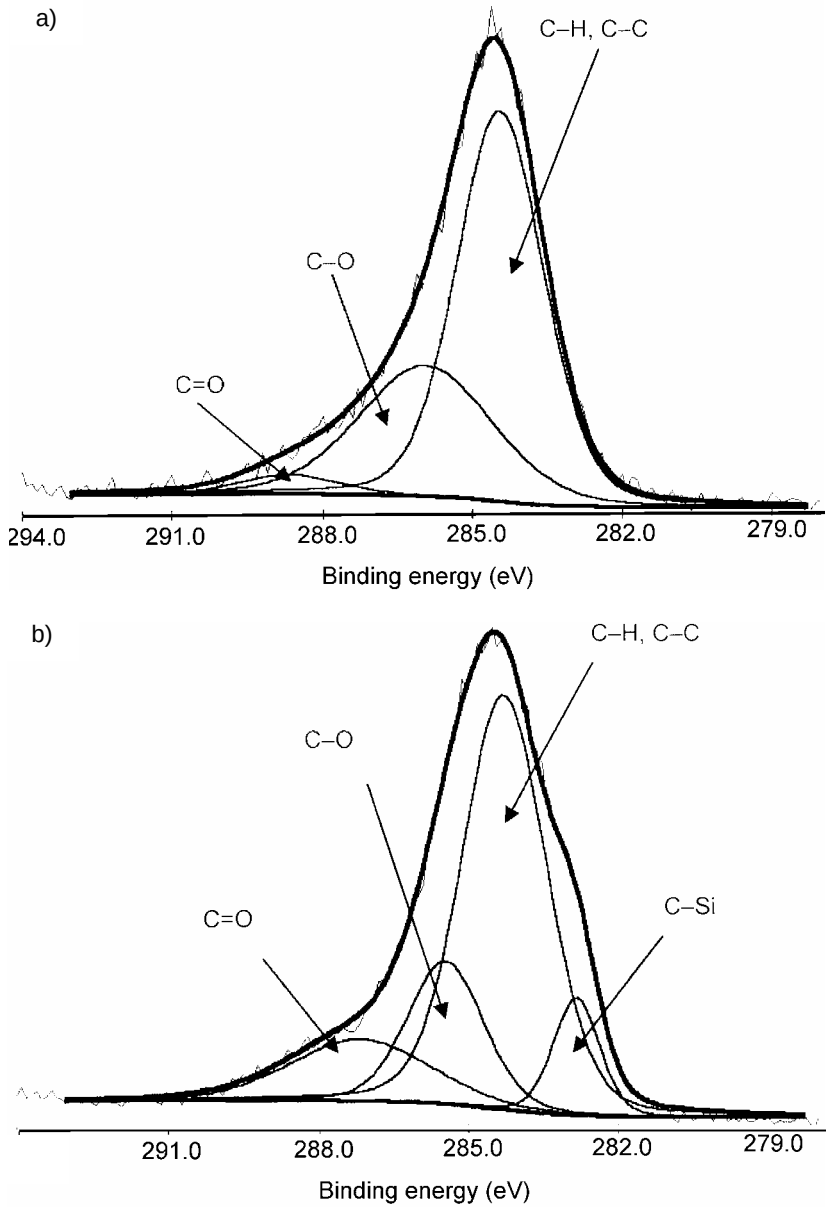

Fig. 4. XPS spectra of C1s region: a) 1:0.2 TEOS to MMA, b) 1:1 TEOS to MMA

binding energy of oxygen O 1s is relatively high (533.1 eV) and characteristic of oxygen in organic polymers having O–C–O and O–C=O bonds [21].

3.4. Spectral properties of the hybrid films

Transmittance spectra were recorded with a Perkin-Elmer Lambda 19 double -beam spectrometer in the range from 200 nm to 2.5 μm with the resolution of 1 nm.

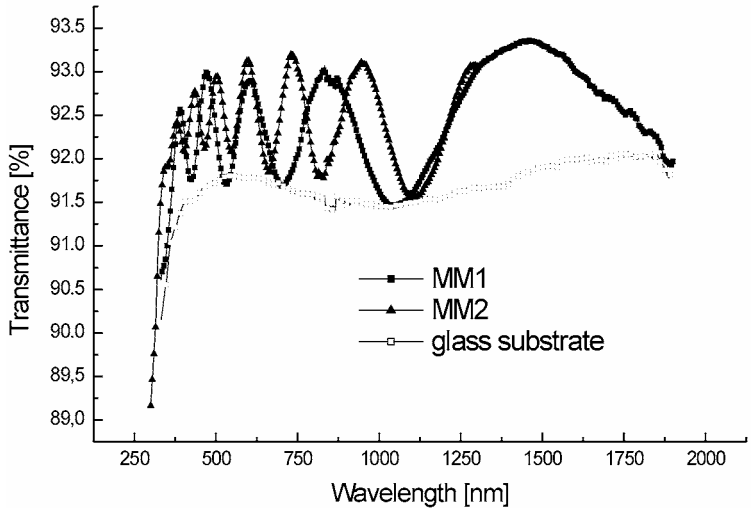

Fig. 5. Transmittance spectra of selected samples (TEOS to MMA): MM1 – 1:0.5, MM2 – 1:1

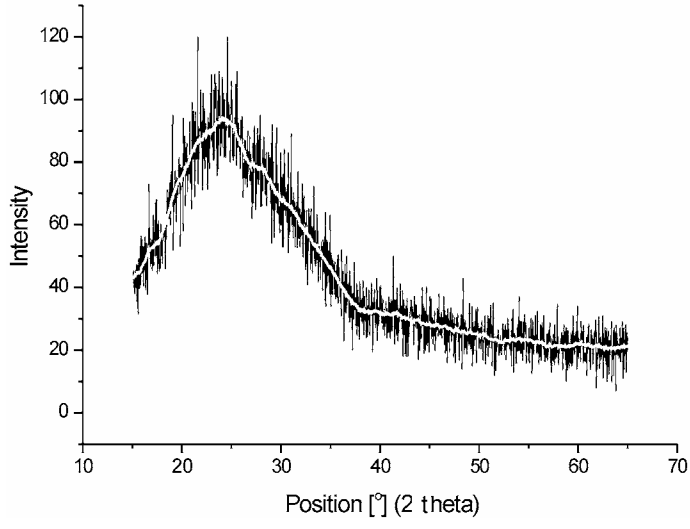

Fig. 6. X-ray low-angle (3°) diffraction analysis of the hybrid layers

Figure 5 shows the transmittance spectra of the hybrid film with the TEOS to MMA molar ratio 1:0.5 and 1:1. All films prepared on glass substrates were uniform, crack-free and transparent in the whole spectral range under investigation. X-ray low

-angle scattering measurements carried out using a Philips X Pert MPD spectrometer with the CuK_α radiation confirm that the layers are amorphous (Fig. 6). The thickness of the films measured with a Taylor-Hobson 'Tallystep' profilometer ranged from 0.7 to 1.5 μm. The thickness of the sample was a function of the MMA content and the reaction time. Thicker layers were obtained in the case of the low MMA-content samples. Increase of the MMA leads to increase in the gellation time and the increase of the viscosity is much slower. The refractive index *n* has been calculated from the results of the profilometer measurements and transmittance spectra from the following relationship:

$$n = \frac{1}{2d} \frac{\lambda_1 \lambda_2}{\lambda_2 - \lambda_1}$$

where *d* is the thickness of the layer from the profilometer measurements, λ_1, λ_2 – the wavelengths of the successive maxima in the transmittance spectra.

The refractive index calculated at 600 nm equals 1.343 for the samples with the components ratio 1:1.

3.5. Microstructure of the layers on glass and steel substrates

Microstructure of the hybrid layers has been studied with a Joel 3000 scanning electron microscope. Examples of the surface morphology are shown in Fig. 7.

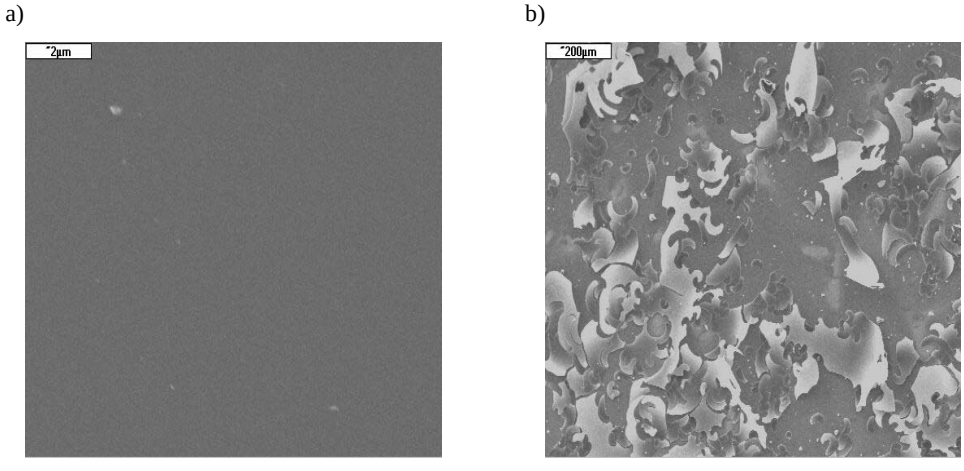

Fig. 7. SEM pictures of the hybrid layers: a) on a glass substrate, b) on a stainless steel substrate

While layers obtained on glass substrates are smooth, uniform and crack-free, layers on steel substrates are cracked with poor adherence to the substrate. The cracking was caused by differences in the thermal expansion coefficients of the hybrid layers and the steel substrates. In the case of the glass substrates, there is a high chemical compatibility between the layer and the glass and the layer is chemically bonded to

the substrate. Adherence of the hybrid layer to the stainless steel substrate is based only on physical and mechanical interactions.

4. Conclusions

The analysis of the carbon region reveals the existence of the C–Si bonds in the samples with high content of MMA. Samples having TEOS to MMA 1:1 molar ratio belong to the class II of hybrid materials; chemical bonds between the silica network and the organic filler are formed. Structures of glasses with lower contents of MMA (1:0.5 and less) are defined by the silica network with precipitates of poly-MMA in the form of short chains. Layers prepared on glass substrates are smooth, uniform and crack-free while layers on stainless steel show poor adherence to the substrates. Both, layers and bulk gels are highly transparent.

Acknowledgement

The authors wish to thank The Polish State Committee for Scientific Research for financial support – grant No. 4T08D00823.

References

[1] HUANG H.-H., ORLEV B., WILKES G.L., Macromolecules, 20 (1987), 1322.
[2] SCHMIDT H., J. Non-Cryst. Solids, 73 (1985), 681.
[3] CHUJO Y., SAEGUSA T., Adv. Polym. Sci., 100 (1992), 12.
[4] MORIKAWA A., IYOKU Y., KAKIMOTO M., UMAI Y., J. Mater. Chem., 2 (1992), 679.
[5] SCHMIDT H., J. Sol-Gel Sci. Technol., 1 (1994), 217.
[6] AVNIR D., LEVY D., REISFELD R., J. Phys. Chem., 88 (1984), 5956.
[7] DONESCU D., TEODORESCU M., SERBAN S., FUSULAN L., PETCU C., Europ. Polym. J., 35 (1999), 1679.
[8] SLOMKOWSKI S., MIKSA B., CHEHIMI M.M., DELMAR M., CABET-DELIVRY E., MOJORAL J.–P., CAMINADE A.–H., Reactive and Functional Polymers, 41 (1999), 45.
[9] CHAN CH., PENG S., CHU J., NI S., Polymer 42 (2002), 4189.
[10] SASSI Z., BUREAU J.C., BAKKALI A., Vibrat. Spectr., 28 (2002), 299.
[11] SASSI Z., BUREAU J.C., BAKKALI A., Vibrat. Spectr., 28 (2002), 251.
[12] LAMBILLY H., KLEIN L.C., J. Non-Cryst. Solids, 102 (1988), 269.
[13] ZHANG H., PANTANO C.G., J. Am. Ceram Soc., 73 (1990), 958.
[14] HENCH L.L., WANG S.H., Phase Trans., 24–26 (1990), 785.
[15] ORGAZ F., RAWSON H., J. Non-Cryst. Solids, 82 (1986), 57.
[16] BRINKER C.J., SCHERER G.W., *Sol-Gel Science.The Physics and Chemistry of Sol-Gel Processing*, Academic Press, New York, 1990, p. 551.
[17] ORCEL G., PHALIPPOU J., HENCH L.L., J. Non-Cryst. Solids, 88 (1986), 114.
[18] KATO K., J. Mater. Sci., 26 (1991), 6777.
[19] BRINKER C.J., BROW R.K., TALLANT D.R., KIRKPATRICK R.J., J. Non-Cryst. Solids, 120 (1990), 26.
[20] MONDRAGON M.A., CASTANO V.M., GRACIA J., TELLEZ C.A., Vibrational Spectr., 9 (1995), 293.
[21] BRIGGS D., *Surface Analysis of Polymers by XPS and Static SIMS*, Cambridge University Press, 1998.

Received 15 June 2003
Revised 21 July 2003

Materials Science, *Vol. 21*, *No. 4*, *2003*

Rheology of silica suspensions stabilized by ethylenediamine

VLADIMIR E. GAISHUN[1*], YNINA A. POTAPENOK[1], OLGA I. TULENKOVA[1], STEPAN V. PAKHOVTCHYSHIN[2], WIESŁAW STRĘK[3]

[1]Francisk Skorina Gomel State University, 104 Sovetskaya St., Gomel, 246019, Belarus

[2]Institute of Surface Chemistry, National Academy of Sciences of Ukraine, 17 General Naumov St., 03680 Kyiv, Ukraine

[3]Institute of Low Temperature and Structure Research, Polish Academy of Sciences, 2 Okólna St., 50-950 Wrocław, Poland

The effect of ethylenediamine bridging, particle size and specific surface area of fumed silica on rheological properties of silica suspensions were studied with a cylinder rheometer. The apparent viscosity of suspensions of aerosils A-50, A-175, A-300 and A-380 irreversibly increases with shearing time at shear rates above a certain value. The critical shear rate for shear-induced bridging coagulation decreases with the increasing ethylenediamine concentration because of lowering of the energy barrier due to a compression of the electrical double layer. The suspensions become elastic pastes after the bridging coagulation.

Key words: silica; suspension; ethylenediamine; rheological properties; viscosity

1. Introduction

The colloidal silica dioxide finds more and more applications in various branches of science and technology: silica gels and glasses produced by the sol-gel method, hydrated cellulose, cellophane, paper, ceramics, for polishing optical and electronic components, etc.

Inter-particle forces determining the dispersion stability of silica particles can be of three types: the London–van der Waals attraction, electrostatic repulsion and forces of interaction of adsorbed long-chain polymer molecules with the silica particles. Important factors are also the bridging attraction and the steric repulsion since the energy barrier

[*]Corresponding author, e-mail: vgaishun@gsu.unibel.by.

for the bridging is determined by the electrostatic contribution to the shear-induced bridging coagulation [1].

Disperse systems integrate the fundamental physicochemical features such as heterogeneity – the presence of an interface and dispersity. The role of these factors in disperse systems (in their aggregative and sedimentation stability) becomes more essential with the decrease of particles sizes and their concentration in a fluid medium.

The flocculation process is especially intensive in lyophobic (aggregative labile) disperse systems upon reaching a critical concentration of particles in the fluid dispersion medium. Main elements of the structural lattice in such systems are contacts between particles in an aggregate generator through the whole volume. The disperse system becomes structured and passes to a new state. In this contribution we explore rheological performances of silica suspensions stabilized by ethylenediamine which exhibit rheopexy and thixotropic properties.

2. Experimental

The suspensions were composed of fumed silica, ethylenediamine ($C_2H_8N_2$) and water. The medium was the solution of ethylenediamine in water. The $C_2H_8N_2$ concentration in aqueous solutions was 1.0–1.4 mol/dm^3. The silica samples were Aerosil A-50, A-175, A-300, A-380 from the Kalush Experimental Plant (KEP, Ukraine) and Aerosil MOX-80 from Degussa Co. (Germany). The particle diameters were 50–70 nm, 10–40 nm, 5–20 nm, 5–15 nm and 10–80 nm, respectively. Silica suspensions were prepared at concentrations up to 12.5 wt %. The technique of preparation of the stabilized aqueous dispersions of silica dioxide includes three stages [2]: stirring of starting components, ultrasonic dispergation and centrifugation. The suspensions were ultrasonicated for 60 min and centrifugated at 2000 min^{-1} for 15 min. Rheological properties of the dispersions were studied with a rotational viscosimeter Reotest 2.1 equipped with a cylindrical system in the range of detrusion rates from 9 to 1312.2 s^{-1}. The temperature of the samples was maintained at 20±0.5 °C.

3. Results and discussion

The study of coagulation of the suspended particles is presented in more detail in this paper than in the contribution by Hunter et al. [3] in which submicron particles are involved and van der Waals forces play an important role. To prevent agglomeration, the particles can be stabilized by ionic charges or a steric barrier if they are suspended in a liquid. Due to its high polarity and for the environmental reasons, water was chosen as the dispersion liquid. It has been observed that the stabilization with large molecules yields suspensions of high viscosity. The steric stabilization, in particular, needs much more space between the particles than the formation of an electric double layer in ionically stabilized suspensions. Conse-

quently, the ionic stabilization is more convenient for low-viscosity aqueous suspensions with high silica concentrations.

According to the DLVO theory [3], the energy barrier between the primary and secondary minima which prohibits a spontaneous agglomeration depends on the ions, their concentrations and the surface potential ψ_0. If the kinetic energy of the particles at room temperature is of the order of the energy barrier, then the coagulation can occur between the dispersed particles if the shear stress vanishes. The agglomeration of the dispersed submicron particles can be described by a second-order kinetic equation [4]:

$$-\frac{dN}{dt} = \alpha_p \frac{4kT}{3\eta} N^2 \tag{1}$$

where N is the number of particles, η is the viscosity of the liquid, and α_p is an operational parameter for the stability ratio describing collisions that lead to permanent agglomeration. The physical meaning of the parameter α_p is the medium size of particles in the colloid. It can be calculated from Eq. (1). If $\alpha_p \leq 1$ then such a colloid system will be inconvertible. The system undergoes a spontaneous agglomeration for $\alpha_p > 1$.

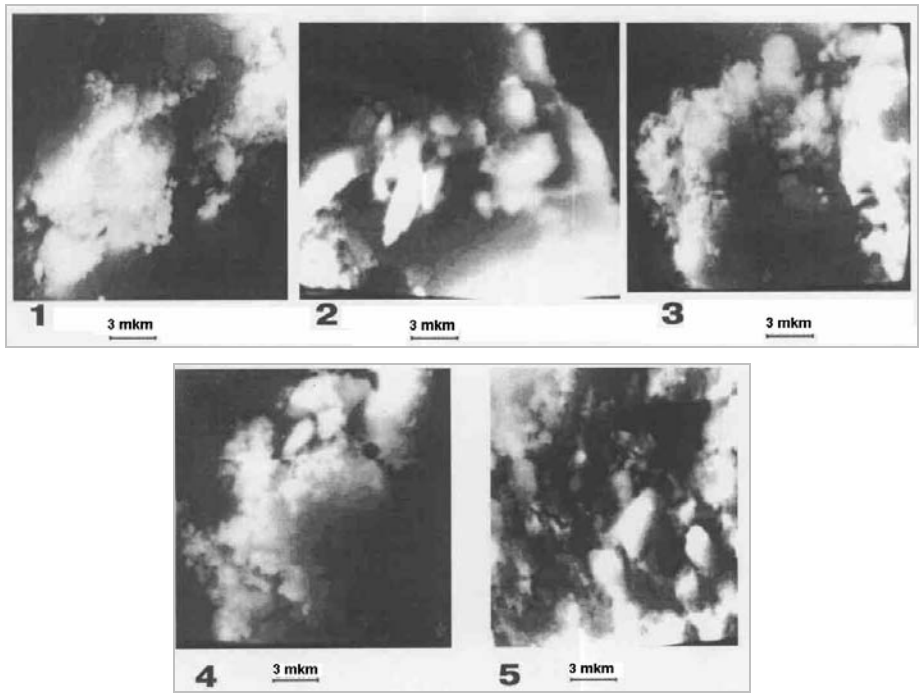

Fig.1. SEM of silica suspensions fabricated from fumed silica:
1 – A-50; 2 – A-175; 3 – A-300; 4 – A-380 (KEP, Ukraine);
5 – MOX-80 (Degussa Co., Germany)

Interacting particles initially connect via hydrogen bonds of the silanol groups on the silica surfaces. As long as only silanol groups are involved in bonding and the siloxane bonds are not formed, the increase of viscosity during the coagulation is reversible and shows a thixotropic behaviour. The thixotropy is largely influenced by the specific surface of silica and ethylenediamine particles because the bonds between the atoms are stronger in this case.

After addition of a small amount (about 6%) of ethylenediamine, low-viscosity suspensions can be prepared by the cross-linking within 3–6 months at room temperature. Figure 1 shows the SEM micrographs of silica particles in the suspensions. The silica particles in the dispersions obtained have a complex morphology.

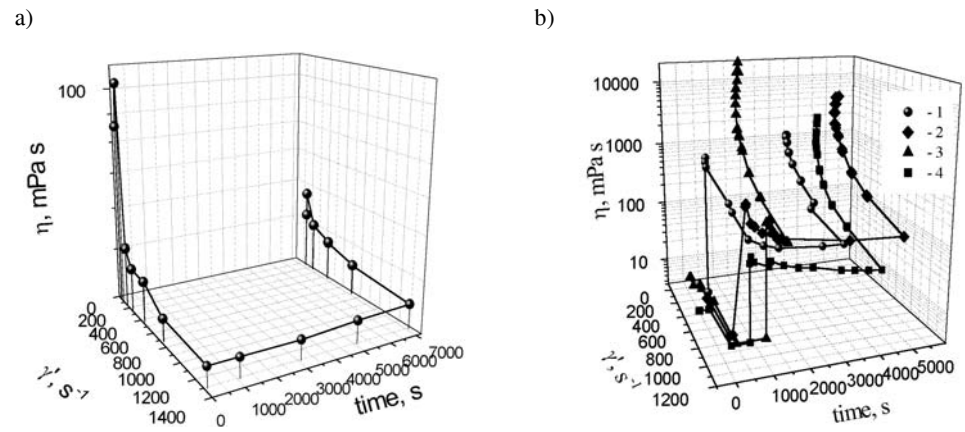

Fig. 2. Shear rate dependence of viscosity for suspensions containing 12.5 wt. % of fumed silica and stabilized by ethylenediamine: a) MOX-80 (Degussa Co., Germany), b) 1 – A-50, 2 – A-175, 3 – A-300, 4 – A-380 (KEP, Ukraine)

As can be seen in Fig. 1, the particles of the MOX-80 aerosil are least susceptible to agglomeration. This allows us to explain the thixotropic behaviour of the suspension prepared from the MOX-80 aerosil (Fig. 2a). The agglomeration of the initial silicas A-50, A-175, A-300 and A-380 with the increase of the shearing rate (γ') leads to irreversible changes in suspensions containing these aerosils (Fig. 2b). Thus, these suspensions exhibit rheopexy. The viscosity of the suspensions prepared increases with the decrease of the specific surface area of the aerosils.

4. Conclusions

We have demonstrated the possibility to process commercially available fumed silicas in order to obtain low-viscosity suspensions. The dispersions of silica nanoparticles (fumed silicas: A-50, A-175, A-300 and A-380 (Ukraine)) stabilized by ethylenediamine exhibit rheopexy. The effective viscosity of dispersions increases

essentially at certain shearing rates. Aqueous, stabilized dispersions of the fumed silica MOX-80 (Degussa, Germany) have the thixotropic properties. The percolation transformation in the dynamic viscosity of silica dioxide dispersions can be important for polishing elements employed in fabricating optical and electronic devices with the silica colloids described in this work.

References

[1] OTSUBO Y., WATANABE K., J. Colloid Interface Sci., 127 (1988), 214.
[2] GAISHUN E., TULENKOVA O.I., MELNICHENKO I.M., BARYSHNIN S.A., POTAPENOK Y.A., XLEBOKAZOV A.P., STRĘK W., Mater. Sci., 20 (2) (2002), 19.
[3] HUNTER R.J., *Zeta Potential in Colloid Science*, Academic Press, New York, 1981.
[4] STUMM W., MORGAN J.J., *Aquatic Chemistry*, Wiley, New York, 1981.

Received 16 July 2003
Revised 6 October 2003

Materials Science, Vol. 21, No. 4, 2003

EPR studies of defects in pure sol-gel matrices and their influence on cytotoxicity of the material

AGNIESZKA ULATOWSKA-JARŻA[1*],
MAŁGORZATA KOMOROWSKA[2], HALINA PODBIELSKA[2]

[1]Bio-Optics Group, Institute of Physics, Wrocław University of Technology,
Wybrzeże Wyspiańskiego 27, 50-370 Wrocław, Poland

[2]Biophysics Group, Institute of Physics, Wrocław University of Technology,
Wybrzeże Wyspiańskiego 27, 50-370 Wrocław, Poland

Sol-gel based biomaterials may be used for various applications, including biomedical ones. In this respect it is important to investigate the influence of sol-gel matrices on biological systems in order to establish their cytotoxic activity. The results of EPR studies of sol-gels are described in this work. They demonstrate that various defects are present in sol-gel matrices: surface defects, peroxy- centres or hydrogen-related centres. These defects arise spontaneously during the gelation, being responsible for cytotoxicity of sol-gels. It was found that the ratio of the number of solvent moles to the number of precursor moles (the molar ratio *R*) is one of the factors determining the level of cytotoxicity. More defects were present in samples prepared with a lower molar ratio *R*. A higher concentration of defects was detected in freshly prepared samples, as compared to samples aged for a longer time.

Key words: sol-gel; xerogel; electron paramagnetic resonance (EPR); cytotoxicity

1. Introduction

A major advantage of the sol-gel technique is the possibility of preparing pure or doped silica xerogels, single- or multicomponent systems at room temperature. This feature can be exploited for the construction of various sensing devices, as well as carriers of biomedical components, e.g. drugs, steroids or cells.

For medical applications, the sol-gel matrix should not be cytotoxic. The absence of cytotoxicity can be confirmed by various biological laboratory tests. Recently, we have described several routes allowing us to obtain non-cytotoxic sol-gels [1]. Our recent studies

[*]Corresponding author, e-mail: Agnieszka.Ulatowska-Jarza@pwr.wroc.pl.

have demonstrated that some of xerogels can cause haemolytic reaction [2–4]. The experiments were done on human erythrocytes obtained from citrated blood 0Rh+, diluted with 150 mmol/l NaCl to the concentration of 10%. Some results are presented in Fig. 1.

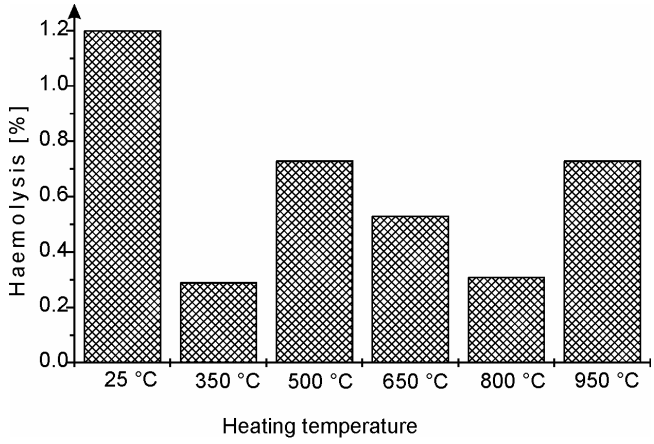

Fig. 1. Percentage of haemolysis depending on the temperature of thermal treatment of a xerogel matrix

The laboratory tests, as well the examination of the haemolytic reactions proved that freshly prepared sol-gels are cytotoxic due to their chemical instability. In order to rule out the problem of biological impurity of the investigated samples, the freshly prepared sol-gel bulks were subjected to the hot steam sterilization process. Interesting conclusions have been drawn from the analysis of the results obtained. The temperature of sterilization does positively influence the haemolytic reactions. This can be the result of a higher chemical stability due to the thermal process. Therefore, further examinations were performed on the xerogels exposed to higher temperatures after the condensation, as well as on materials aged for 6 months at room temperature (25 °C). For long-aged and heated materials the haemolysis is below the toxic values (< 1%).

A promising technique that can be used to describe and explain the material properties is the electron paramagnetic resonance (EPR). Some applications of the EPR technique to doped sol-gel materials have been reported [5–7]. The results include analysis of EPR spectra of pure sol-gel matrices (no dopants added). These materials, prepared by the sol-gel route, have been γ-ray irradiated and vacuum dried [8], heated at 700 °C and irradiated with X-rays [9] or dried at 920 °C and X-ray irradiated [10].

In the present work, we report the studies of paramagnetic defect centres in silica -based sol-gel materials that were produced at room temperature during the gelation process with various solvent amounts (different R values). Endogenous defects in the materials were examined. No exogenous defects caused by irradiation or additives were introduced.

2. Materials and methods

The samples were prepared from TEOS (Tetraethoxysilane, $Si(OC_2H_5)_4$, Aldrich), mixed with suitable amount of solvent (96% ethyl alcohol) for 4 h. The following molar ratios *R* were chosen: 5, 15, 32, and 50. The mixtures were acidified with 36% $HCl_{aq.}$ to obtain pH = 2 during the hydrolysis. The sol-gels were prepared in the form of bulks in plastic containers and left for drying after gelation stimulated by addition of ammonia solution. One-week-old samples were examined by means of UV-VIS spectroscopy. After one-month storage at room temperature the samples were powdered and weighed. Then, 9.44 GHz electron spin resonance spectra of the sol-gel materials were recorded by means of an EPR spectrometer made at the Wrocław University of Technology (EPR spectra were obtained with a standard SE/X-28 spectrometer operating in the X band). The MX-20/R microwave unit with a frequency counter was applied. The magnetic field was modulated at 100 kHz and the spectra were displayed as the first derivative of the absorption curves. All spectra were recorded at room temperature.

3. Results and discussion

Defects in amorphous SiO_2 with and without OH^- ions has been reviewed by Weil [11], Halliburton [12] and Griscom [13]. The description of these centres according to notation given by Ikeya [14] will be used in our further considerations (Table 1). The EPR spectra of the examined sol-gel matrices are presented in Fig. 2.

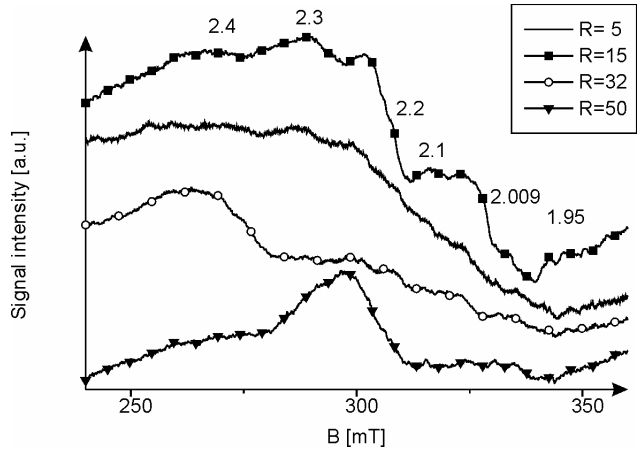

Fig. 2. EPR spectra of the sol-gel matrices dependent on the molar ratio *R*, recorded in the range of 240–360 mT

Figures 2 and 3 demonstrate that EPR signals of the sol-gel materials are mainly the broad structured bands with the average factor $g = 2.06$ (width of about 70 mT).

Table 1. Possible defects observed in silica materials by EPR and UV spectroscopy

Normal glassy structure	≡Si–O–Si≡	Each Si atom has 4 oxygen atoms tetrahedrally positioned, two different bond lengths: 1.62 Å and 1.60 Å. Si–O–Si angle 144°
g parameters		
E_1' centre	≡Si • Si≡ 2.00179 2.00053 2.00030	The centre is an electron trapped in the oxygen vacancy, produced at room temperature by γ-irradiation, annealed out above 373 K. The EPR signal is easily saturated at microwave power of 10^{-2} mW. Optical absorption at 212 nm.
E_2' centre E_4' centre	2.0022, 2.0006 2.00154, 2.00065, 2.00060	Absorption band at 225 nm. H^0 in an O^{2-} vacancy with a different relaxation.
Surface *E*′-like centre CO^{3-}- type centre	2.0017, 2.0003 centre: 2.0007 2.0048, 2.0063, 2.0248	Not stable when the sample contacts with water due to formation of gaseous H_2. Adsorption of CO_2 on the surface of *E*′-like centre.
Peroxy centre: two types OHC (dry OHC) NBOHC (non bonding oxygen hole centre). wet OHC	 ≡Si–O–(–O •)–Si≡ 2.0014, 2.0074, 2.067 (av.*) ≡Si–O • 2.0010, 2.0095, 2.078 (av.)	Oxygen-associated trapped hole centres. Peroxy radical, oxygen interstitial. Model: a complimentary centre of E_1' in a Frenkel pair (interstitial oxygen ion O^- which bonds with O^{2-}). Optical absorption at 325 nm. Usually observed as a shoulder of the OHC. Model: proton is released from Si–OH and a hole is trapped at the remaining oxygen in nonbonding 2p orbital. Optical absorption at 260 nm and 630 nm.
O_2^-	2.318, 1.992, 1.959	
Hydrogen centres	$[(OH)_4]^+$ 2.0911, 2.0103, 2.0002 $O(HO)_3$ 2.1351, 2.0047, 1.9962	Trapping a hole in p orbital of oxygen associated with one of four hydrogen atoms replacing a Si site $[H_4O_4]$ one proton is released

*Av. – average value of the *g* parameter.

With the increase of the solvent amount (increasing *R*), the fine structure of the EPR signal is more visible. For $R = 15$ three dominating groups of signals are observed: a low-field group with 2 signals $g_1 = 2.3–2.4$ and a more intensive $g_2 = 2.2$; mid-field with signals $g_3 = 2.1$ and more intensive $g_4 = 2.06$; high-field with narrow signals g_5 and g_6 between 2.009–1.95. For higher *R* factors, the dominating characteristics are low-field signals, although other signals are present as well (Fig. 2). The amount of

defects is strongly dependent on *R*. For small values of *R*, the number of defects is larger, what is demonstrated by wide bands with slightly marked fine structure of the spectrum.

With the increase of *R*, the amount of defects clearly decreases, particularly in the mid-field and high-field areas. In Figure 3, the EPR spectra are shown of the sol-gel matrices produced with $R = 15$ and 50 recorded in the range of 310–350 mT.

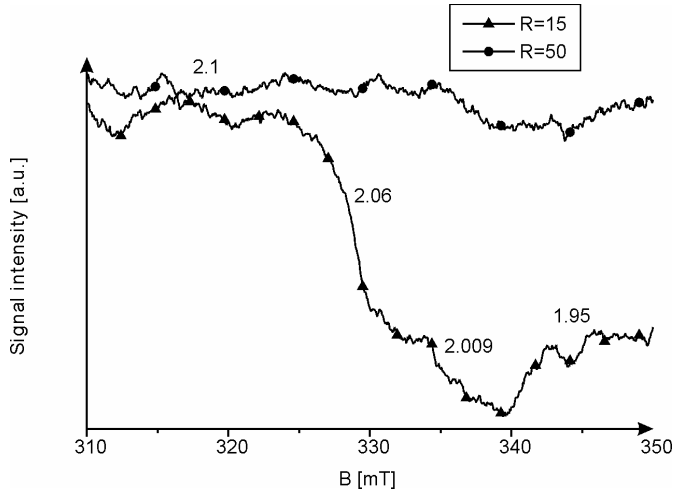

Fig. 3. EPR spectra in the range of 310–350 mT of the sol-gel matrices prepared with the molar ratios $R = 15$ and $R = 50$

Drying time at room temperature influences the amount of defects as well. For the shorter-dried sample (A), the highest concentration of centres in the high-field area is observed. The defects disappear with the increase of the ageing time (sample B). The centres with signals in the low-field part of the spectrum are prevalent (Fig. 4).

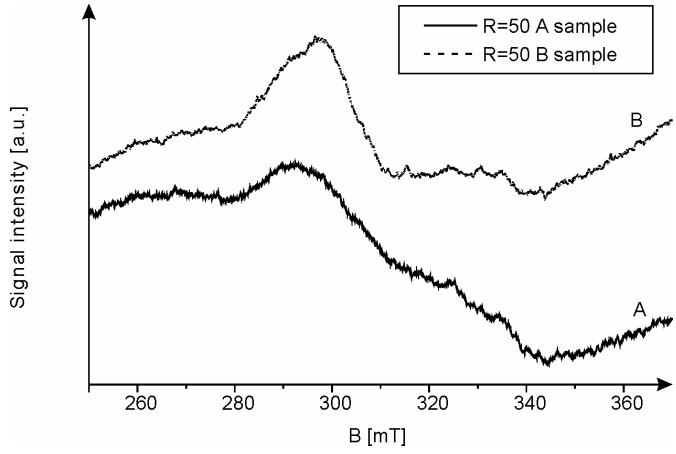

Fig. 4. The comparison of the EPR spectra depending on the ageing time of sol-gel matrices

Since some defects (for example E' – easily saturated) are better observed by the UV spectroscopy, the absorption spectra of matrices with R = 15 and 50 were measured (Fig. 5). For R = 15, two absorption bands with the maxima at 225 (E_2' centre) and 260 nm (peroxy centre) are observed. For R = 50 a third band with maximum at 212 nm appears (E_1' centre). The number of centres which absorb at 260 nm is constant and does not depend on the R factor. However, the 212 nm and 225 nm bands occur for the larger R factors.

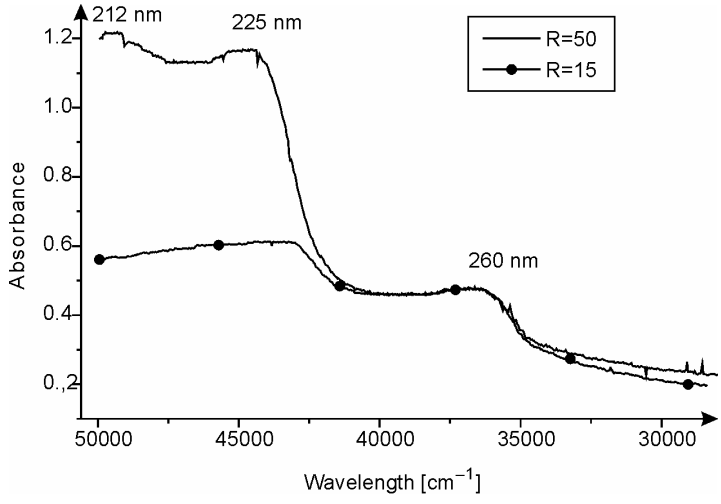

Fig. 5. UV-VIS spectra of sol-gels prepared with R = 15 and R = 50

Table 2. Absorption bands (UV spectra)

Parameter R	Absorption band at [nm]	Absorbance	I_{225}/I_{260}
15	225	0.9	1.1
	260	0.8	
50	212	1.2	2.4
	225	1.2	
	260	0.5	

Regarding the g factor, the presence of peroxy-centres: OHC (g_1 = 2.0014, g_2 = 2.0074, g_3 = 2.067 (av.)) and NBOHC (2.0010, 2.0095, 2.078 (av.)) can be assumed. E_1' centres cannot be detected by EPR because of saturation, even at low-power microwaves (50 mW used in experiment). Surface centres E' are unstable in contact with water, therefore they are present only in areas with the smallest amount of solvent. These centres are responsible for signals in the mid-field and high-field areas, therefore the defect concentration for these signals is much higher at the low R factors than

at the higher R values. Signals observed in the low-field and high-field areas (g about 1.9) may be related to the presence of the O^{2-} centres. The value of $g = 2.13$ may indicate the presence of hydrogen-related centres. Table 3 contains the summary of the above considerations.

Table 3. Proposed assignments of defects in the samples studied

Defect in a sample	g values	Absorption bands [nm]	Remarks
E_1'	not available	212	Yes. Invisible in EPR spectra because of saturation, stated by UV spectrometry.
E_2' E_4'	high magnetic field	225	Yes. The concentration is higher with the increasing parameter R
Surface like E_1'	high magnetic field	No UV absorption observed	Probably. Unstable in the presence of water. Dominating for lower R
O^{2-}	low and high magnetic field	No UV absorption observed	Yes The most stable. Dominating for high R values
Peroxy centres OHC NBOHC	mid and high magnetic field	260	Yes Dominating for lower values of the R parameter
Hydrogen -related defects $[(HO)_4]^+$, $[O(HO)_3]^+$	mid and high magnetic field	No UV absorption observed	Yes

4. Possible influence of the defects observed on cytotoxicity

Macroporous silica gels can be exploited as carriers for cells, bacterias or other microorganisms, provided they are biocompatible. Gels may be cytotoxic since the hydrolysis of alcohol-based reactants leads to creation of non-biocompatible materials. In addition, our studies have demonstrated that all types of E' defects can be present. Thus when the samples contact with water, free electrons or hydrogen atoms are produced. Both products could act as redox reagents.

According to the results obtained, the toxicity is expected to be higher when samples are freshly prepared or prepared with a lower R ratio. Increased R value accelerates the reaction of hydrolysis and causes more complete hydrolysis of monomers before condensation occurs. As a consequence, the gelation time increases. Longer gelation times reduce the amount of defects formed during gelation. For lower R values the alcohol-producing condensation mechanism is favoured, whereas the water-forming condensation is favoured at higher values of the R ratio.

5. Conclusions

The number of defects in sol-gel matrices, which can be responsible for cytotoxicity, depends on the *R* ratio and the ageing time. This confirms the results of laboratory and biological testing of aqueous extracts of sol-gels presented in our previous papers [2, 3]. We have proved that it was possible to produce the sol-gel derived materials that are non-haemolytic. This can be achieved by heating the materials at elevated temperatures or by ageing them for a suitably long time (minimum 6 months). Examination of the haemolytic reaction showed that freshly prepared xerogels are cytotoxic due to their chemical instability. EPR can be exploited as a suitable method for searching for defects responsible for cytotoxicity in the materials tested.

Acknowledgements

The financial support by the State Committee for Scientific Research (KBN), grant No. 4T11E 01124), and by the Centre for Advanced Materials and Nanotechnology of the Wrocław University of Technology is gratefully acknowledged. A. Ulatowska-Jarża is granted by the Foundation for Polish Science FNP with an Annual Award for Young Scientists.

References

[1] CONROY J.F.T., POWER M.E., MARTIN J., EARP B., HOSTICKA B., DAITCH C.E., NORRIS P.M., J. Sol-Gel Sci. Technol., 18 (2000), 296.
[2] ULATOWSKA-JARŻA A., PODBIELSKA H., SZYMONOWICZ M., STANISZEWSKA-KUŚ J., PALUCH D., Polym. Med., 30 (2000), 45.
[3] ULATOWSKA-JARŻA A., PODBIELSKA H., HOŁOWACZ I., LECHNA-MARCZYŃSKA M., SZYMONOWICZ M., STANISZEWSKA-KUŚ J., PALUCH D., SPIE Proc. vol. 4597 (2001), 81.
[4] ULATOWSKA-JARŻA A., *Elaboration of project for enzymatic optode based on the own results of examination of the sol-gel matrices properties*, Ph.D. Thesis, Wrocław University of Technology, Wrocław, 2001.
[5] KŁONKOWSKI A., KLEDZIK K., OSSOWSKI T., JANKOWSKA-FRYDEL A., J. Mater. Chem., 8 (1998), 1245.
[6] KŁONKOWSKI A., KOEHLER K., WIDERNIK T., GROBELNA B., J. Mater. Chem., 6 (1996), 579.
[7] KŁONKOWSKI A., WIDERNIK T., GROBELNA B., MOZGAWA W., JANKOWSKA-FRYDEL A., Microporous Mesoporous Mater., 31 (1999), 175.
[8] KORDAS G., WEEKS R.A., KLEIN L.C., J. Non-Cryst. Solids, 71 (1985), 327.
[9] WOLF A.A., FRIEBELE E.J., TRAN D.C., J. Non-Cryst. Solids, 71 (1985), 345.
[10] GRISCOM D.L., BRINKER C.J., ASHLEY C.S., J. Non-Cryst. Solids, 92 (1987), 295.
[11] WEIL J.A.,Phys. Chem. Miner., 10 (1984), 149.
[12] HALLIBURTON L.E., Appl. Radiat. Isot., 40 (1989), 859.
[13] GRISCOM D.L., Rev. Solid State Sci., 4 (1990), 565.
[14] IKEYA M., *New Applications of Electron Spin Resonance: Dating, Dosimetry and Microscopy*, World Scientific Publ., London, 1993.

Received 15 June 2003
Revised 25 July 2003

Materials Science, Vol. 21, No. 4, 2003

Silica gel glasses after laser irradiation

S.V. SHALUPAEV, A.V. SEMCHENKO*, Y.V. NIKITYUK

Gomel State University, Sovetskaya 104, Gomel 246699, Belarus

The paper describes a 'combined' sol-gel process allowing us to fabricate large-sized silica glasses. A comparative analysis of the laser thermosplitting of fused and gel silica glasses is also presented. Basic characteristics and main specific features of the silica-gel glasses obtained are given. The distribution of thermoelastic fields in fused and gel-silica glasses after exposing them to laser thermosplitting is analyzed. Regularities in splitting silica glasses by the laser thermosplitting method have been found. To achieve reliable thermosplitting effects and stable dividing microcracks, special conditions are needed, favouring the formation of initiating microcracks.

Key words: sol-gel method, silica glasses, thermosplitting, microcracks

1. Introduction

Theoretical and experimental studies of the problem of splitting brittle non-metallic materials by laser methods are described in a great number of papers. However, new materials recently developed require an adaptation of known technologies to make them applicable for treatment of these materials. Quality of cutting silica glasses, especially gel glasses, is one of the most important problems [1]. This method yields high-purity activated silica glasses for fibre optics, optoelectronics and laser optics at low temperatures eliminating the fusion stage. The sol-gel transition occurs due to polycondensation, hydrolysis and gel formation followed by heat treatment yielding dense gels. Unlike fused glasses, the sol-gel ones contain fewer impurities resulting from the quality of the initial materials. They are also synthesized at lower temperatures. The sol-gel technology is believed to be an energy- and resource-saving process [2]. Its another advantage is simplicity of the necessary equipment.

At present, three directions of the sol-gel technology are employed to produce silica glasses suitable for optical applications. The first variant is the alkoxide method.

* Corresponding author, e-mail:semchenko@gsu.unibel.by.

Glass is formed by hydrolysis, polycondensation of products of hydrolysis and heat densification of gels to the state of pore-free glass. The drawbacks of this technique are time-consuming process of synthesis, high probability of cracking when bulks are dried and sintered and small bulk size.

The other technique involves polymerization of colloids of ultradispersed silicate powders in liquid environment. Large-sized gels obtained by this technique can be dried without cracking. Yet, the process requires elevated temperatures of sintering (over 1450 °C) and does not allow one to obtain complex compositions and homogeneously activated glasses.

The third technique is a combination of the two. It comprises the advantages of the former two variants [2]. The initial components are usually ethoxy- and methoxysilanes with aerosils or other ultradispersed powders serving as fillers. The introduction of aerosols into sols increases the concentration of the solid phase in the liquid and the gel strength, facilitates and accelerates the drying of the porous bulks. Vitrification temperatures of such combined systems are usually within the range of 1200–1350 °C, depending, among others, on the filler content. Such systems are most prospective from the viewpoint of industrial application – yet, their properties are poorly understood.

A number of processes occurring during the production of gel glasses and inside the samples formed are not fully understood. A comparative analysis of the regularities of the laser thermosplitting of fused and silica glasses is also an important task.

2. Experiment and materials

The glasses studied were obtained by the ‘combined’ sol-gel process. The schematic diagram of the process is presented in Fig. 1. Certain characteristics of these glasses are similar to those of fused silica glasses (Table 1) [3]. This is why common methods used to study silica glasses were applied in our case. Bulks of gel glass may have large sizes making them suitable for practical applications. However, their structure on the submicron scale is different than that of fused glasses. The glasses have more chaotic structure and contain more defects.

Table 1. Comparison of characteristic features of gel lasses and fused glasses

Characteristic	Gel glasses	Fused glasses
Density, g/cm^3	2.201	2.206
Specific heat, J/(kg×°C)	1325	880
Heat conductivity, W/(m×°C)	0.7	1.34
Linear thermal expansion coefficient, (1/K)×10^{-7}	5.7	5
Yung’s modulus, GPa	7.3	7.8
Poisson’s ratio	0.158	0.165
Microhardness, MPa	7000–8500	6860–8850
Refractory index	1.458	1.458

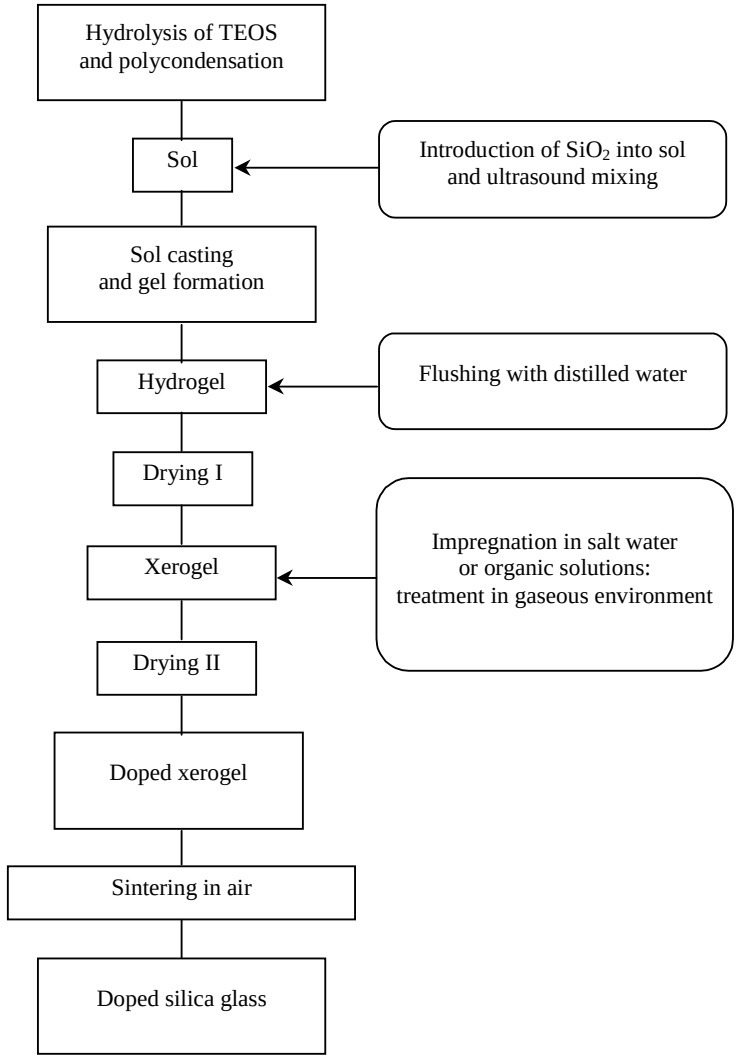

Fig. 1. Schematic diagram of the sol-gel process to obtain silica glasses

Experimental studies of the laser thermosplitting of fused and gel-silica glasses were performed using a set-up comprising the following units: a CO_2 laser with the power of output radiation of 60 W operating in the continuous mode at λ = 10.6 μm, an *xyz* positioner with the software control, an optical-mechanical device of the radiation energy channel.

Experimental studies have yielded the technology of laser cutting of fused and silica gel glasses. Optimal technological parameters providing the best results are listed in Table 2.

Table 2. Optimal technological parameters for the technology of laser cutting of glasses

Material	Laser beam	Sizes of glasses, mm		Cutting speed, mm/s	Power density of a laser radiation, 10^6 W/m^2
		Thickness	Cross-section		
Fused quartz glass	ellipse A = 4.5 mm B = 1.1 mm	2	30×30	10	5
Silica gel glass	ellipse A = 2 mm B = 0.5 mm	2	30×30	17	3.2

Our studies have shown that the processes of cutting gel and fused silica glasses by laser thermosplitting are similar. This occurs provided that special measures are applied to attain conditions favourable for formation of the initial microcracks. In such a case, preliminary softening of glass due to the generation of a defect zone along the cutting line is inefficient.

The main features of the technology developed are: the supply of the air–water mixture into the cutting zone which acts as a refrigerant and the initiation of the thermosplitting process by glass softening within the region where the refrigerant is supplied.

3. Numerical analysis of thermoelastic fields

The analysis of thermoelastic fields is of practical importance since it allows one to study the features of the mechanism of dividing microcrack formation. Due to difficulties arising when using analytical methods in calculating thermoelastic fields in the non-linear problem formulation, the finite-element method [4] was used.

Thermal characteristics of silica glasses depend to a great extent on temperature while with the laser thermosplitting the temperature of silica glass varies within a broad range. To eliminate large errors in calculations, one should take into account these dependencies. According to literature data [5], we suggest that upon increasing temperature from the ambient value to the vitrification temperature, the glass thermal conductivity increases two times and the specific heat increases by the factor of 1.5. To achieve high-quality glass by laser thermosplitting, the temperature of the specimens to be cut should not exceed the vitrification temperature. Thus, in calculations we have taken into account that the temperature of glass within the region of laser beam action can vary from 20 to 1100 °C.

We used the supply of the cooling air–water mixture into the cutting zone previously heated by a laser beam. The mixture rate was 0.8 m/s [6], which gives the heat transfer coefficient of 6800 W/(m^2×K) used in our calculations.

As the initial size of the region heated depends on the depth of radiation penetration into the material, the model of a surface heat source was applied to simulate the

effect of laser radiation. When a CO_2 laser is used to cut silica glasses, this depth is comparable with the radiation wavelength.

To calculate temperature stresses, we employed the formulation of the quasi-static problem implying that the stress state stabilises sufficiently faster than the thermal equilibrium. The error of the values of the temperature stress caused by the neglect of the inertial effects is very small [7].

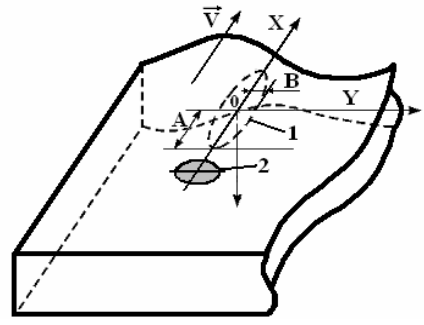

Fig. 2. Scheme of arrangement of the laser beam and cooling agent in a plane of processing: 1 – elliptical laser beam, 2 – cooling agent

Figure 3 shows the temperature fields on the surface of the specimen during cutting. The solid lines are isotherms corresponding to the temperature values shown in the plots. The maximum surface temperature of gel silica glass reaches 1152 °C. Thus, the brittle fracture mode occurs in the specimens.

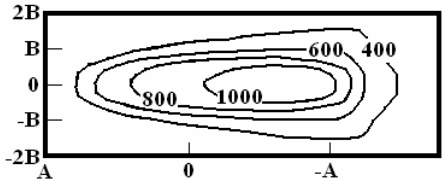

Fig. 3. Distribution of temperature fields (in °C) on the surface of a quartz glass synthesized by the sol-gel method

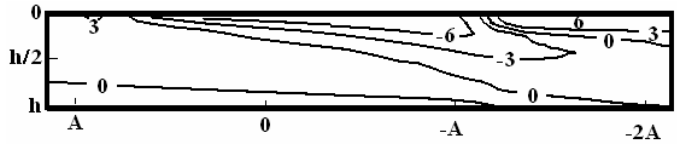

Fig. 4. Distribution of fields of σ_{22} stresses (in MPa) in a plane of splitting of a silica glass synthesized by the sol-gel method

In Figures 4 and 5, the distribution of fields of stresses (σ_{22}) which give the largest contribution to the development of the dividing microcracks in the splitting plane of the silica glass obtained by the sol-gel method is shown. One can conclude that the maximum values of σ_{22} occur on the sample surface in the zone of action of the cooling agent. These values do not exceed 10 MPa. That is not enough for splitting the

sample without formation of the initial microcrack. Thus, as has been mentioned above, the necessary requirement of the reliable thermosplitting process is initializing of the dividing microcrack in the zone of action of the cooling agent.

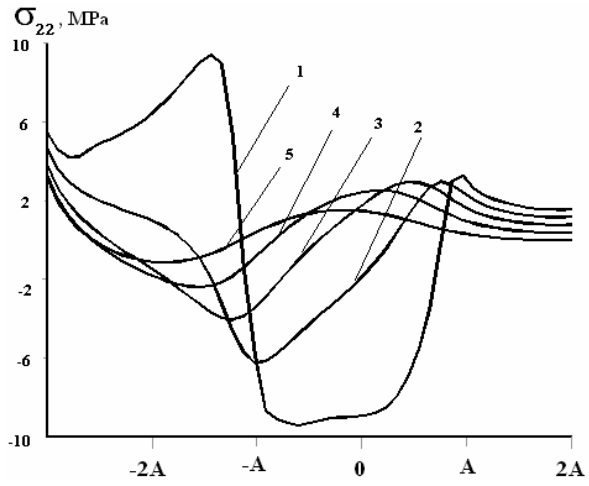

Fig. 5. Dependence of stresses σ_{22} (in MPa) to spacing interval up to the centre of an elliptical laser beam in silica glass synthesized by the sol-gel method (Y = 0 mm), 1 – Z = 0, 2 – Z = 0.3 mm, 3 – Z = 0.6 mm, 4 – Z = 0.9 mm, 5 – Z = 1.2 mm

A further development of the crack is governed by the distribution of compressive stresses caused by the laser beam. The zones of location of these stresses stretch around the zone of tensile stresses resulting from the cooling agent action. This enables division of the silica glass in the controlled thermosplitting mode involving the first stage of the sample damage yielding high quality of surfaces of articles being processed.

References

[1] EMELYANOV V.A., KONDRATENKO V.S., TANASEYCHUK A.S., SHALUPAEV S.V., SHERSHNEV E.B., Electron technology. Laser technology and optoelectronics, 3 (1991), 90.
[2] GAISHUN V.E., BOIKO A.A., SEMCHENKO A.V., MELNICHENKO I.M.,PODDENEZHNY E.N., SPIE, 1995, 263.
[3] PODDENEZHNY E.N., MELNICHENKO I.M., PLYTSH B.V., KAPSHAI M.N., RUNTSO N.K., Inorganic Materials, 38 (1999), 1525.
[4] SHABROV N.N. *Finite element method in calculations of elements of thermal engines* (in Russian), Engineering, Leningrad, 1983.
[5] MATHYLKA G.A., *Laser processing of a glass*, Soviet Radio, Moscow, 1979.
[6] BOGUSLAVSKI I.A., *High-strength well-tried glasses* (in Russian), Publishing House of Building Literature, Moscow, 1969.
[7] NOVATSKI V., *Theory of elastic strength* (in Russian), World, Moscow, 1975.

Received 15 June 2003
Revised 9 September 2003